We put science to work.™

Savannah River National Laboratory™

OPERATED BY SAVANNAH RIVER NUCLEAR SOLUTIONS

A U.S. DEPARTMENT OF ENERGY NATIONAL LABORATORY • SAVANNAH RIVER SITE • AIKEN, SC

Sludge Batch 9 Simulant Runs Using the Nitric-Glycolic Acid Flowsheet

D. P. Lambert

M. S. Williams

C. H. Brandenburg

M. C. Luther

J. D. Newell

W. H. Woodham

November 2016

SRNL-STI-2016-00319, Revision 0

SRNL.DOE.GOV

DISCLAIMER

Printed in the United States of America

Prepared for
U.S. Department of Energy

SRNL-STI-2016-00319
Revision 0

Keywords: *DWPF, SRAT, Sludge, SB9, CPC*

Retention: *Permanent*

Sludge Batch 9 Simulant Runs Using the Nitric-Glycolic Acid Flowsheet

D. P. Lambert
M. S. Williams
C. H. Brandenburg
M. C. Luther
J. D. Newell
W. H. Woodham

November 2016

Prepared for the U.S. Department of Energy under contract number DE-AC09-08SR22470.

Savannah River National Laboratory™
OPERATED BY SAVANNAH RIVER NUCLEAR SOLUTIONS

REVIEWS AND APPROVALS

AUTHORS:

D. P. Lambert, Process Technology Programs Date

M. S. Williams, Process Technology Programs Date

J. D. Newell, Process Technology Programs Date

W. H. Woodham, Process Technology Programs Date

TECHNICAL REVIEW:

C. J. Martino, Process Technology Programs, per E7 2.60 Date

APPROVAL:

F. M. Pennebaker, Manager Date
Process Technology Programs

D. E. Dooley, Director, Date
Environmental & Chemical Process Technology Research Programs

R. E. Edwards, Manager Date
SRR Nuclear Safety and Engineering Integration

E. J. Freed, Manager Date
SRR DWPF/Saltstone Engineering

PREFACE OR ACKNOWLEDGEMENTS

The thirteen runs were completed between February 2 and March 18, 2016. The following people and groups listed below were instrumental in completing this testing:

Thanks to the technicians responsible for the testing, Jon Duvall, Vickie Williams, Phyllis Workman, David Healy, Kim Wyszynski, Courtney Burkhalter, and Madison Caldwell. The technicians worked twelve-hour day or night shifts for 4 weeks.

Thanks to Frances Williams, John Pareizs, Matt Williams, and Jack Zamecnik for moving, setting up, calibrating and running the GC, MS and FTIR offgas instruments that collected so much data during these runs. Thanks also to John Pareizs, Matt Williams, and Jack Zamecnik for collecting and analyzing the offgas data and completing the mass balances needed for understanding not just the peak concentrations but also the total mass produced or consumed.

Thanks to Joel Jones and Kenn Gibbs for developing the LabVIEW automation and control software for the 1/216th scale rig. Thanks to Frances Williams for her support for the procurement of the equipment to support the 1/216th scale testing.

Thanks to Kim Wyszynski, Beverly Wall, Whitney Riley, and Courtney Burkhalter for analyzing nearly one-thousand samples to support this testing. Each of these samples had multiple analytes and/or repeat analyses, not to mention all the dilutions, standards, and blanks that had to be prepared and analyzed.

Thanks to Holly Hall for coordinating all of the samples including preparing/labeling the sample bottles, preparing the sample request forms, and arranging delivery of all the samples.

Thanks to Tom White and Chuck Coleman for their work in developing an improved method of glycolate analysis. Thanks to Tom for analyzing and reanalyzing so many SRAT and SME products from these runs for anions and ammonium.

EXECUTIVE SUMMARY

Testing was completed to develop a Sludge Batch 9 (SB9) nitric-glycolic acid chemical process flowsheet for the Defense Waste Processing Facility's (DWPF) Chemical Process Cell (CPC). CPC simulations were completed using SB9 sludge simulant, Strip Effluent Feed Tank (SEFT) simulant and Precipitate Reactor Feed Tank (PRFT) simulant. Ten sludge-only Sludge Receipt and Adjustment Tank (SRAT) cycles and four SRAT/Slurry Mix Evaporator (SME) cycles, and one actual SB9 sludge (SRAT/SME cycle) were completed. As has been demonstrated in over 100 simulations, the replacement of formic acid with glycolic acid virtually eliminates the CPC's largest flammability hazards, hydrogen and ammonia. Recommended processing conditions are summarized in section 3.5.1.

Testing demonstrated that the interim chemistry and Reduction/Oxidation (REDOX) equations are sufficient to predict the composition of DWPF SRAT product and SME product. Additional reports will finalize the chemistry and REDOX equations. Additional testing developed an antifoam strategy to minimize the hexamethyldisiloxane (HMDSO) peak at boiling, while controlling foam based on testing with simulant and actual waste.

Implementation of the nitric-glycolic acid flowsheet in DWPF is recommended. This flowsheet not only eliminates the hydrogen and ammonia hazards but will lead to shorter processing times, higher elemental mercury recovery, and more concentrated SRAT and SME products. The steady pH profile is expected to provide flexibility in processing the high volume of strip effluent expected once the Salt Waste Processing Facility starts up.

Conclusions

- Successfully validated interim chemistry equations
    - Interim REDOX model predicts resulting REDOX trends.
- Demonstrated very low generation of two of DWPF's potential flammable gases, hydrogen and ammonia.
- Except for the first tests where the antifoam strategy was being developed, significant foaming was observed only during boiling, prior to completion of dewater, for the coupled run (NG62).
- The antifoam strategy developed during additional SB9 flowsheet testing, similar to the reduced antifoam addition strategy used during SC-18 qualification, should be implemented by DWPF for SB9 nitric-glycolic flowsheet processing. The peak HMDSO SRAT generation at boiling was 0.0041±0.0004 mmol/min at the experiment scale.
- The Koopman Minimum Acid (KMA) operating window for SB9 processing is 77% to 100% for SRAT product total solid concentration of <30 wt % and can be extended to 123% for SRAT product total solid concentration of <20 wt %. Note the SB9 antifoam strategy was only tested up to 110% KMA.
- Mercury stripping and collection in the Mercury Water Wash Tank (MWWT), averaging 71% mercury recovery in the MWWT during 100% KMA runs at design basis boilup, was much better than has been achieved in previous testing.
- In all experiments, nitrite was destroyed to <500 mg/kg. This is similar to the SC-18 actual-waste demonstration (at a relatively low 78% KMA) where the nitrite concentration was 304 mg/kg in the SRAT product slurry and 380 mg/kg in the SME product slurry.
- The peak carbon dioxide in the SRAT varied from 640 to 730 lb/hr at DWPF scale, significantly higher than the 342 lb/hr measured in the SC-18 actual-waste demonstration. The peak carbon dioxide in the SME varied from 4.9-6.1 lb/hr, significantly lower than the 19 lb/hr measured in the SC-18 shielded cells run.

- The peak nitrous oxide ranged from 0.23-1.0 vol% in the SRAT and <0.069 vol% in the SME. The peak nitrous oxide in the SC-18 actual-waste demonstration was 0.57 vol% in the SRAT and 0.08 vol% in the SME.
- Rheology is the most important processing parameter in defining the CPC operating window for this flowsheet. The rheology was a strong function of acid stoichiometry. The highest acid stoichiometry runs (NG52, 54 and 59) had yield stress and consistency results that were higher than the DWPF SRAT product design basis. The rest of the runs had low yield stress and consistency values, often below the SRAT product design basis.
- Run NG58 was the closest simulant run for comparison to the SC-18 actual-waste demonstration. The NG58 SRAT product had a yield stress of 0.6 Pa and a consistency of 5.6 cP. The SC-18 shielded cells run had a SRAT product yield stress of 0 Pa and a consistency of 2.8 cP. Both SRAT products were rheologically thin. Since the NG58 SRAT product was higher in total solids (30% versus 25% for SC-18) it would be expected to have a higher yield stress and consistency.
- The final concentration of mercury in the SRAT product ranged from 0.02-0.61 wt% of the total solids, which was below the 0.45 wt% target in all runs except NG52.

Recommendations

Based on the results of this simulant study, SRNL recommends implementation of the nitric-glycolic acid flowsheet in DWPF. The following

- Except for runs NG52 and NG54, which both had thick rheology and high rod temperatures, Hydrogen generation was near or below the GC detection limit of <0.006 volume % or <0.0037 lb/hr DWPF scale.
- Throughout the SB9 qualification testing, no significant foaming was observed. DWPF should consider implementing a reduced antifoam addition strategy developed for SB9 in testing with simulants and actual waste
- Testing with simulants and actual waste confirmed that the Caustic Quench method previously developed should be used for anion measurement by IC for SRAT and SME product slurries and SRAT receipt slurry.

The following are recommendations for follow-on work utilizing the data from this study:

- Use SRAT and SME product data from these tests in regressions to refine the nitric-glycolic flowsheet CPC chemistry equations.
- Use SRAT and SME product from these tests and additional REDOX measurements to finalize the nitric-glycolic flowsheet REDOX model.
- Based on findings from additional study of mercury within the liquid waste flowsheet, it is recommended that future simulant work include Cold Vapor Atomic Absorption Spectroscopy for mercury analysis to compare method sensitivities during simulant tests.

Based on testing results and observations, SRNL recommends the following future testing to better align simulant studies with the facility in an effort to maximize mercury recovery. These recommendations are not tied to the implementation of the flowsheet for SB9.

- Complete back to back DWPF prototypic SRAT testing that includes a heel of mercury in the MWWT and SMECT, hot SRAT condenser outlet temperature, to better simulate prototypic DWPF processing.

- Determine if mercury collection is increased by refluxing the SRAT condensate (not dewatering) for the first 3 hours of SRAT boiling. This would return any dissolved mercury back to the SRAT allowing collection in the MWWT at a time when the condensate is less acidic.
- Determine whether pH control of the MWWT and/or SMECT can increase mercury recovery.
- Determine whether a coalescer will improve the recovery of mercury in the MWWT

In future sludge batches, testing for CPC processing qualification can be radically changed due to elimination of catalytically generated hydrogen. Little chemistry is happening in the SME cycle, thus much more can be learned by focusing on SRAT cycle testing. The following testing at prototypic processing conditions is recommended:

- Complete SRAT cycle testing at the extremes of the expected processing (80% to 110% KMA).
- Define rheological window.
- Complete one sludge-only SRAT/SME cycle and several coupled SRAT/SME cycles with varying PRFT and SEFT volumes to bound expected processing.
- Complete one shielded cells SRAT/SME cycle with actual sludge, actual PRFT, and SEFT simulant. Use recommended acid stoichiometry and REDOX target from simulant tests.
- Validate the Aspen plus CPC model using data generated in CPC testing.

TABLE OF CONTENTS

LIST OF TABLES

LIST OF FIGURES

LIST OF ABBREVIATIONS

ACTL	Aiken County Technology Laboratory
ADPs	Antifoam Degradation Products
CPC	Chemical Processing Cell
CSTR	Continuous Stirred Tank Reactor
CVAA	Cold Vapor Atomic Absorption Spectroscopy
DWPF	Defense Waste Processing Facility
FAVC	Formic Acid Vent Condenser
FTIR	Fourier Transform Infrared Spectroscopy
GC	Gas Chromatography
GMA	Glycolic Minimum Acid
HMDSO	Hexamethyldisiloxane
HNMR	Hydrogen Nuclear Magnetic Resonance
IC	Ion Chromatography
ICP-AES	Inductively Coupled Plasma – Atomic Emission Spectroscopy
KMA	Koopman Minimum Acid
M&TE	Measuring and Test Equipment
MAR	Measurement Acceptability Region
MS	Mass Spectrometry
MS&E	Measurement Systems and Equipment
MST	Monosodium titanate
MWWT	Mercury Water Wash Tank
N/A	Not Applicable
NR	Not Reported
NGS	Next Generation Solvent
NIST	National Institute of Standards and Technology
PID	Proportional Integral Derivative
PRA	Percent Reducing Acid (molar)
PRFT	Precipitate Reactor Feed Tank
R&D	Research and Development
REDOX	Reduction Oxidation Ratio
SB9	Sludge Batch 9
SEFT	Strip Effluent Feed Tank
SME	Slurry Mix Evaporator
SMECT	Slurry Mix Evaporator Condensate Tank

SRAT	Sludge Receipt and Adjustment Tank
SRNL	Savannah River National Laboratory
SVOA	Semi-Volatile Organic Analysis
TGA	Thermal Gravimetric Analysis
TIC	Total Inorganic Carbon
TiDG	Tris (isodecyl) guanidine
TMS	Trimethylsilanol
TOC	Total Organic Carbon
TS	Total Solids
TTR	Technical Task Request
UV-Vis	Ultraviolet-Visible
VOA	Volatile Organic Analysis

1.0 Introduction

Sludge Batch 9 (SB9) simulant testing was performed using the nitric-glycolic flowsheet as requested by the DWPF Technical Task Request[1] and as described in the Task Technical and Quality Assurance Plan.[2] The objective of this work was to perform DWPF Chemical Process Cell (CPC) Sludge Receipt and Adjustment Tank (SRAT) and Slurry Mix Evaporator (SME) simulant flowsheet testing to validate the sludge-only flowsheet and establish a coupled operation flowsheet for use with SB9 using the new antifoam addition strategy and nitric-glycolic flowsheet. Objectives were achieved by monitoring the chemistry of the CPC experiments through sampling the condensate, sludge, and offgas. The testing focused on the chemistry of the SRAT cycles, which allows flexibility in frit and waste loading in future studies of rheology and REDOX. Separate studies were conducted for frit development and glass properties.[3-5]

The lab-scale CPC runs were performed with a blend of Tank 51H and Tank 40H simulants deemed SB9A, the same simulant used for SB9 Nitric-Formic Flowsheet testing. Testing was completed at the Aiken County Technology Laboratory (ACTL). The 4-L laboratory scaled CPC runs were performed using round-the-clock operations.

Ten SRAT-only runs were designed to develop the operating window for implementation of the nitric-glycolic flowsheet in DWPF and determine the impact the change of acid stoichiometry and the blend of nitric and glycolic acid as it impacts various processing variables over a wide processing region. In addition, the resulting SRAT products could be used for further analysis or could be blended together to better understand certain segments over this region.

Three SRAT/SME lab-scale simulations each had additional objectives. NG60 was performed at DWPF processing conditions by using design basis boil up rates. NG61 was performed at half the boil up rate of the DWPF design basis, unlike the other experiments, and included six canister decontamination simulant additions that were added at the start of the SME cycle. NG62 was performed to validate the coupled operations, in which Precipitate Reactor Feed Tank (PRFT) simulant (without monosodium titanate or MST) was added at the beginning of the SRAT cycle, and Strip Effluent Feed Tank (SEFT) simulant was added after dewater in the SRAT cycle.

A recommendation for the performance of the SRNL shielded cells qualification SRAT and SME run(s), with a blend of actual waste SB9 Tank 51H and SB8 Tank 40H samples, was based on the conditions used in test NG60.[6] The results of the SRNL shielded cells qualification SRAT and SME run are documented in a separate report.[7]

2.0 Experimental Procedure

The simulant makeup, equipment set-up, experimental run parameters, offgas analysis, liquid sampling, and quality assurance are described in this section.

2.1 Simulant Makeup

Four different simulants were generated to meet the objectives of the study: SB9 sludge, PRFT, SEFT, and canister decontamination. These simulants are outlined below.

2.1.1 Sludge Simulant

Two simulant batches were prepared, one representing SB8 Tank 40H and another representing SB9 Tank 51H.[8] The simulant used for SB9 qualification testing was prepared by blending the SB8 Tank 40H and SB9 Tank 51H simulants. The blended simulant is referred to as SB9A. Inputs to the Measurement

Acceptability Region (MAR) assessment included the projected chemical compositions of SB9 Tank 51H and SB9 Tank 40H, the targeted blend ratio provided by SRR, and the Tank 51H/Tank 40H insoluble solids ratio targeted in the "September 1, 2015 Restart (Case 1)" for nominally a 1.0 M [Na] end point of washed Tank 51H[5]That case assumed consumption of SB8 at the rate of 150 canisters per year at 36% waste loading between September 1, 2015 and June 1, 2016. [9]

The simulant development was completed during a six step process:

1. Manganese Dioxide (MnO_2) Preparation: Manganese dioxide was prepared by feeding potassium permanganate at 40 °C to a manganese nitrate solution at 40°C

2. Metal nitrate solution precipitation in Continuously Stirred Tank Reactor (CSTR): The metal oxides were co-precipitated in the CSTR. A 50 wt % NaOH solution and combined MnO_2 and metal nitrate solutions were fed to the CSTR at a rate sufficient to produce a precipitate at a pH of ~9.5

3. Precipitation of Insoluble Carbonate Species: Sodium carbonate was added to precipitate the insoluble carbonate species.

4. Washing and Concentration Adjustment of Slurry: The slurry was batch washed in a 55 gallon drum with inhibited water (0.001 M NaOH and 0.001 M $NaNO_2$).

5. Add the final insoluble compounds to the washed slurry: The remaining insoluble species were added to the washed slurry.

6. Add the final soluble compounds to the concentrated washed slurry: The remaining soluble species that would have been removed during washing were added to the washed slurry.

Samples were obtained and analyzed during the preparation process as required to meet the Savannah River Remediation (SRR) System Planning projections seen in 7.1 Appendix A: Sludge Batch 9. The results of the SRR projection are included in the second column of Table 2-1 through Table 2-3.

SB9A simulant was used in testing. The column labelled "SB9A simulant initial analysis" was analyzed prior to nitric-formic flowsheet testing. This SB9A simulant initial analysis data was used in all acid calulationsThe column labelled "SB9A-NG, reanalysis" was analyzed during the nitric-glycolic flowsheet testing to confirm the results used in the acid calculations. Calcined elemental data is presented in Table 2-1. Anion and physical property data are presented in Table 2-2 and Table 2-3. .

Table 2-1. SB9A Blended Tank 40H Elemental Calcined Solids, wt %

Calcine Solids	SRR Projection Normalized Target	SB9A Simulant Initial Analysis	SB9A-NG,reanalysis
Al	9.78	9.83	10.03
B	0.016	<0.100	<0.100
Ba	0.066	0.094	0.151
Ca	1.40	1.53	1.58
Ce	0.275	0.162	Not Analyzed
Cr	0.057	0.132	0.091
Cu	0.054	0.098	<0.100
Fe	24.3	25.2	24.5
K	0.149	<0.100	0.179
La	0.040	<0.100	Not Analyzed
Li	0.011	<0.100	Not Analyzed
Mg	0.313	0.293	0.283
Mn	7.77	8.74	7.80
Na	20.5	15.0	17.1
Ni	1.76	1.78	2.39
Pb	0.026	<0.100	Not Analyzed
S	0.368	0.263	0.333
Si	1.94	2.41	1.32
Ti	0.011	<0.100	Not Analyzed
Zn	0.021	<0.100	<0.100
Zr	0.051	<0.100	0.218

Based on a comparison of SB9A simulant, initial analysis and the SRR Projection, normalized target, all species but Ba, Ce, Cr, Cu, Mn, Na, S and Si are within 10% of target. Ba, Ce, Cr, and Cu are minor components of the sludge. Sulfur is difficult to measure. Si remains inert during SRAT and SME processing. Mn is 12.5% over target, which will cause increased acid consumption. There is an obvious difference in the projected sodium concentrations and measured concentrations in the simulants. This difference results from the amount of insoluble sodium present in the actual sludge. Currently, there is no strategy for simulating insoluble sodium. Therefore, the supernatant sodium concentration was targeted. Insoluble sodium does not contribute to the chemical reactions occurring during CPC processing. It does, however, have an impact on glass formulation of the SME product. For this reason, it was decided that sodium hydroxide would be trimmed into the SME product prior to making glass in order to achieve a final sodium concentration comparable to the targeted concentration. Sodium hydroxide was selected to add sodium because it would not adversely affect glass chemistry. Sodium chloride and sodium nitrate impact glass chemistry and sodium carbonate significantly offgases during simulated melter work.

Table 2-2. SB9A Blended Tank 40H Anion Composition, mg/kg slurry

	SRR Projection Normalized Target	SB9A Simulant , Initial Analysis	SB9A-NG, reanalysis
NO_2^-	10,640	10,200	10,300
NO_3^-	6,318	5,725	5,830
SO_4^{-2}	1,619	1,235	1,210
$C_2O_4^{-2}$	2,062	3,980	3,330
TIC	1,292	1,619	NA

Table 2-3. SB9A Blended Tank 40H Physical Properties Simulant (Acid Calculation Inputs)

	SRR Projection Normalized Target	SB9A Simulant Initial Analysis
Total Solids, wt%	15.9	15.3
Insoluble Solids, wt%	10.8	10.6
Calcined Solids, wt%	12.4	11.7
Soluble Solids, wt%	5.15	4.70
Slurry Density, g/mL	1.13	1.12
Supernate Density, g/mL	1.05	1.04

Noble metals are added into the sludge immediately before each experiment at 125% of the SB9 projection. Note, ruthenium was added as 1.5 wt% Ruthenium(III) nitrosyl nitrate solution. Mercury is added at 105% of the projected mercury concentration as seen in Table 2-4.

Table 2-4. Trimmed Sludge Noble Metal and Mercury Targets (Acid Calculation Inputs)

Metal	Concentration
Ag	0.0139
Pd	0.0037
Rh	0.0156
Ru	0.0762
Hg	2.48

Each individual noble metal was weighed out dry, then slurried using DI water and a vortex mixture. The metal slurry is then poured into the vessel. The bottle is then flushed with DI water that is added to the vessel as well.

Using the SB9A simulant analytical data, the inputs in Table 2-5 were developed for use in the acid calculation.

Table 2-5. Target Sludge Simulant Parameters (Acid Calculation Inputs)

Parameter	SB9A Simulant	Parameter	SB9A Simulant
Target Sludge (untrimmed) added to 4-L vessel, g	3,330	Fresh Sludge Nitrite, mg/kg	10,200
Trimmed Sludge Target Ag metal content, wt %	0.0139	Fresh Sludge Nitrate, mg/kg	5,725
Trimmed Sludge Target wt% Hg dry basis	2.48	Fresh Sludge Sulfate, mg/kg	1,235
Trimmed Sludge Target Pd metal content, wt %	0.0037	Fresh Sludge Oxalate, mg/kg	3,514
Trimmed Sludge Target Rh metal content, wt %	0.0156	Fresh Sludge Manganese (% of Calcined Solids)	8.74
Trimmed Sludge Target Ru metal content, wt %	0.0762	Fresh Sludge Calcium (% of Calcined Solids)	1.53
Fresh Sludge Weight % Total Solids	15.25	Fresh Sludge Magnesium (% of Calcined Solids)	0.293
Fresh Sludge Weight % Calcined Solids	11.74	Fresh Sludge Slurry TIC, mg/kg slurry	1,619
Fresh Sludge Weight % Insoluble Solids	10.55	Fresh Sludge Base Equivalent molarity pH = 7	0.483
Fresh Sludge Density, g/mL	1.122	Fresh Sludge Supernate TIC, mg/L Supernate	1,671

2.1.2 PRFT Simulant

PRFT simulant was generated to simulate the PRFT addition to the SRAT. The PRFT simulant was made by slowly combining the compounds in Table 2-6, then mixing for 1+ hour. MST was not added to the simulant because currently integrated salt disposition processing is running the "No MST flowsheet." MST does not impact CPC chemistry, but it could change rheology and glass properties. The resulting composition is summarized in Table 2-7 and Table 2-8.

Table 2-6. PRFT Simulant

Compound	Molecular Formula	Target wt%
DI Water	H_2O	90.28%
Sodium Hydroxide	NaOH	4.82%
Aluminum Nitrate	$Al(NO_3)_3.9H_2O$	1.19%
Sodium Carbonate	Na_2CO_3	0.69%
Sodium Sulfate	Na_2SO_4	0.13%
Sodium Oxalate	$Na_2C_2O_4$	0.84%
Sodium Nitrate	$NaNO_3$	1.57%
Sodium Nitrite	$NaNO_2$	0.47%

Table 2-7. PRFT Simulant Anions and Cations

Al, mg/Kg	Ca, mg/Kg	Cu, mg/Kg	K, mg/Kg	Na, mg/Kg	S, mg/Kg	NO_2^-, mg/Kg	NO_3^-, mg/Kg	SO_4^{-2}, mg/Kg	$C_2O_4^{-2}$, mg/Kg	CO_3^{-2} mg/Kg
899	1.73	0.21	1.69	41,570	315	3,517	17,570	847	5,492	3,907

Table 2-8. PRFT Simulant Anions and Cations

Total Solids, wt%	Soluble Solids, wt%	Insoluble Solids, wt%	Calcined Solids, wt %	pH	Density, g/cc
7.57%	7.53%	<0.10%	4.93	13.7	1.05

2.1.3 Strip Effluent Simulant

The strip effluent simulant was prepared by combining two streams, a boric acid solution and 87 mg/kg of Next Generation Solvent (NGS) solvent. The aqueous stream was prepared by making a 0.015 M boric acid solution and adding sodium hydroxide to duplicate the pH 8 with strip effluent.

The blend solvent used in these studies was previously used for NGS flowsheet testing at SRNL[10] and SB9 Formic Flowsheet development[11] to simulate solvent entrainment in the strip effluent. The composition of the solvent is summarized in Table 2-9.

Table 2-9. BOBCalixC6-NGS Analysis

Analysis		Results, mg/L	50/50 Blend Target, mg/L	% of Nominal
Isopar-L	FT-HNMR	6.23E+05	6.23E+05	100.0%
	TGA	6.31E+05		101.2%
Modifier	HPLC	1.65E+05	1.69E+05	97.6%
	FT-HNMR	1.71E+05		101.0%
	TGA	1.67E+05		98.5%
TiDG	Titration	1.29E+03	1.44E+03	83.8%
	FT-HNMR	7.49E+02		52.0%
TOA	Titration	4.80E+02	5.30E+02	90.6%
MaxCalix	FT-HNMR	4.84E+04	4.44E+04	109.0%
	TGA	4.15E+04		93.4%
BOBCalixC6	HPLC	4.46E+03	4.03E+03	109.0%
Solvent Density		0.8333	0.8384	N/A
Solvent pH		12.87	~ 6	N/A
Cs	ICPMS	11.83	N/A	N/A
Cu	ICPMS	2.35	N/A	N/A
Sr	ICPMS	0.32	N/A	N/A
Zr	ICPMS	0.20	N/A	N/A
Mo	ICPMS	0.34	N/A	N/A
Sn	ICPMS	0.15	N/A	N/A
Ba	ICPMS	0.47	N/A	N/A
Pb	ICPMS	0.28	N/A	N/A

2.1.4 Canister Decontamination Simulant

Canister decontamination simulant was added to the SME. The laboratory simulant contains DI water only and does not contain frit. The simulant experiment added the same amount of scaled frit; however, only during the frit addition portion of the SME.

2.2 Equipment Set-up

4-L runs are performed at the same time using two separate hoods located in 999-W Lab 132. LabVIEW was used to automate the CPC experiments and record real time data. Collected data includes:

- SRAT slurry temperature
- Bath temperatures for the cooling water to the SRAT condenser and Formic Acid Vent Condenser (FAVC)
- Slurry pH
- SRAT mixer speed and torque
- Air and helium purge flows (He is used as an internal standard and is set to 0.5% of the nominal SRAT air purge flow)
- Raw GC data
- Heating rod temperature and power
- Heat transfer coefficient of the heating rods
- Hood temperature
- Scrubber temperature
- Condenser flowrates
- MWWT temperature

Two heating rods were used for each CPC run. During heating to 93 °C a proportional-integral-derivative (PID) control algorithm is used to reach the temperature set point while limiting the temperature differential between the hottest rod and the sludge to 30 °C (in runs NG52 and NG54, the 30°C was raised to allow temperature control). Above 93 °C, a PID algorithm is used to target a wattage set point. The wattage is adjusted by personnel to target the desired boil-up rate. Boil-up rate was determined using the graduated markings on the MWWT and a stopwatch. The pH of the sludge was monitored and the automation temperature corrected the pH to 25 °C. The 4-L laboratory scale CPC setup is shown in Figure 2-1.

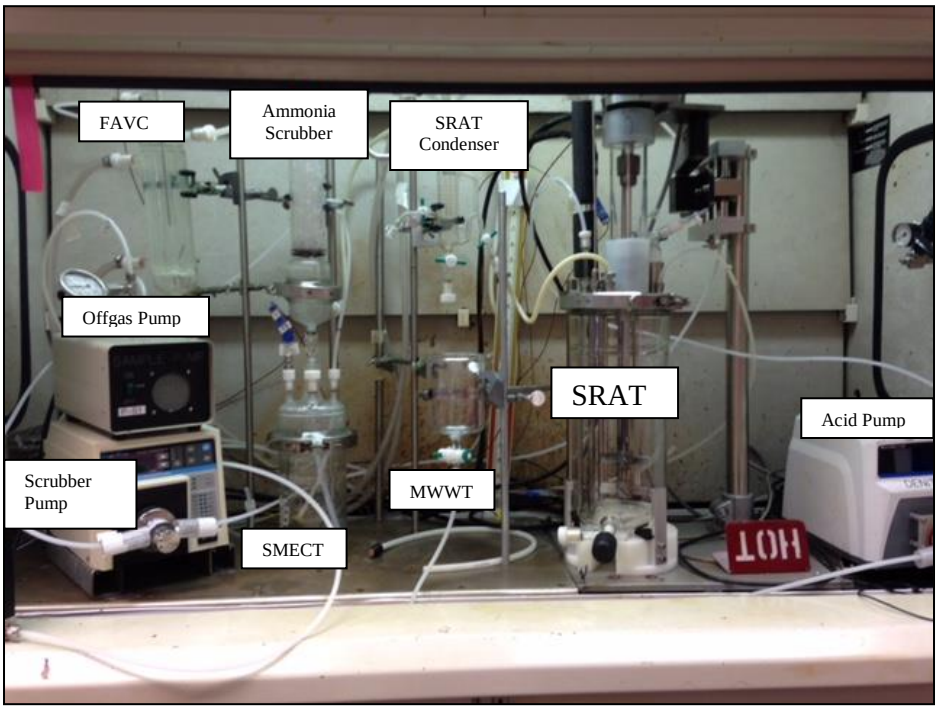

Figure 2-1. CPC 4-L Setup

Offgas passes through the SRAT/SME vessel then passes through a condenser operated at 25 °C that drops SRAT/SME condensate vertically into the MWWT. The MWWT is filled with ~30 mL of DI water prior to starting the run. Offgas flows from the condenser through the ammonia scrubber. The reservoir below the ammonia scrubber was charged with a solution of 749 g of de-ionized water and 0.1 mL of 50 wt% nitric acid (pH ~2). The dilute acid reservoir solution was recirculated by a MasterFlex driven Micropump gear pump at 120 mL per minute to a spray nozzle at the top of the packed section. The lab-scale ammonia scrubber absorbs ammonia vapor from the SRAT/SME condenser offgas for quantification of ammonia generation. The offgas next passes through the FAVC, which is operated at 4°C. The offgas then passes through the Nafion® dryer after which the gas is sampled for analysis before exhausting to the hood. Offgas is analyzed by gas chromatography (GC) and mass spectrometry (MS) for all runs and Fourier Transform Infrared (FTIR) spectroscopy for half of the 4-L laboratory scale setups.

2.3 Experimental Run Parameters

The chemistry and DWPF processing parameters described below were used to develop the R&D directions based on mass balances that are scaled to the DWPF process. The total acid was calculated based on the KMA requirement equation[12] (all terms have units of moles/L slurry).

$$\frac{\boldsymbol{moles\ acid}}{\boldsymbol{L\ slurry}} = \boldsymbol{base\ equiv.} + \boldsymbol{Hg} + \boldsymbol{soluble\ TIC} + \boldsymbol{NITRITE} + \mathbf{1.5}(\boldsymbol{Ca} + \boldsymbol{Mg} + \boldsymbol{Mn}) \quad \text{Equation 1}$$

An acid equation (Glycolic Minimum Acid or GMA) for the nitric-glycolic acid flowsheet has been proposed[12,13]:

$$\frac{\boldsymbol{moles\ acid}}{\boldsymbol{L\ slurry}} = \boldsymbol{base\ equiv.} + \frac{\boldsymbol{Hg}}{\mathbf{3}} + \boldsymbol{soluble\ TIC} + \mathbf{0.75} \times \boldsymbol{NITRITE} + \mathbf{1.5}(\boldsymbol{Ca} + \boldsymbol{Mg}) + \mathbf{0.8} \times \boldsymbol{Mn}$$

Equation 2

DWPF has used the Hsu equation[14] for their acid calculations:

$$\frac{moles\ acid}{L\ slurry} = base\ equivalents + Hg + 2 \times slurry\ TIC + 0.75 \times NITRITE + 1.2 \times Mn$$

Equation 3

It is important to note the calculated stoichiometry is based on the sum of the sludge simulant acid demand and the PRFT simulant acid demand in the case of the coupled flowsheet.

The mass balance then adjusts the ratio of glycolic acid to total acid to meet a target REDOX given the input parameters. The input parameters are the assumptions for destruction and/or conversion of the acids. The input parameters are adjusted as needed between experimental runs to meet the REDOX target and ensure processability.

Acid stoichiometry of experiments ranged from 76.9% to 123% of the KMA equation, which is equivalent to a range of 80.3% to 129% of the Hsu minimum acid factor. The percent reducing acid was also varied to cover a wide REDOX range. For the SRAT-only experiments, 100% destruction of nitrite, and SRAT product total solids of 25 wt% were targeted. For the SRAT/SME experiments, 100% destruction of nitrite, SRAT product total solids of 25 wt% were targeted and SME product total solids of 48 wt%. The values for the conversion of nitrite to nitrate, destruction of glycolic acid, and destruction of nitrate were calculated using the CPC predicted reaction chemistry.[13] The conversion of nitrite to nitrate, destruction of glycolic acid, and destruction of nitrate are listed in Table 2-10.

Table 2-10. Experimental Matrix

	Acid in Excess Stoichiometric Ratio			Conversion of Nitrite to Nitrate in SRAT	Destruction of Glycolate charged in SRAT		Destruction of Nitrate
Run ID #	Koopman	Hsu	Glycolic		SRAT Cycle	SME Cycle	SME Cycle
NG51	83.7%	87.5%	99.5%	41.39%	24.38%	N/A	N/A
NG52	116.3%	121.5%	138.2%	31.34%	13.27%	N/A	N/A
NG53	83.6%	87.4%	99.4%	38.19%	24.41%	N/A	N/A
NG54	116.6%	121.8%	138.6%	37.10%	13.17%	N/A	N/A
NG55	100.0%	104.5%	118.8%	35.51%	18.83%	N/A	N/A
NG55A	100.0%	104.5%	118.9%	35.49%	18.81%	N/A	N/A
NG56	100.2%	104.7%	119.1%	39.90%	18.75%	N/A	N/A
NG57	99.9%	104.4%	118.7%	33.75%	18.85%	N/A	N/A
NG58	76.9%	80.3%	91.4%	41.26%	26.70%	N/A	N/A
NG59	123.2%	128.8%	146.5%	32.98%	10.90%	N/A	N/A
NG60	100.2%	104.7%	119.1%	38.32%	18.76%	0.00%	0.00%
NG61	100.2%	104.7%	119.1%	38.34%	18.75%	0.00%	0.00%
NG62*	97.4%	103.3%	113.7%	24.93%	19.70%	0.00%	0.00%

* Coupled run (PRFT and SEFT included)

2.3.1 Scaled Parameters

Purge rates, acid addition flow rates, and boil-up rates were scaled by mass to the DWPF rates used for a DWPF SRAT receipt volume of 6,000 gallons. The DWPF SME purge rates and antifoam additions are scaled to the predicted SME starting volume. DWPF inputs used for scaling and limits are summarized in Table 2-11 for runs NG51-62. In addition, inputs used for scaling and limits for the additional runs to develop the antifoam strategy (NG63-67) are also summarized in Table 2-11 The predicted SME starting volume accounts for the starting mass of the trimmed sludge after acid addition, nitrite destruction, conversion of nitrite to nitrate, formate and oxalate generation, nitrate destruction, dewatering, and sampling. Thus, the predicted SME volume is highly dependent on the input parameters. It is important to note that after performing the experiment and receiving all results, a mass balance is performed to better estimate the SME starting volume, since the original predictions only account for the theoretical gas generation losses, which are often lower than actual.

Table 2-11. DWPF Processing Parameters (DWPF Scale)

Run	NG51-59	NG60	NG61	NG62	NG63-64	NG65	NG66	NG67	Units
SRAT Starting Volume	6,000	6,000	6,000	6,000	6,000	6,000	6,000	6,000	gallons
PRFT Addition Volume	N/A	N/A	N/A	1,000	N/A	N/A	N/A	1,000	gallons
SEFT Addition Volume	N/A	N/A	N/A	12,000	N/A	N/A	N/A	N/A	gallons
Volume per Decon. Canister	N/A	N/A	6× 1,000	N/A	N/A	N/A	N/A	6× 1,000	gallons
Antifoam Addition Volume	0.5-1.5	0.5-1.5	0.5-1.5	0.5-1.5	1.5	0.25	0.25	0.25	gallons
SRAT Air Purge	93.7	93.7	93.7	93.7	186	186	93.7	186	scfm
SME Air Purge	N/A	72	72	72	N/A	N/A	N/A	72	scfm
Nitric Acid Addition Rate	179	179	179	179	179	179	179	179	moles/min
Glycolic Acid Addition Rate	179	179	179	179	179	179	179	179	moles/min
SRAT Boil-up Rate	5,000	5,000	2,500	5,000	5,000	5,000	5,000	5,000	lbs/hr
SME Boil-up Rate	N/A	5,000	2,500	5,000	N/A	N/A	N/A	5,000	lbs/hr
SRAT Product Hg	0.45	0.45	0.45	0.45	N/A	N/A	N/A	0.45	wt % TS
SRAT Steam Stripping Factor	750	750	750	750	N/A	N/A	N/A	750	g steam/g Hg
SRAT Hydrogen Limit#	0.65	0.65	0.65	0.65	N/A	N/A	N/A	0.65	lbs/hr
SME Hydrogen Limit#	N/A	0.223	0.223	0.223	N/A	N/A	N/A	0.223	lbs/hr

DWPF plans to reduce hydrogen limit[15]

Antifoam additions were scaled from the DWPF addition size for a 6,000 gallon SRAT receipt to the starting mass of the material in the laboratory scaled setup. Undiluted Antifoam 747 (Lot # 110684-0413) manufactured by Siovation was used for all additions. The DWPF 100 gallon water flush that follows the antifoam addition was also scaled to the laboratory size. SME antifoam additions and the flush water are scaled to the predicted SME starting volume. Each antifoam addition was weighed out in the same syringe; however, the empty syringe was not reweighed to verify the actual mass that was added.

2.3.2 Procedures and Methods

CPC experiments are performed by R&D directions to supplement procedure L29 ITS-0094, Laboratory Scale Chemical Process Cell Simulations. [16] Sludge is added to the kettle. The mixer is started then noble metals and mercury are trimmed uniquely into the sludge at the beginning of each SRAT run. The trimmed SRAT receipt volume was 3.1 L for the 4 L laboratory scale. The trimmed sludge is allowed to mix for a

minimum of thirty minutes prior to sampling and beginning the SRAT cycle. Experiments used concentrated acids during the SRAT and frit 803 in the SME.

2.3.3 Antifoam Addition Strategy Used in This Testing

The antifoam strategy used for the SB9 nitric-glycolic flowsheet runs was based on the initial strategy requested for the nitric-formic flowsheet. In an effort to minimize the antifoam used, the technicians were directed to use antifoam only if needed. In most of the later runs, no antifoam was added during SRAT dewater or reflux. In two of the runs, no antifoam was added during acid addition.

Initial testing during SB9 nitric-glycolic acid flowsheet development identified that the peak concentration of Hexamethyldisiloxane (HMDSO) was approximately three times higher than for similar testing of the nitric-formic acid flowsheet. In each of these tests, the HMDSO peak occurred at the initiation of boiling just after acid addition was complete. The antifoam strategy for each test is summarized in Table 2-12.

Table 2-12. Antifoam Addition in SRAT and SME Testing, DWPF Volume and Frequency

Run	Sludge Simulant	Pre PRFT	Late Nitric	Post Acid	SRAT boiling	Decon Dewater	Frit Dewater
NG51	SB9A	NA	1.5 gal	1 gal	1.5 gal	NA	NA
NG52	SB9A	NA	1.5 gal	1 gal	2×1 gal	NA	NA
NG53	SB9A	NA	1.5 gal	1.5 gal	1 gal	NA	NA
NG54	SB9A	NA	1.5 gal	1.5 gal	1 gal	NA	NA
NG55	SB9A	NA	1.5 gal	1 gal	None	NA	NA
NG55A	SB9A	NA	None	1.5 gal	None	NA	NA
NG56	SB9A	NA	1.5 gal	1 gal	None	NA	NA
NG57	SB9A	NA	1.5 gal	1 gal	None	NA	NA
NG58	SB9A	NA	None	1.5 gal	None	NA	NA
NG59	SB9A	NA	1.5 gal	1.5 gal	1 gal	NA	NA
NG60	SB9A	NA	1.5 gal	1 gal	None	NA	2×0.5 gal
NG61	SB9A	NA	1.5 gal	1.5 gal	None	0.5 gal	2×0.5 gal
NG62	SB9A	1 gal	1.5 gal	1.5 gal	None	NA	2×0.5 gal
NG63	SB8F	NA	1.5 gal	1.5 gal	NA	NA	NA
NG64	SB8F	NA	1.5 gal	1.5 gal	NA	NA	NA
NG65	SB8F	NA	0.25 gal	0.25 gal	NA	NA	NA
NG66	SB8F	NA	0.25 gal	0.25 gal	NA	NA	NA
NG67	SB8F	0.25 gal	0.25 gal	0.25 gal	2×0.25 gal	6×0.25 gal	2×0.25 gal

SRR requested additional SB9 flowsheet testing to determine the peak HMDSO concentration in a series of tests designed to better understand the previous testing and to find processing conditions that minimize the HMDSO peak. The SB9 nitric-glycolic acid flowsheet task and quality assurance plan[17] was modified to add the additional testing. A number of meetings were held between SRR and SRNL to ensure the testing was focused on providing SRR with the data needed for developing an SB9 flammability strategy that could handle the nitric-formic acid flowsheet, the nitric-glycolic acid flowsheet, and transition between both flowsheets. A run plan[18] documented the details for the planned testing and the decision matrix.

Four abbreviated SRAT (NG63-66) and one SRAT/ SME (NG67) simulations were completed to develop processing conditions to minimize the HMDSO peak. An SB8 simulant[9] was used along with the SB9 levels of noble metals and mercury (same as was used in the SB9 flowsheet testing). In these experiments, antifoam was added about 45 minutes into nitric acid addition and just prior to boiling. Since the primary focus of this study was to develop a strategy to minimize peak HMDSO offgassing, which occur after initiation of post-acid boil, abbreviated SRAT cycles were used. This run strategy maximized efficiency for data collection during the peak HMDSO region.

Once an antifoam strategy successfully reduced the HMDSO peak at boiling to an acceptable level, a complete SRAT and SME simulation was completed to successfully demonstrate that the antifoam strategy was effective throughout processing as demonstrated in Run NG67. The antifoam strategy used in NG67 is summarized in Table 3-40.

2.4 Offgas Analysis (Additional Task g in TTR[1])

Offgas was monitored by GC, MS, and/or FTIR. The specific monitors used in each offgas analysis are detailed in Table 2-13.

Table 2-13. Offgas Monitoring Used

Run	GC	MS	FTIR
NG51	X	X	
NG52	X	X	X
NG53	X	X	X
NG54	X	X*	X
NG55	X	X	
NG55A	X	X	
NG56	X	X	X
NG57	X	X	X
NG58	X	X	
NG59	X	X	X
NG60	X	X	X
NG61	X	X	X
NG62	X	X	X*

* Not available for part of run

The chilled offgas leaving the FAVC was passed through a Nafion® dryer in counter-current flow with a dried air stream to reduce the moisture content of the gases to the analyzers. The GC internal pump pulled a sample at approximately four minute intervals from this offgas line. A separate sample pump was used to transport samples from the offgas line to the MS and FTIR. Mass flow controllers were used to regulate the amount of gases sent to the MS (~50 mL/min) and FTIR (~150 mL/min). If simultaneous runs were performed, the FTIR sampled only one of the runs, and the MS alternately sampled each stream. The total sample flow pumped from the offgas system had to be maintained below the total offgas flow from the SRAT/SME equipment so that ambient air would not be drawn into the system and give erroneous results.

Raw chromatographic data were acquired by the GC using separate computers interfaced to the data acquisition computer. Each experiment had a dedicated Agilent (or Inficon) 3000A dual column micro GC. Column-A can collect data related to He, H_2, O_2, N_2, NO, and CO, while column-B can collect data related

to CO_2, N_2O, and water. Data for NO, CO, and water are only qualitative. The GCs were calibrated with a standard calibration gas containing He, H_2, O_2, N_2, CO_2 and N_2O. The calibration was verified prior to starting the SRAT cycle and after completing the SME cycle. Room air was used to give a two point calibration for N_2. Raw chromatographic data were acquired by the GC from the FAVC offgas stream samples using a separate computer interfaced to the data acquisition computer. Sampling frequency was approximately one chromatogram every four minutes. The GC data were additionally post-processed to adjust for inaccuracies in the measured N_2 and O_2 concentrations. The concentrations of N_2 and O_2 measured in air at the beginning and end of each run were used to perform linear interpolation corrections of the N_2 and O_2 data.

An Extrel CMS MAX300LG MS was used to measure H_2, He, N_2, O_2, NO, NO_2, CO_2, and Ar. The MS is calibrated by a series of gas mixtures that are used to measure background intensity, ion fragmentation, and sensitivity. All gases used were National Institute of Standards and Technology (NIST) traceable. The certificates of analysis are documented in the SRNL Electronic Lab Notebook (ELN). In addition, qualitative intensity measurements of specific ion masses that might be expected from antifoam degradation products were also measured. HMDSO was monitored at masses 148, 147, 131, and 73 and trimethylsilanol (TMS) was monitored at mass 75. HMDSO and TMS are potentially flammable volatile products from decomposed antifoam. Measurements of H_2 by MS were somewhat inaccurate due to the extremely low values that were subject to error due to drift in the MS background signal. For some runs, the He calibration drifted and was corrected by a linear interpolation between the calibration value and the post-calibration check value.

For two simultaneous runs, the MS alternately measured the two systems. Each system was measured for about 110 sec with a 28 sec delay in between to flush out the other system's sample. The sampling rate was about one sample per 8-10 seconds. The presence of N_2O in the process gas samples introduces interferences in the measurements of CO_2, NO, and N_2 because it has fragment ions at the measurement masses of each of these gases. The MS cannot be calibrated for N_2O because the relative amount of N_2O to the other gases is too small to give a reliable calibration. For example, the presence of 1.2 volume % N_2O would result in the measurement of N_2 being high by about 0.12 volume %, NO being high by about 0.24 volume %, and CO_2 being high by about 0.86 volume %. An N_2O calibration gas was used to determine these ratios and the N_2, NO, and CO_2 data were adjusted post-run using the N_2O measured by the GC or FTIR. When the N_2O from the GC or FTIR was added to the adjusted MS data, the sum was generally within 99.9 to 100.1%.

For simultaneous tests, the MKS MG2030 FTIR spectrometer was connected to the two SRAT/SME offgas systems like the MS, but was manually valved into one or the other for the duration of the run. The FTIR measures CO, CO_2, NO, NO_2, N_2O, H_2O, and HMDSO concentrations. Although the GC detects water, the FTIR gives a quantitative concentration for moisture in the chilled offgas leaving the Nafion® drier. The FTIR obtained data roughly every 15 seconds.

A summary listing offgas species and analyzer is seen in Table 2-14.

Table 2-14. Analyzer Used in Quantifying Offgas Species

Offgas Species	GC	MS	FTIR
H_2	X	X	
CO_2	X	X	X
NO		X	X
NO_2		X	X
N_2	X	X	
N_2O	X		X
O_2	X	X	
He	X	X	
Ar		X	
NH_3			X
HMDSO			X

2.5 Liquid Sampling

Samples were analyzed by Semivolatile Organic Analysis (SVOA), Volatile Organic Analysis (VOA), Inductively Coupled Plasma – Atomic Emission Spectroscopy (ICP-AES), Ion Chromatography (IC) Anions, IC Cations, Total Inorganic Carbon (TIC), Total Organic Carbon (TOC), ICP-AES for mercury, Ultraviolet-Visible (UV-Vis) spectrophotometry, weight, and rheology. Condensate samples were taken from the MWWT, FAVC, ammonia scrubber, and the SRAT/SME dewater material. Slurry samples were taken before processing, during processing and after processing. Two mercury samples were analyzed by Cold Vapor Atomic Absorption (CVAA) Spectroscopy for mercury and ICP-AES for impurities in the mercury.

Samples taken during the SRAT cycle were used to monitor mercury and the progress of major reactions. Samples to be analyzed for mercury were pulled directly into digestion vials to eliminate potential segregation of mercury during sub-sampling steps. Major anions in the slurry were evaluated immediately after acid addition. Selected cations were evaluated in the SRAT supernate and the SRAT condensates. The SRAT and SME product slurries were sampled once the vessel contents had cooled slightly, but still while mixing. SRAT and SME product samples were analyzed for cation and anion composition in addition to solids analyses and rheological characterization. The MWWT and FAVC were drained after both the SRAT and SME cycles. The condensates were weighed and elemental mercury was separated from the aqueous phase in the post- SRAT MWWT sample, and the mass of the mercury-rich material was determined.

Although there was some variation in the sample plan between runs, the basic sample plan can be seen in Table 2-15. The sample plan is consistent with previous simulant flowsheet work and what has been specified in the TTQAP.[10] Based on findings from additional study of mercury within the liquid waste flowsheet, it is recommended that future simulant work include CVAA for mercury analysis to compare method sensitivities during simulant tests.

Table 2-15. Sample Plan

Vessel	Sample Description	Analysis
SRAT	SRAT post noble metals Addition (Mixing >30 min)	Hg (digest then ICP-AES), ICP-AES
MWWT	MWWT post formic addition	SVOA, VOA
SRAT	SRAT post acid mercury sample	Hg (digest then ICP-AES)
SRAT	SRAT post acid slurry (NaOH quench)	IC
SRAT	SRAT post acid: supernate	ICP-AES
SCRUBBER	Post acid ammonia scrubber solution	IC Cations- NH_4
Dewater (SMECT)	SRAT dewater condensate	SVOA, VOA, TOC, IC, ICP-AES
SRAT	SRAT Post dewater Hg sample (from SRAT)	Hg (digest then ICP-AES)
SRAT	SRAT slurry 5 hrs into reflux (NaOH quench)	IC
SRAT	SRAT 5 hrs into reflux: supernate	ICP-AES
SRAT	SRAT 8 hrs into reflux Hg sample	Hg (digest then ICP-AES)
SRAT	SRAT slurry 10 hrs into reflux (NaOH quench)	IC
SRAT	SRAT 30 minutes before end of reflux (NaOH quench)	IC
SRAT	SRAT product	ICP-AES, IC, pH, density, TS, IS, SVOA, VOA, TIC/TOC, IC Cations- NH_4, rheology, Hg (digest then ICP-AES),
MWWT	MWWT dewater	TS, ICP-AES, SVOA, VOA
MWWT	MWWT (mercury bead phase)	weight
FAVC	SRAT FAVC	SVOA, VOA
SCRUBBER	Ammonia scrubber at end of SRAT	SVOA, VOA, IC Cations- NH_4
Dewater (SMECT)	SME 1st Frit dewater	SVOA, VOA
Dewater (SMECT)	SME 2nd Frit dewater	SVOA, VOA
SME	SME product	TS, IS, SS, pH, density, ICP-AES, TIC/TOC, IC Cations- NH_4, SVOA, VOA, rheology, Hg (digest then ICP-AES),, REDOX
SCRUBBER	Ammonia scrubber acid at end of SME	SVOA, VOA, IC Cations- NH_4

All analytical instruments used except pH probes were Measurement Systems and Equipment (MS&E). Balances and pipettes used are a part of the Measuring and Test Equipment (M&TE) program.

Total solids, soluble solids, and calcined solids were analyzed in the slurry. Total solids content was determined by weighing a 5 to 10 g aliquot of the slurry sample after it was dried in a platinum crucible at 110 °C in an oven for about 12 hours. The dried total solids are then calcined in an 1100 °C furnace for 1 hour to determine amount of calcined solids. Dissolved solids content was determined by weighing a dried 5 to 10 g of 0.45 μm filtered, centrifuged slurry sample. The filtered sample was dried in a platinum crucible at 110 °C in an oven for about 12 hours. Insoluble solids are calculated by taking the difference between total solids and soluble solids.

An Agilent 730 ES ICP-AES was used to analyze for metals in the supernate, slurry, and dewater using L29, ITS-0079. The ICP-AES is calibrated before each run and NIST certified standards are analyzed with each set of samples to verify the calibration. Dewater samples were diluted as needed prior to performing ICP-AES. Mercury was determined by ICP-AES after digesting the sludge by aqua regia and diluting. Slurry samples are eluted through a 0.45 μm filter and then diluted as needed before being analyzed to determine Ag, Al, B, Ba, Ca, Cr, Cu, Fe, K, Li, Mg, Mn, Na, Ni, P, Pd, Rh, Ru, S, Si, Sn, Ti, Zn, and Zr in the supernate. If solids were still visible, aqua regia was added to the filtrate prior to analysis. To determine metals in the slurry, the calcined solids were ground with a mill grinder, and then sieved to collect a powder that is less than 149 μm particle size. The powder was digested by peroxide fusion (L29 IST-0040) to

determine B and Li and also by lithium metaborate (L29 ITS-0071) and lithium tetraborate (L29 ITS-0070) to determine all other metals.

A Dionex DX-500 and ICP-5000 IC were used to measure anions in the slurry and dewater via L29 ITS-0027. The IC is calibrated before each set of samples being run and NIST certified standards are run with each set to verify the calibration. Dewater was diluted as needed prior to IC. Two grams of 50 wt% NaOH is added to a 10 g aliquot of slurry if the sample was not immediately caustically quenched after being pulled. At points in the process when a significant amount of chemistry is occurring, Two mL of 50 wt% NaOH is added to the sample to prevent the chemical reactions from continuing further. The aliquot is then diluted 100x, 500x, and 5000x and filtered with a 0.45µm filter prior to being analyzed for F^-, Cl^-, NO_2^-, NO_3^-, SO_4^{-2}, $C_2H_3O_3^-$, $C_2O_4^{-2}$, and HCO_2^-.

For the SRAT cycle runs, frit 803 was added to the SRAT product to target a waste loading of 38 wt %. The SME product or SRAT product with frit 803 was converted to glass per L29 ITS-0052 after adding 50 g of 50 wt% NaOH per kilogram of product to account for the difference in insoluble sodium between the simulant and the projections. The SME product (or the SRAT product with added frit) was dried at 40 to 50 °C range until resembling a thick paste without freestanding liquid, and then placed in a sealed crucible. The crucibles were added to a furnace at 1150 °C for at least 1 hour to vitrify the material. The glass was then submitted for iron analysis by UV-Vis to determine REDOX using L29 ITS-0042. UV-Vis is used to determine the Fe^{+2} content and total iron content. The Fe^{+2} was subtracted from the total iron to determine the Fe^{+3} in the glass. A blank is run to validate the calibration.

A Dionex ICS-3000 Reagent-Free IC was used to analyze for ammonia via L16.1 ADS-2310. The sample was diluted with DI water to within the calibration curve range of 1-50 mg/L prior to being run through the IC. Calibration is performed prior to performing analysis and a quality control sample is run with each sample set.

TIC and TOC were analyzed separately. Sludge samples were analyzed using wet chemical oxidation (sodium persulfate addition) on an OI Analytical 1030W Total Organic Carbon Analyzer using procedure L16.1 ADS-1209 r2Approximately 0.1 g of sample was weighed and mixed with 40 mL of water. The samples were run in triplicate with one sample per set spiked with standards. Inorganic carbon was determined by acidification with 20% phosphoric acid followed by infrared detection.

The elemental Hg samples were dissolved at room temp with HNO_3 + HCl. The digested samples were diluted with water and analyzed with the ICP-AES for impurities and CVAA for mercury.

2.6 Quality Assurance

Requirements for performing reviews of technical reports and the extent of review are established in manual E7 2.60. SRNL documents the extent and type of review using the SRNL Technical Report Design Checklist contained in WSRC-IM-2002-00011, Rev. 2.

A functional classification of Safety Class is selected in the TTR[1]Thus, the technical review was performed as a design verification by document review. The following items were identified in the TTR[1] as being used in DWPF Technical Safety Requirement Safety Administrative Controls and were thus given the greatest scrutiny during the technical review:

- Dried weight percent solids (soluble, insoluble, and total) measurements and Density
- Hydrogen Generation/Nitrous Oxide Concentration: Hydrogen generation rate for SRAT and SME on 6000 gallon basis. Volume percent of nitrous oxide produced during the SRAT cycle.
- Ammonium concentration for the condensate generated from the SRAT and SME
- Antifoam degradation product data

3.0 Results and Discussion

The results and discussion from the ten SRAT only cycles and the three SRAT/SME cycles are included in this section

3.1 Testing to Define Operating Window

SRAT testing was planned to determine the operating window for CPC processing. Ten SRAT-only runs (runs NG51-NG59) were completed, to address wide ranges of acid stoichiometry (KMA 76.8%-123%, Hsu 80.5%-130.5%, and GMA 91.5% to 146 %) and REDOX by varying the molar percent of glycolic acid or percent reducing acid (PRA) from 52-64%. Curves of constant REDOX are drawn in red based on the interim REDOX equation for the nitric-glycolic acid flowsheet.[1] The resulting matrix for the ten runs is summarized in Figure 3-1. Note that one run (center point runs NG55 and NG55A) was repeated. Also, the three SRAT/SME cycles are included for completeness (Runs NG60-NG62).

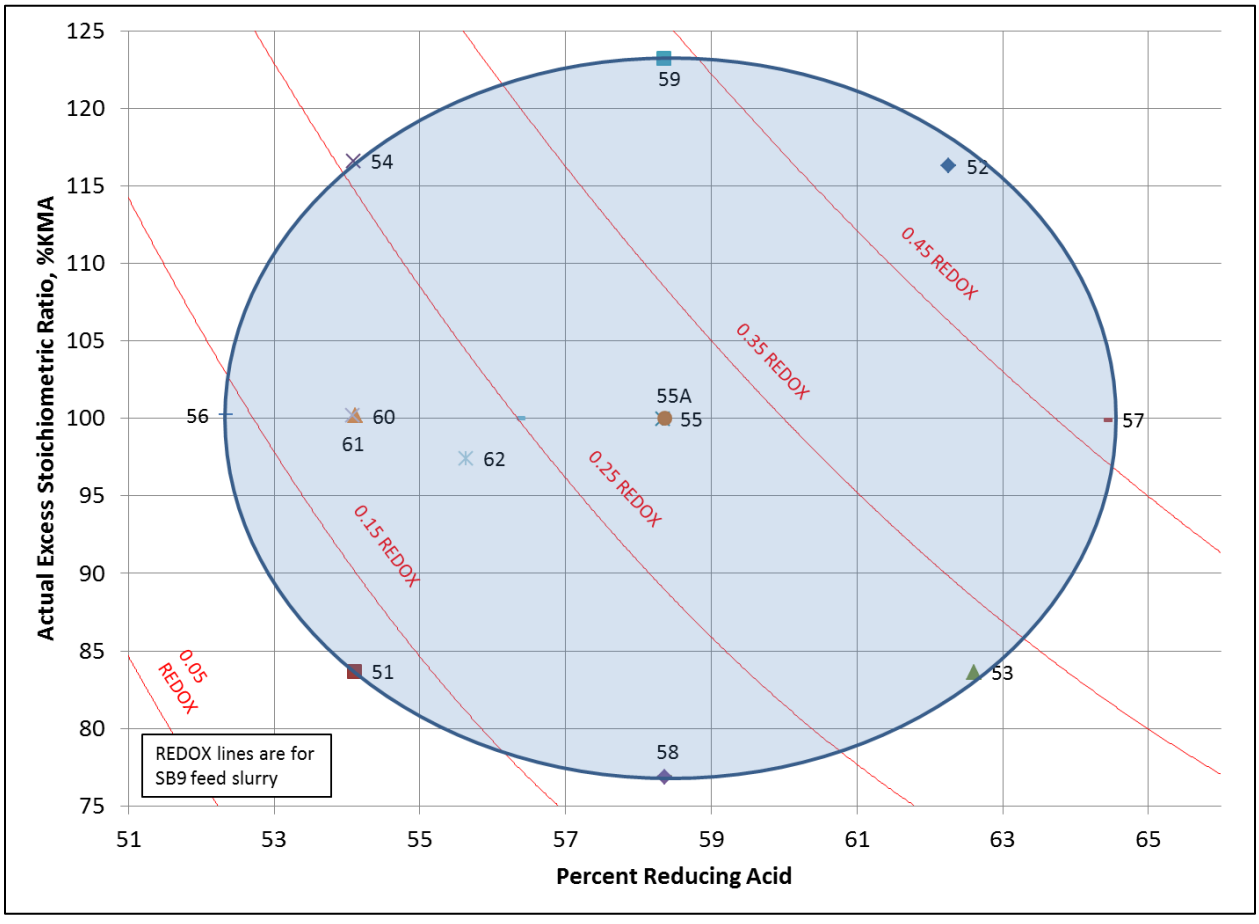

Figure 3-1. SRAT-only Matrix Showing Acid Stoichiometry and Percent Reducing Acid

Note that this figure will be repeated throughout the report to visually show the change of various parameters with acid stoichiometry and PRA.

A summary of some of the results from all runs is included in Table 3-1 and Table 3-2.

Table 3-1. Summary of Actual NG51 through NG59 Results

	NG51 No FTIR	NG52	NG53	NG54	NG55 No FTIR	NG55A No FTIR	NG56	NG57	NG58 No FTIR	NG59
Percent KMA Stoichiometry	83.7	116	83.6	117	100	100	100	99.9	76.9	123
Untrimmed Sludge, g	3300	3300	3299	3300	3300	3300	3300	3299	3300	3300
Ratio of Glycolic to Total Acid, %	54.1	62.3	62.6	54.1	58.3	58.4	52.3	64.4	58.4	58.4
Nitric Acid Added, moles	1.471	1.680	1.197	2.049	1.594	1.594	1.828	1.361	1.225	1.964
Glycolic Acid Added, moles	1.733	2.771	2.004	2.413	2.233	2.235	2.008	2.463	1.717	2.752
Total Acid Added, moles	3.204	4.451	3.201	4.462	3.827	3.829	3.836	3.824	2.943	4.716
REDOX ($Fe^{+2}/\Sigma Fe$)	0.06	0.62	0.57	0.22	0.32	0.34	<0.03	0.53	0.04	N/A
Total Solids wt%	30.8%	26.4%	29.9%	27.7%	34.2%	24.9%	30.9%	31.0	29.8	27.4
Max CO_2 lb/hr, FTIR or MS	705.8	684.4	678.4	701.0	636.3	671.1	663.2	631.2	662.0	640.1
Max N_2O lb/hr, FTIR or GC	1.62	6.66	1.78	2.72	2.38	2.45	1.50	2.55	2.76	3.07
Max H_2 lb/hr, GC	<0.0037	0.0098*	0.0010	0.0155*	0.0009	0.0008	0.0008	0.0010	<0.0037	<0.0037
Max NO lb/hr, FTIR or MS	37.9	1.2	19.2	1.4	69.7	69.2	40.3	74.9	71.6	1.4
Max NO_2 lb/hr, FTIR or MS	15.3	4.8	7.5	4.6	12.2	12.9	9.1	12.9	11.7	6.4

* Hydrogen data generated while heating rod temperatures exceeded 160 ˚C.

Table 3-2. Summary of Actual NG60 through NG62 Results

	NG60	NG61	NG62	NG60	NG61	NG62
	SRAT			SME		
Percent KMA Stoichiometry	100	100	97.4			
Untrimmed Sludge, g	3299	3299	3300			
Percent Reducing Acid	54.1	54.1	55.6			
Nitric Acid Added, moles	1.759	1.744	1.848			
Glycolic Acid Added, moles	2.075	2.055	2.318			
Total Acid Added, moles	3.834	3.799	4.166			
REDOX ($Fe^{+2}/\Sigma Fe$)	N/A	N/A	N/A	0.14	<0.03	0.09
Total Solids wt%	25.7	26.9	25.9	46.0	37.1	37.2
Sludge Oxide Contribution (Waste Loading) based on Fe_2O_3	N/A	N/A	N/A	43.0	41.3	43.6
Max CO_2 lb/hr, GC	733.2	694.7	671.7	2.5	3.4	4.1
Max N_2O lb/hr, FTIR or GC	1.52	1.43	5.55	0.02	0.01	<0.51
Max H_2 lb/hr, GC	<0.0037	<0.0037	0.0014	<0.0023	<0.0028	0.0014
Max NO lb/hr, FTIR or MS	37.3	25.5	36.9	0.1	0.1	0.2
Max NO_2 lb/hr, FTIR or MS	10.4	9.7	14.2	0.2	0.1	0.4

3.1.1 Process Data and Observations (Additional Task i in TTR[1])

LabVIEW was used to record process data for all runs. In addition, records collected by the technicians and their observations were noted and can be found in the E-Notebook.[19] These were reviewed to look for any observations that might be pertinent to DWPF as the nitric-glycolic acid flowsheet is implemented. A separate section discusses process temperature, pH profile, mixing, offgas deposits, and solids noted in the glycolic acid feed line and glycolic acid bottle.

3.1.1.1 Temperature profile

The temperature trends for the SRAT only cycles (Runs 51-59) can be seen in Figure 3-2. During SRAT processing acid addition is performed at 93±2 °C. Dewater and reflux was performed at boiling (~102 ˚C). Due to the thick rheology in two high acid stoichiometry runs, NG54 and NG52, mixing and heat transfer were limited at agitator speeds up to 700 revolutions per minute (rpm). The 30 wt% total solids targets for these runs are higher than the 21.1 wt% total solids that DWPF is averaging in SB8 SRAT products. The highest acid stoichiometry run, NG59, was completed without any mixing issues by lowering the total solids target to 20 wt%.

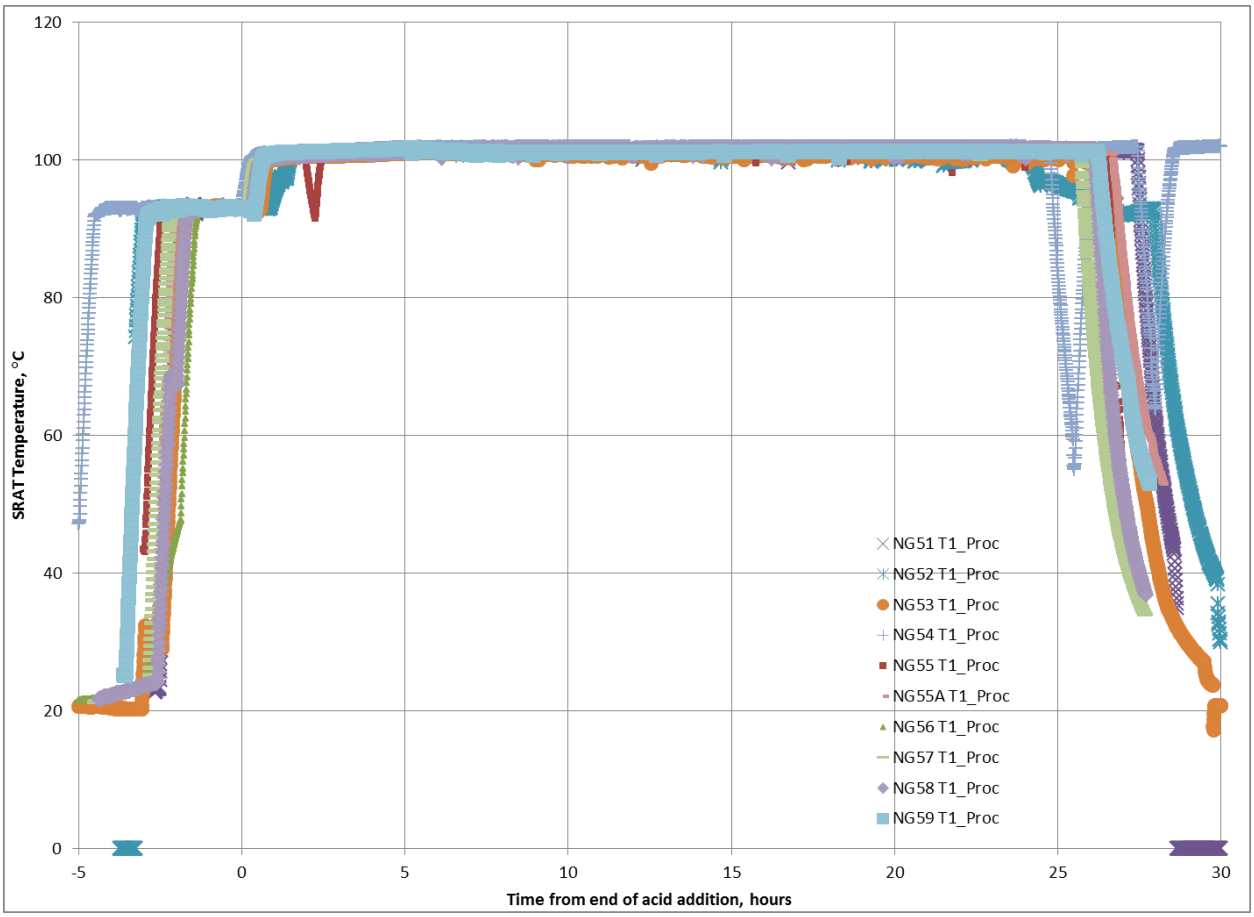

Figure 3-2. SRAT Cycle Slurry Temperature, ˚C

The temperature trends for the SRAT/SME cycles (Runs 60-62) can be seen in Figure 3-3. NG60 and NG62 had two process frit additions but no decon canister water additions. NG61 had six additions of decon canister water and two process frit additions. The SME heat was turned off and the slurry was cooled to about 90 ˚C prior to making additions of water, frit, and antifoam, which further cooled the slurry.

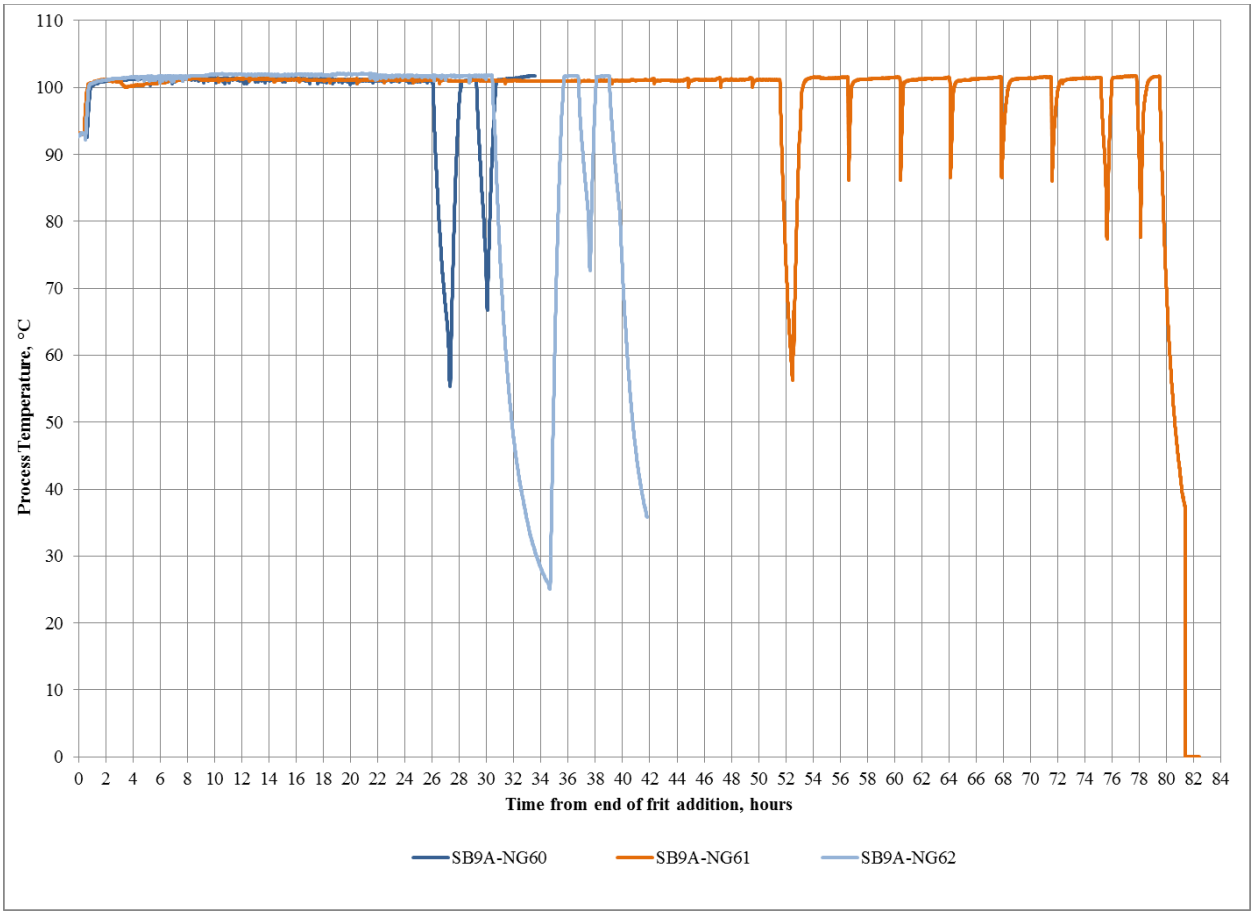

Figure 3-3. SME Cycle Slurry Temperature, ˚C

3.1.1.2 pH profile (Task 1l in TTR[1])

The slurry pH was measured throughout testing. The pH reported in Figure 3-4 is the temperature corrected pH to 25 ˚C. In run NG60 the PSAL measured SME product pH was 4.43 compared to 5.00 for the SRAT product. The online pH probe measured approximately the same pH for both the SRAT and SME product (approximately 4.) The post calibration check of the pH probe was about 0.8 pH units low so the final pH should have been about 4.8, similar to the measured pH of the SRAT product.

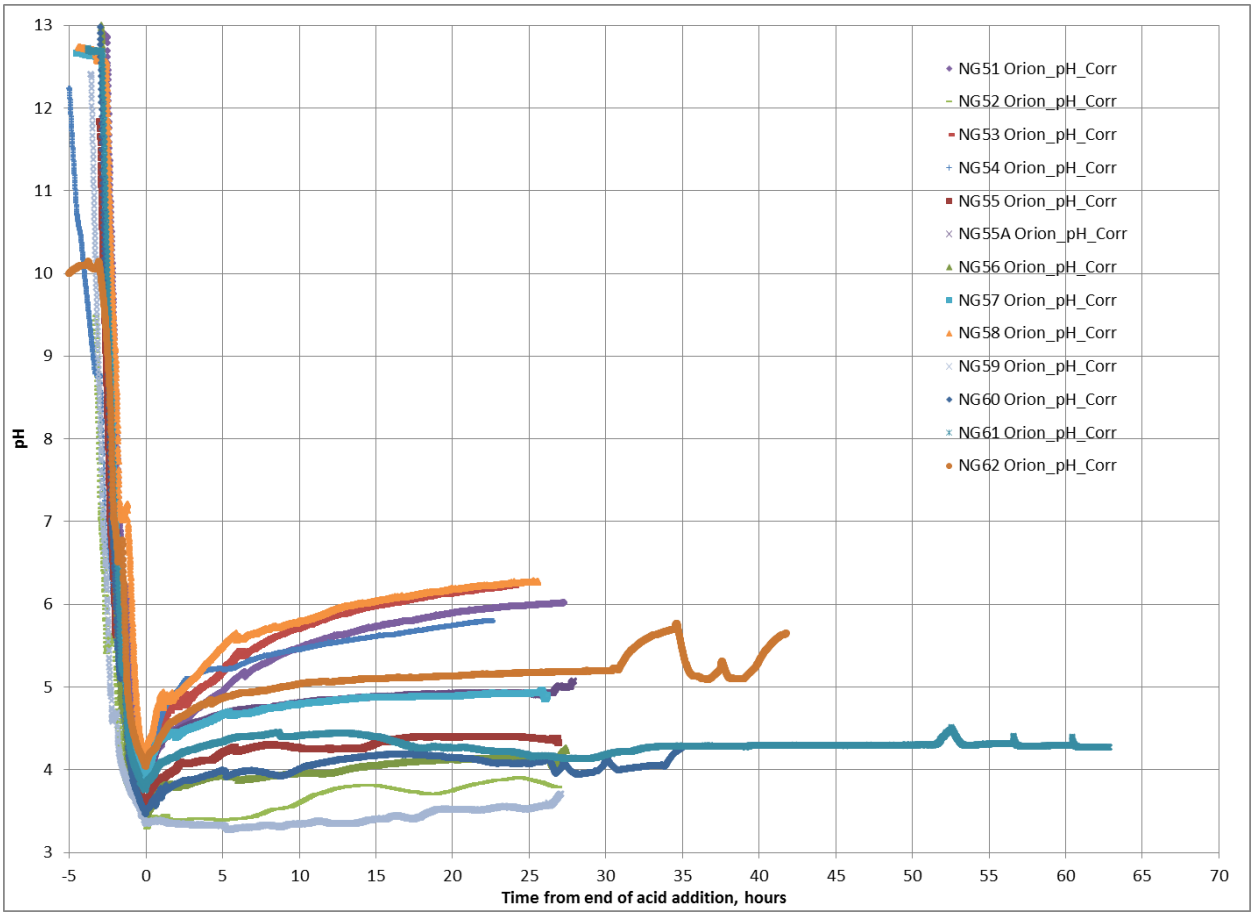

Figure 3-4. SRAT Cycle pH Profile for All Runs

The pH reaches a minimum upon completion of acid addition. The minimum pHs are presented in Table 3-3.

Table 3-3. Minimum, Post SRAT and Post SME pH

NG Run #	KMA	Process pH	PSAL pH	Process pH
		Minimum pH	SRAT Product	
51	83.7%	3.22	7.45	6.02
52	116%	3.04	4.36	3.89
53	83.6%	4.01	7.61	6.26
54	117%	4.00	4.14	3.45
55	100%	3.56	5.12	4.35
55A	100%	3.86	5.39	4.93
56	100%	3.41	4.97	4.12
57	99.9%	3.92	5.65	4.92
58	76.9%	4.19	7.75	6.27
59	123%	3.27	3.94	3.57
60	100%	3.46	5.00	4.10
61	100%	3.75	4.93	4.30
62	97.4%	4.03	5.93	5.19
			SME Product	
60	100%	NA	4.43	3.94
61	100%	NA	4.94	4.24
62	97.4%	NA	6.09	5.09

3.1.1.3 Mixing, Heat Transfer and Rod Fouling

The calculated heat transfer coefficient was about 0.2 $W/m^2/^{\circ}C$ during normal processing. In the two high acid stoichiometry runs targeting 30 wt% total solids (NG52 and NG54), the heat transfer coefficient began dropping late in the SRAT cycle (Figure 3.6). The heat transfer coefficient drops due to thick rheology leading to heating rod fouling (Figure 3.5). Due to the poor heat transfer, the boilup rate could not be maintained if the heating rod temperature was limited to 160 ˚C. Both of these runs had extended processing times and high rod temperatures in an attempt to maintain the boilup target. These were the only time during the testing where significant hydrogen was generated. The mass of the solid deposits on the heating rods in NG54 was 488 g or about 20% of the slurry mass. The higher acid stoichiometry run, NG59, was processed at a SRAT product total solids concentration of 20 wt %. In NG59, the heat transfer coefficient was steadier but was still dropping through the SRAT cycle.

Figure 3-5. Fouled Heater Rods in NG52

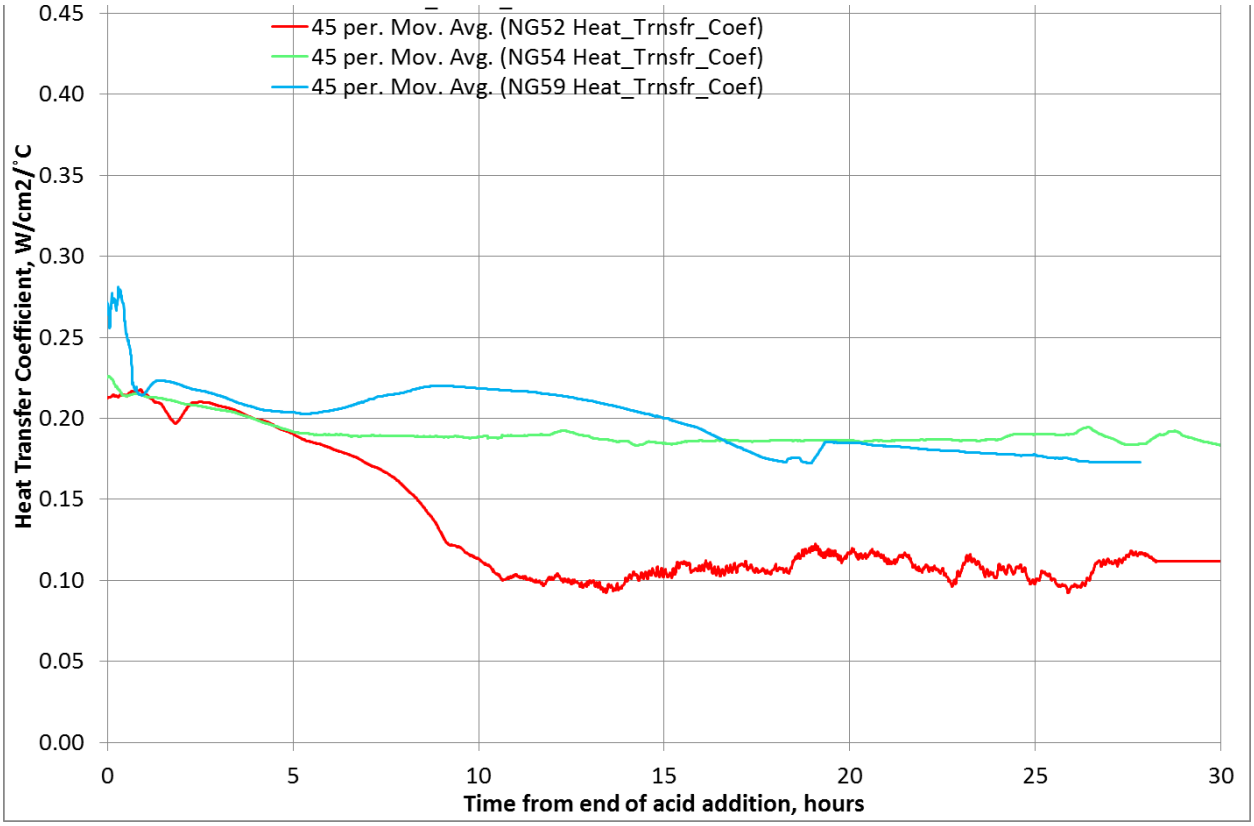

Figure 3-6. Heat Transfer Coefficient, W/cm^2/°C, during NG 52, 54 and 59 SRAT cycles

3.1.1.4 Offgas Deposits

Two items related to offgas deposits were noted in these runs. In most runs, solids were noticed in the horizontal offgas line between the SRAT and SRAT condenser. The deposits appeared to be fine sludge solids. Figure 3-7 is a photo showing the deposits. The kettle was very full in this run due to the addition of ARP, nitric and glycolic acid. White deposits were also noticed in the MS filter during several of the runs.

Figure 3-7. Solids in NG67 Offgas Line Run Post SME Cycle

3.1.1.5 Glycolic Acid Line Deposits

At the completion of NG67, deposits were noted in the horizontal section of the glycolic acid feed line (Figure 3-8).

Figure 3-8. Solids in Glycolic Acid Feed Line Run NG63

It was noted that the glycolic acid reagent bottle used in run NG63 (one of the additional tests to minimize the HMDSO peak) was almost empty. The remaining solution was filtered and the solids were easily removed. In discussions with the technical experts at Chemours, they believe that the glycolic acid may have been allowed to get too cold (50 ˚F or 10 ˚C)[3] during storage, allowing the solids to precipitate. Redissolving the solids requires heating the glycolic acid to a higher temperature (>30 ˚C). If the solids were glycolic acid precipitate, the glycolic acid may have been slightly under added in runs NG51-62.

3.1.2 SRAT and SME Products (Task 1a-1h in TTR[1])

The SRAT and SME product analytical results will be reported in this section. Table 3-4 gives the properties of the untreated sludge, as well as SRAT and SME products from each applicable run.

Table 3-4. Properties of SRAT Receipt, SRAT and SME Products

NG Run #	Solids					Density (g/mL, 20 °C)		
	Total	Insoluble	Calcined	Dissolved	Soluble	Slurry	Supernate	pH
SB9A	15.3%	10.6%	11.7%	5.25%	4.70%	1.12	1.04	NM
SRAT Product								
51	30.8%	19.3%	17.2%	14.2%	11.5%	1.2165	1.0958	7.45
52	26.4%	14.2%	13.9%	14.3%	12.3%	1.1798	1.0971	4.36
53	29.9%	17.5%	16.8%	15.0%	12.3%	1.2176	1.0922	7.61
54	27.7%	14.9%	14.8%	15.1%	12.8%	1.1792	1.0970	4.14
55	34.2%	19.1%	18.4%	18.6%	15.0%	1.2465	1.1255	5.12
55A	19.8%	10.1%	10.9%	10.8%	9.7%	1.1432	1.0728	5.39
56	30.9%	16.1%	16.7%	17.6%	14.8%	1.2368	1.1202	4.97
57	31.0%	16.6%	17.1%	17.2%	14.4%	1.2383	1.1150	5.65
58	29.8%	17.4%	17.5%	15.0%	12.4%	1.2280	1.0940	7.75
59	18.7%	8.49%	9.59%	11.2%	10.2%	1.1334	1.0779	3.94
60	25.7%	12.9%	13.9%	14.7%	12.8%	1.1495	1.0977	5.00
61	26.9%	14.3%	14.6%	14.7%	12.6%	1.2013	1.0976	4.93
62	25.9%	12.2%	14.2%	15.6%	13.7%	1.1966	1.0999	5.93
SME Product								
60	46.0%	33.7%	34.8%	18.6%	12.3%	1.3775	1.1256	4.43
61	37.1%	27.4%	27.9%	13.4%	9.7%	1.3118	1.0856	4.94
62	37.2%	25.8%	27.4%	15.4%	11.5%	1.2911	1.0959	6.09

SRAT product total solids content varies across the 13 experiments, ranging from 18.7% (NG59) to 34.2% (NG55). The total solids targets for NG51-58 were 30 wt%, NG55A and 59 were 20 wt %, and NG60-62 were 25 wt%. Similarly, insoluble solids values range from 8.49% (NG59) to 19.3% (NG51). SRAT product pH correlates well with KMA (R^2=0.898, linear relationship), as expected. SME products have higher slurry densities than their SRAT product counterparts (1.38 g/mL vs. 1.15 g/mL for NG60, 1.31 g/mL vs. 1.20 g/mL for NG61, and 1.29 g/mL vs. 1.20 g/mL for NG62, respectively), largely due to the increased solids loadings. SME product pH values fall within 0.6 pH units of the SRAT product pH (4.43 vs. 5.00 for NG60, 4.94 vs. 4.93 for NG61, and 6.09 vs. 5.93 for NG62, respectively).

Table 3-5 gives the elemental composition of each SRAT and SME product, reported as % of calcined solids.

Table 3-5. Elemental Composition of SRAT and SME Product Calcined Solids (given as % of calcined solids)

Run	Al	B	Ca	Cr	Fe	Li	Mg	Mn	Na	Ni	S	Si	Zr
SB9A	9.83	<0.1	1.53	0.13	25.2	<0.1	0.29	8.74	15.0	1.78	0.26	2.41	<0.10
SRAT Product*													
51	9.73	NR	1.44	0.13	23.30	NR	0.30	8.32	16.85	1.76	0.34	1.95	0.11
52	9.84	NR	1.35	0.13	23.00	NR	0.28	8.00	16.40	1.73	0.31	1.97	0.11
53	9.46	<0.1	1.50	0.12	24.30	<0.1	0.28	8.18	17.05	1.74	0.23	1.66	0.11
54	10.15	<0.1	1.41	0.13	24.85	<0.1	0.29	8.49	16.15	1.83	0.37	1.91	0.11
55	9.83	<0.1	1.49	0.13	23.60	<0.1	0.29	8.09	16.60	1.78	0.35	2.00	0.11
55A	10.30	<0.1	1.52	0.13	23.25	NR	0.30	8.72	15.75	1.76	0.38	1.98	0.11
56	9.81	<0.1	1.45	0.13	23.40	<0.1	0.28	7.98	16.40	1.75	0.35	1.97	0.11
57	10.50	NR	1.45	0.13	23.00	NR	0.29	8.05	16.60	1.73	0.33	1.93	0.11
58	10.55	NR	1.48	0.12	23.25	NR	0.28	8.07	17.45	1.74	0.33	1.92	0.11
59	10.15	<0.1	1.51	0.13	23.45	NR	0.31	8.71	15.70	1.78	0.36	2.03	0.11
60	9.89	<0.1	1.47	0.13	23.80	<0.1	0.30	8.21	16.30	1.80	0.34	1.96	0.11
61	10.35	NR	1.41	0.13	22.30	NR	0.27	8.73	16.75	1.68	0.34	1.83	0.11
62	9.34	NR	1.33	0.12	21.25	NR	0.26	7.67	19.55	1.59	0.35	1.73	<0.101
SME Product													
60	3.95	1.51	0.50	0.05	9.14	1.75	0.11	3.25	10.05	0.57	0.13	24.00	<0.1
61	4.22	1.60	0.51	0.06	9.22	1.63	0.11	3.54	10.50	0.59	0.12	22.15	<0.1
62	4.21	1.56	0.49	0.06	9.26	1.52	0.11	3.42	11.80	0.58	0.14	21.75	<0.1

"NR" = Not Reported. *Ag, Ba, Cu, K, P, Pd, Rh, Ru, Sn, Ti, & Zn are below detection limits in every case.

For the most part, the elemental compositions of SRAT product calcined solids are comparable to the composition of the untreated sludge simulant. The measured composition of sodium in SRAT products averages about 10% higher than that measured in the untreated sludge, while the SRAT product compositions of manganese and iron are 5% and 7% lower respectively. These differences suggest slight variability in the composition of the sludge used in the SB9 nitric-formic acid runs versus the SB9 nitric-glycolic acid runs or in the addition of sludge to the experimental apparatus (sodium is assumed to be present primarily in the supernatant phase of the sludge simulant, while iron is assumed to be present primarily in the solid phase). The differences between NG62 and the other runs (e.g. an 18% increase in sodium composition relative to the average of all other runs) are largely due to the increased salinity of the SRAT product caused by the addition of PRFT simulant feed stream during the SRAT cycle. SME products generally exhibit a marked decrease in percent composition of Al, Ca, Cr, Fe, Mg, Mn, Na, Ni, and S and a similarly significant increase in percent composition of B, Li, and Si relative to their corresponding SRAT products. These changes are due to the addition of glass frit, which is primarily composed of Si, B, Li, Na, and O.

In addition to the elemental composition of calcined slurry solids, the concentration of these species in the supernatant phase of each SRAT product is measured. The supernatant elemental concentration data is shown in Table 3-6.

Table 3-6. Elemental Concentration of SRAT/SME Product Supernatant Phase (given as mg/L)

Run	Al	B	Ba	Ca	Cr	Cu	Fe	K	Li	Mg	Mn	Na	Ni	Rh	Ru	S	Si	Sn	Ti	Zn	Zr
SRAT Product*																					
51	192	NR	2	179	1	1	79	188	NR	216	3760	37600	31	4	25	729	54	<1	0.4	<0.1	3
52	705	NR	4	1250	43	57	4390	161	NR	254	6910	28900	790	19	117	560	254	<1	0.6	29	33
53	301	60	2	136	2	1	158	198	47	194	3750	35450	43	5	36	774	77	3	<0.1	<0.1	4
54	890	97	3	1815	45	49	2685	277	62	278	8050	31000	822	15	109	549	58	22	<0.1	<0.1	34
55	773	127	3	1070	22	35	1760	239	72	306	11050	40300	1410	21	15	805	48	16	<0.1	17	64
55A	478	65	1	550	8	4	832	165	NR	156	4355	19650	485	8	51	406	13	<1	<0.1	7	14
56	1165	107	3	1060	19	41	2165	236	61	271	12250	36200	1205	19	13	669	44	15	<0.1	16	56
57	1225	NR	3	923	24	8	3170	167	NR	255	9160	34500	1145	21	124	743	49	<1	0.4	15	75
58	207	NR	2	68	1	1	110	194	NR	173	4330	35050	21	3	21	817	20	<1	0.2	<0.1	2
59	1030	59	2	1205	38	45	4070	96	NR	182	6465	17200	1050	13	77	341	35	<1	0.1	26	41
60	899	89	2	907	14	23	1590	150	50	235	11100	29400	1050	15	10	551	33	12	<0.1	13	35
61	998	NR	2	794	16	29	737	150	NR	250	9645	28950	385	14	90	580	43	<1	0.3	9	28
62	257	NR	1	483	4	9	248	126	NR	177	7355	34850	515	6	34	665	46	<1	0.3	5	6
SME Product																					
60	1385	151	3	1140	24	37	2155	200	185	309	12250	37900	1185	21	13	722	107	17	<0.1	17	50
61	877	113	2	661	15	26	624	135	128	228	7870	26900	203	12	74	512	93	<1	0.3	7	19
62	223	308	1	463	4	5	152	117	122	174	6530	32850	488	6	32	661	188	<1	0.3	4	5

"NR"=Not Reported. *Ag, P, and Pd are below detection limits in every case

Trends in supernatant metal concentration appear to be dictated by the aqueous solubility of the same metals. As expected, sodium exhibits no trend across the multiple runs (likely due to its high solubility in water), while metals such as calcium exhibit a reasonable correlation to pH (R^2=0.828), suggesting a dependence of solubility on solution acidity. Interestingly, no strong trend is detected in manganese concentration, suggesting that other parameters may dictate the solubility of Mn (e.g. extent of reduction to Mn(II), concentration of glycolate, etc.). No significant trends are identifiable in the transition from SRAT to SME product.

The data from Table 3-4, Table 3-5, and Table 3-6 can be combined to directly calculate the extent of solubility of each metal cation via Equation 4:

$$\%\, Solubility_i = \frac{[i]_{sup}(1-\%IS)}{\rho_{sup}*\%CS*\%i_{CS}*100} \qquad \text{Equation 4}$$

where % Solubility$_i$ is the percentage of component i that is soluble in the supernatant phase (expressed as a number between 0 and 100), $[i]_{sup}$ is the supernatant concentration of component i in units of mg/L, %IS is the fraction of the slurry mass composed of insoluble solids (expressed as a number between 0 and 1), %CS is the fraction of the slurry mass remaining after calcination at 1150 °C (expressed as a number between 0 and 1), ρ_{sup} is the density of the supernatant phase in units of kg/L, and $\%i_{CS}$ is the percentage of calcined solids attributable to the mass of component i (expressed as a number between 0 and 100). Such values are calculated for selected species and shown in Table 3-7. Note that an element that is completely soluble should have a solubility of approximately 80-120% due to analytical uncertainties.

Table 3-7. Percent Solubilities of Selected Metals in SRAT and SME Products

Run	%KMA	Al	Ca	Cr	Fe	Mg	Mn	Na	Ni	S	Si	Zr
SRAT Product												
51	84	0.8	5.3	0.4	0.1	31	19	96	0.8	93	1.2	1.2
52	116	4.0	52	19	11	50	49	99	26	103	7.3	16
53	84	1.4	4.1	0.6	0.3	32	21	94	1.1	154	2.1	1.9
54	117	4.6	68	18	5.7	50	50	101	24	78	1.6	16
55	100	3.1	28	6.8	2.9	42	53	95	31	89	0.9	22
55A	100	3.6	28	4.4	2.7	40	38	96	21	82	0.5	9.7
56	100	5.3	33	6.6	4.1	43	69	99	31	86	1.0	23
57	100	5.1	28	8.2	6.0	39	50	91	29	98	1.1	30
58	77	0.8	2.0	0.5	0.2	27	23	87	0.5	108	0.5	1.0
59	123	9.0	71	25	15	52	66	97	52	84	1.5	32
60	100	5.9	39	8.0	4.0	46	64	103	35	93	0.1	NR
61	100	5.2	30	6.8	1.8	49	59	92	12	92	1.3	14
62	97	1.5	20	1.9	0.7	39	54	100	18	107	1.5	NR
SME Product												
60	100	5.3	35	7.2	3.6	41	57	57	32	84	0.1	NR
61	100	5.0	31	5.9	1.6	48	53	61	8.3	101	0.1	NR
62	97	1.3	24	1.5	0.4	38	47	69	21	117	0.2	NR

As mentioned earlier, the solubilities of elements like sodium and sulfur (present primarily as sulfate ion) exhibit no obvious trends, likely due to the high solubility of these species. Solubilities of metals like calcium and magnesium exhibit a strong correlation to pH (R^2 > 0.85), suggesting a possible role of hydroxide/hydronium ions in the solubility of these metals. The solubilities of the remaining metals (aluminum, chromium, iron, manganese, and nickel) exhibit varying strengths of correlation to pH, suggesting that multiple processing parameters play a role in the dissolution of these species. Elemental

solubilities of the SRAT and SME products are roughly equivalent, suggesting that only minor changes in solution composition occur during the SME cycle.

Similar analyses can be conducted with the anions present in the SRAT and SME products. Table 3-8 gives the anion content of the SRAT and SME products (reported on a mg/kg slurry basis). The SB9A Sludge Slurry TIC was 1619 mg/kg and the Supernate TIC was 1671 mg/L.

Table 3-8. Concentrations of Anions* in SRAT and SME Products (mg/kg slurry basis)

Run	NO_2^-	NO_3^-	$C_2H_3O_3^-$	SO_4^{-2}	$C_2O_4^{-2}$	HCO_2^-	CO_3^{-2}
SB9A	10,200	5,725	-	1,235	3,514	-	8,090
SRAT Product							
51	<500	56200	45150	1875	11350	846.5	NA
52	<500	54950	63050	1475	7115	694	3,100
53	<500	46350	47450	1825	11200	1560	NA
54	<500	66900	54500	1505	6745	<500	NA
55	<500	65700	59500	1930	11650	<500	NA
55A	<500	46000	38400	1175	6495	<500	NA
56	<500	68000	49650	1745	10650	<500	NA
57	<500	56900	70650	1990	10750	<500	NA
58	<500	50100	46950	2035	12800	1225	3,160
59	<500	48450	44000	986	4695	573.5	NA
60	<500	54850	43650	1460	7605	<500	<200
61	<500	56350	39850	1545	11100	<500	<200
62	<500	54950	46450	1610	6905	626	<200
SME Product							
60	<500	51650	40750	1400	7710	<500	<200
61	<500	42150	28850	1160	10100	<500	<200
62	<500	45550	38950	1350	6130	623	<200

* F^-, Cl^-, and PO_4^{-3} are all below detection limit of <500 mg/L

In every run the amount of nitrite is below the detection limit of 500 mg/kg, indicating that the nitric - glycolic flowsheet is capable of destroying nitrite ions in sludge slurries. However, formate is apparently formed during the SRAT cycle, albeit in small amounts compared to the amount of glycolate remaining after the run (e.g. 1,225 mg formate/kg slurry vs. 46,950 mg glycolate/kg slurry in the SRAT product of NG58). Despite the formation of formate, no measurable amount of hydrogen is seen in the offgas data. This suggests that the concentrations of formate formed are too low to yield a significant rate of formation of hydrogen or that the chemistry formerly seen in the formic-glycolic flowsheet has been fundamentally altered with the presence of glycolate. A follow-up report will be written on the nitric-glycolic acid flowsheet based on the data from this report and other testing as needed.

Table 3-9 gives the concentration of anions in the supernatant phase of the SRAT and SME products produced in runs NG51 through NG62 (given on a mg/L basis).

Table 3-9. Supernatant Concentration of Anions* in SRAT and SME Products (mg/L basis)

Run	Cl^-	NO_2^-	NO_3^-	$C_2H_3O_3^-$	SO_4^{-2}	$C_2O_4^{-2}$	HCO_2^-
SRAT Product							
51	<100	<100	75900	32650	1925	385	836
52	<100	<100	70600	31050	1410	1600	470
53	122.5	<100	56450	45755	2180	691	861.5
54	<100	<100	89900	24700	1440	2790	482.5
55	141.5	<100	93500	47400	2060	922	547
55A	<100	<100	43900	30800	1025	951.5	323
56	133.5	<100	92600	43000	1675	1845	465
57	141.5	<100	70150	53550	1900	603	487
58	133.5	<100	63650	41250	2150	1540	1350
59	<100	<100	47150	29300	862	3145	720.5
60	<100	<100	70600	39850	1355	2230	478.5
61	<100	<100	73150	33550	1400	1990	335
62	<100	<100	70450	43650	1750	486	617
SME Product							
60	111.5	<100	93000	47600	1815	1595	605.5
61	<100	<100	66900	28250	1295	2265	370
62	<100	<100	67050	40700	1665	342	704.5

* F^-, and PO_4^{-3} are all below detection limit of <100 mg/L

It is clear that nitrite has been destroyed to sufficiently low levels in the nitric-glycolic flowsheet, achieving less than 100 mg nitrite/L supernatant in every case. Concentration of oxalate varies throughout the runs, reaching values as low as 385 mg/L (NG51) and as high as 3145 mg/L (NG59). Formate concentration is also variable throughout the runs, ranging from 323 mg/L in NG55A to 1350 mg/L in NG58.

Using the data in Table 3-8 and Table 3-9, percent solubilities can be calculated for each anion using the following equation:

$$\%\, i_{soluble} = \frac{[i]_{sup}(1-\%IS)}{\rho_{sup} * [i]_{slurry}} * 100 \qquad \text{Equation 5}$$

where $\%i_{soluble}$ is the percentage of anion i that is soluble in the sludge (expressed as a number between 0 and 100), $[i]_{sup}$ is the concentration of anion i in the supernatant phase (in units of mg/L), ρ_{sup} is the density of the supernatant phase (in units of g/mL), $[i]_{slurry}$ is the concentration of anion i in the heterogeneous slurry mixture (in units of mg/kg), and %IS is the fraction of slurry mass contributable to the insoluble solid phase (expressed as a number between 0 and 1). Percent solubilities for selected anions are reported in Table 3-10.

Table 3-10. Percent Solubilities of Selected Anions in SRAT and SME Products

Run	NO_3^-	$C_2H_3O_3^-$	SO_4^{-2}	$C_2O_4^{-2}$	HCO_2^-
SRAT Product					
51	99	53	76	2	73
52	100	39	75	18	53
53	92	73	90	5	42
54	104	35	74	32	NR
55	102	57	77	6	NR
55A	80	67	73	12	NR
56	102	65	72	13	NR
57	92	57	71	4	NR
58	96	66	80	9	83
59	83	57	74	57	107
60	102	72	74	23	NR
61	101	66	71	14	NR
62	102	75	87	6	79
SME Product					
60	106	69	76	12	NR
61	106	65	75	15	NR
62	100	71	84	4	77

"NR" = Not Reported.

Anions that are traditionally water-soluble (such as nitrate and sulfate) exhibit relatively constant solubilities across all runs, with nitrate returning an average of 97% solubility across all runs and sulfate returning an average solubility of 76%. Oxalate ($C_2O_4^{-2}$) solubility appears to exhibit a weak correlation to pH, which suggests a difference in solubility between the non-protonated ($C_2O_4^{-2}$), partially-protonated ($HC_2O_4^-$, $pK_a = 4.14$), and fully protonated ($H_2C_2O_4$, $pK_a = 1.25$) species. Upon initial inspection, no trends are evident in the glycolate ($C_2H_3O_3^-$) or formate (HCO_2^-) solubility data. A significant amount of noise is expected in the solubility data for formate due to the proximity of the measured concentration to the lower detection limit for formate in the slurry (Table 3-8).

3.1.3 Mass Balance

A mass balance was completed for each of the runs. The details used for completing the mass balance are located in Appendix A. The summary of the balance is summarized below.

3.1.3.1 C Balance

A mass balance was completed for all analyzed compounds containing carbon. Note that there is no detectable carbon or antifoam in the condensate samples (there would be if there is a foam-over). As a result, the carbon mass balance can be completed by knowing the sludge anions (carbonate, oxalate, formate and glycolate), the added glycolic acid, the SRAT product anions (oxalate, formate and glycolate, carbonate), and the cumulative offgas (CO, CO_2, and HMDSO).

The inputs and outputs to the carbon balance are summarized in Table 3-11 and Table 3-12. The % carbon from glycolate, oxalate, formate, CO_2, CO and antifoam in the output streams is summarized in Table 3-13. The results of each anion's carbon conversion (glycolate destruction, oxalate generation, formate generation) are included in Table 3-14. A balance trying to explain which reactions led to the formation of CO_2 is summarized in Table 3-15.

Table 3-11. Inputs to SRAT-only Cycle Carbon Balances, mol carbon

Carbon Inputs	NG51	NG52	NG53	NG54	NG55	NG55A	NG56	NG57	NG58	NG59
Sludge CO_3^{2-}	0.089	0.089	0.089	0.089	0.089	0.089	0.089	0.089	0.089	0.089
Sludge oxalate	0.264	0.264	0.263	0.263	0.263	0.263	0.263	0.263	0.263	0.263
Glycolic acid	3.466	5.574	4.007	4.827	4.465	4.469	4.015	4.925	3.434	5.504
Total in Feed	3.819	5.927	4.360	5.179	4.818	4.822	4.368	5.278	3.787	5.857

Table 3-12. Outputs to SRAT-Only Carbon Balances, mol carbon

Carbon Outputs	NG51	NG52	NG53	NG54	NG55	NG55A	NG56	NG57	NG58	NG59
Glycolate	2.585	4.171	2.785	3.398	3.288	3.474	3.085	4.114	2.662	4.412
Formate	0.040	0.038	0.076	0.000	0.049	0.000	0.000	0.000	0.058	0.050
Oxalate	0.554	0.401	0.560	0.352	0.482	0.453	0.496	0.534	0.619	0.362
TIC	NA	0.026	NA	NA	NA	NA	NA	NA	0.022	NA
TOC	NA	3.276	NA	NA	NA	NA	NA	NA	2.524	NA
CO and CO_2	0.824	0.800	0.771	0.744	0.728	0.784	0.671	0.815	0.802	0.795
Total in Products	4.004	5.539	4.193	4.494	4.547	4.710	4.253	5.463	4.253	5.618
C Delta	0.171	0.744	0.523	1.041	0.627	0.468	0.470	0.170	-0.110	0.594
% Closure	96%	88%	89%	81%	88%	91%	90%	97%	103%	90%

Table 3-13. % Carbon in Output Streams

Carbon Outputs	NG51	NG52	NG53	NG54	NG55	NG55A	NG56	NG57	NG58	NG59
Glycolate	64.6	77.1	66.4	75.6	72.3	73.8	72.5	75.3	64.3	78.5
Oxalate	13.8	7.4	13.4	7.8	10.6	9.6	11.7	9.8	14.9	6.4
Formate	1.0	0.7	1.8	0.0	1.1	0.0	0.0	0.0	1.4	0.9
TIC	NA	2.3%	NA	NA	NA	NA	NA	NA	2.6	NA
CO_2	20.6	14.8	18.4	16.5	16.0	16.6	15.8	14.9	19.4	14.1
CO	0.0	0.0	0.0	0.0	0.0	0.0	0.0	0.0	0.0	0.0

Table 3-14. Carbon Conversion Calculations, %

Carbon Outputs	NG51	NG52	NG53	NG54	NG55	NG55A	NG56	NG57	NG58	NG59
SRAT glycolate Destruction	25.4	25.2	30.5	29.6	26.4	22.3	23.2	16.5	22.5	19.8
SRAT oxalate Production	110.3	52.3	112.7	33.5	82.9	71.8	88.4	102.6	134.9	37.3
SRAT formate Destruction	NA	NA	NA	NA	NA	NA	NA	NA	NA	NA

Table 3-15. Carbonate/CO_2 Balance, mol C

Carbonate/CO_2 Balance	NG51	NG52	NG53	NG54	NG55	NG55A	NG56	NG57	NG58	NG59
Carbonate in Sludge	0.445	0.445	0.445	0.445	0.445	0.445	0.445	0.445	0.445	0.445
CO_2 generation	0.824	0.800	0.771	0.744	0.728	0.784	0.671	0.815	0.802	0.795
CO_2 from other reactions	0.379	0.355	0.327	0.299	0.283	0.339	0.226	0.370	0.357	0.350
Carbonate in Product	NA	0.128	NA	NA	NA	NA	NA	NA	0.112	NA

3.1.3.2 N Balance

A mass balance was completed for all analyzed compounds containing nitrogen. The nitrogen mass balance can be completed by knowing the incoming nitrate and nitrite in the sludge, the added nitric acid, the nitrate in the SRAT product, and the offgas NO, NO_2, and N_2O.

The inputs and outputs to the nitrogen balance are summarized in Table 3-16 and Table 3-17. The percent of nitrite that decomposed to form various oxides of nitrogen in the offgas, to nitrate in condensate, and to nitrate in SRAT are summarized in Table 3-18. A balance trying to explain which reactions led to the formation of the various oxides of nitrogen (those not scrubbed in the SRAT, condenser, scrubber or FAVC) is summarized in Table 3-19.

Table 3-16. Inputs to SRAT-only Cycle Nitrogen Balances, mol nitrogen

Nitrogen Inputs	NG51	NG52	NG53	NG54	NG55	NG55A	NG56	NG57	NG58	NG59
Sludge nitrite	0.73	0.73	0.73	0.73	0.73	0.73	0.73	0.73	0.73	0.73
Sludge nitrate	0.30	0.30	0.30	0.30	0.30	0.30	0.30	0.30	0.30	0.30
Nitric Acid	1.47	1.66	1.20	2.05	1.59	1.59	1.83	1.36	1.23	1.96
Total in Feed	2.51	2.70	2.23	3.08	2.63	2.63	2.86	2.40	2.26	3.00

Table 3-17. Outputs to SRAT-Only Nitrogen Balances, mol nitrogen

Nitrogen Outputs	NG51	NG52	NG53	NG54	NG55	NG55A	NG56	NG57	NG58	NG59
SRAT Product nitrate	1.95	2.20	1.65	2.72	2.20	2.02	2.37	2.01	1.72	2.45
NO_x measured ($NO + NO_2 + 2*N_2O$)	0.092	0.100	0.087	0.087	0.108	0.109	0.083	0.147	0.125	0.083
Scrubber nitrate	0.15	0.12	0.12	0.05	0.14	0.06	0.07	0.05	0.07	0.10
Dewater nitrate	0.16	0.01	0.20	0.04	0.11	0.09	0.08	0.13	0.17	0.01
MWWT nitrate	0.00	0.00	0.00	0.00	0.00	0.00	0.00	0.00	0.00	0.00
Total condensate	0.32	0.13	0.32	0.09	0.24	0.15	0.15	0.18	0.25	0.11
Total NH3	0.000	0.000	0.000	0.000	0.000	0.000	0.000	0.000	0.000	0.000
total nitrite to offgas	0.41	0.23	0.40	0.18	0.35	0.26	0.23	0.33	0.38	0.19
Total in Products	2.36	2.43	2.05	2.90	2.55	2.28	2.60	2.34	2.09	2.64
Delta	0.15	0.27	0.18	0.18	0.08	0.36	0.27	0.06	0.17	0.36
% Closure	94	90	92	94	97	87	91	97	93	88

Table 3-18. % Nitrite in Output Streams

Nitrogen Outputs	NG51	NG52	NG53	NG54	NG55	NG55A	NG56	NG57	NG58	NG59
% of nitrite to offgas	12.6	13.6	11.8	11.8	14.8	14.9	11.4	20.2	17.0	11.3
% nitrite to condensate	43.3	17.8	43.2	13.0	33.5	20.3	20.2	25.2	34.3	15.1
% nitrite to SRAT nitrate	44.1	68.5	44.9	75.2	51.8	64.7	68.4	54.6	48.7	73.6

Table 3-19. Nitrogen Oxides in Offgas

Nitrogen Oxides Balance	NG51	NG52	NG53	NG54	NG55	NG55A	NG56	NG57	NG58	NG59
NO, mmol	35.2	27.1	23.4	20.1	58.5	53.3	35.7	73.3	54.3	24.2
NO_2, mmol	46.0	42.1	43.8	41.2	39.6	46.7	40.4	63.1	46.2	40.9
N_2O,mmol	5.6	15.3	9.7	12.7	4.9	4.7	3.6	5.5	12.0	8.8
Total N mmol	92.5	99.8	86.5	86.7	108.0	109.3	83.3	147.5	124.6	82.7
Offgas Percent N as NO	38.1	27.1	27.1	23.2	54.2	48.7	42.9	49.7	43.6	29.2
Offgas Percent N as NO_2	49.8	42.2	50.6	47.6	36.7	42.7	48.5	42.8	37.1	49.4
Offgas Percent N as N_2O	12.2	30.6	22.4	29.3	9.1	8.6	8.6	7.5	19.3	21.3

3.1.4 Anion Reactions

The anion conversion calculations are summarized in sections 3.1.3.1 and 3.1.3.2. The discussion below will focus on the SRAT product trends for nitrate, glycolate, oxalate and formate. The anion results were overlaid on a graph showing the testing matrix (see Figure 3-1 for correlating these points to a run number). To simplify run comparisons, the anion data was corrected by the following equation:

$$anion_{corrected} = anion_{measured} * \frac{25}{\%\, Total\ Solids} \quad \text{Equation 6}$$

The first anion to be discussed is oxalate. In early testing, the poor quality of the oxalate data prevented knowing whether oxalate was being generated or consumed. Due to the improvements in quantifying oxalate using the caustic quench method, the following can be concluded about oxalate (Figure 3-9):

- Oxalate is generated in all runs.
- There is an increase in oxalate generation with a decrease in acid stoichiometry. The oxalate generation is maximized at the lowest acid stoichiometry.
- There is an increase in oxalate generation with percent reducing acid but this may be because there is more reducing acid added and is not as strong an effect as acid stoichiometry.

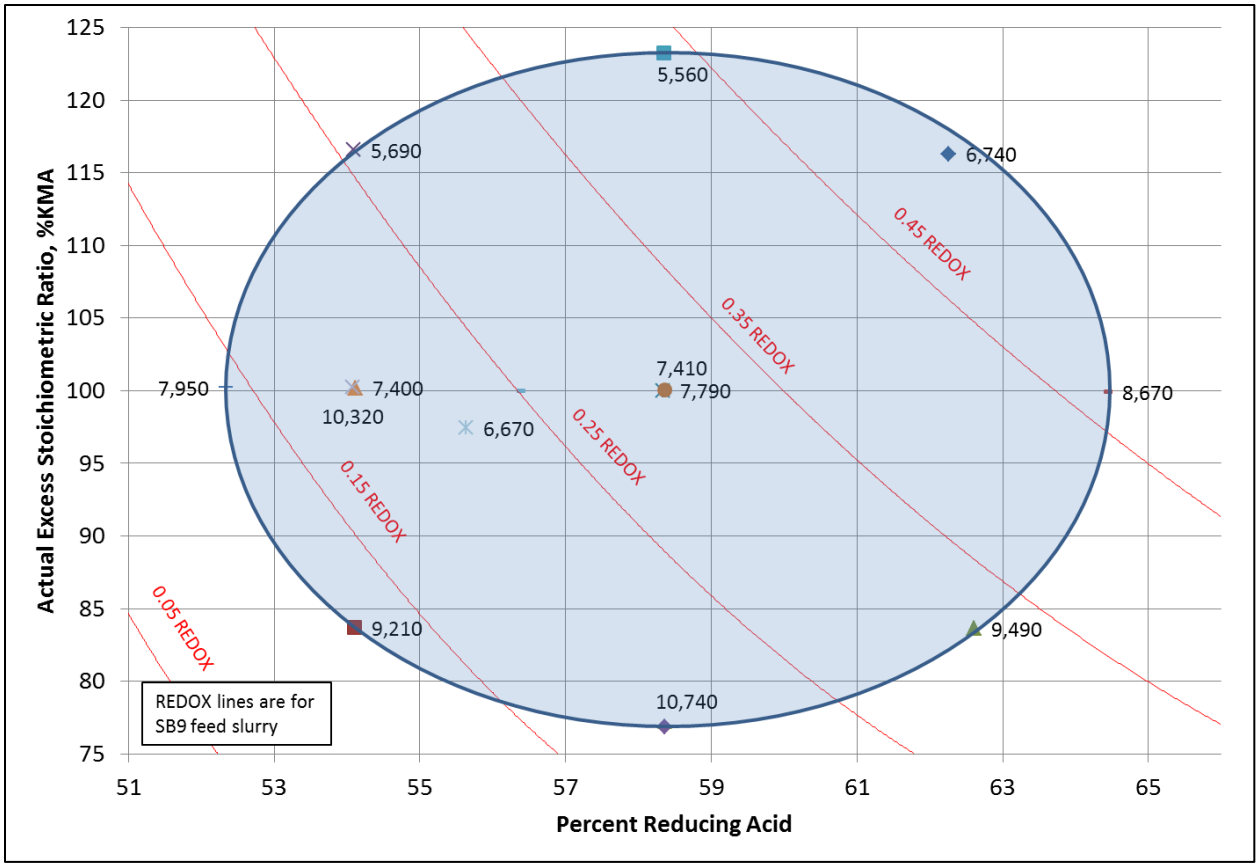

Figure 3-9. SRAT Product Oxalate Trends, mg/kg

The most concentrated anion is glycolate. Due to the improvements in the caustic quench method, the following can be concluded about glycolate (Figure 3-10):

- Glycolate is consumed in all runs, primarily acid/base and reduction reactions.
- The glycolate concentration is roughly parallel to the red REDOX lines. This is expected as producing the desired REDOX is essentially balancing glycolate and nitrate.

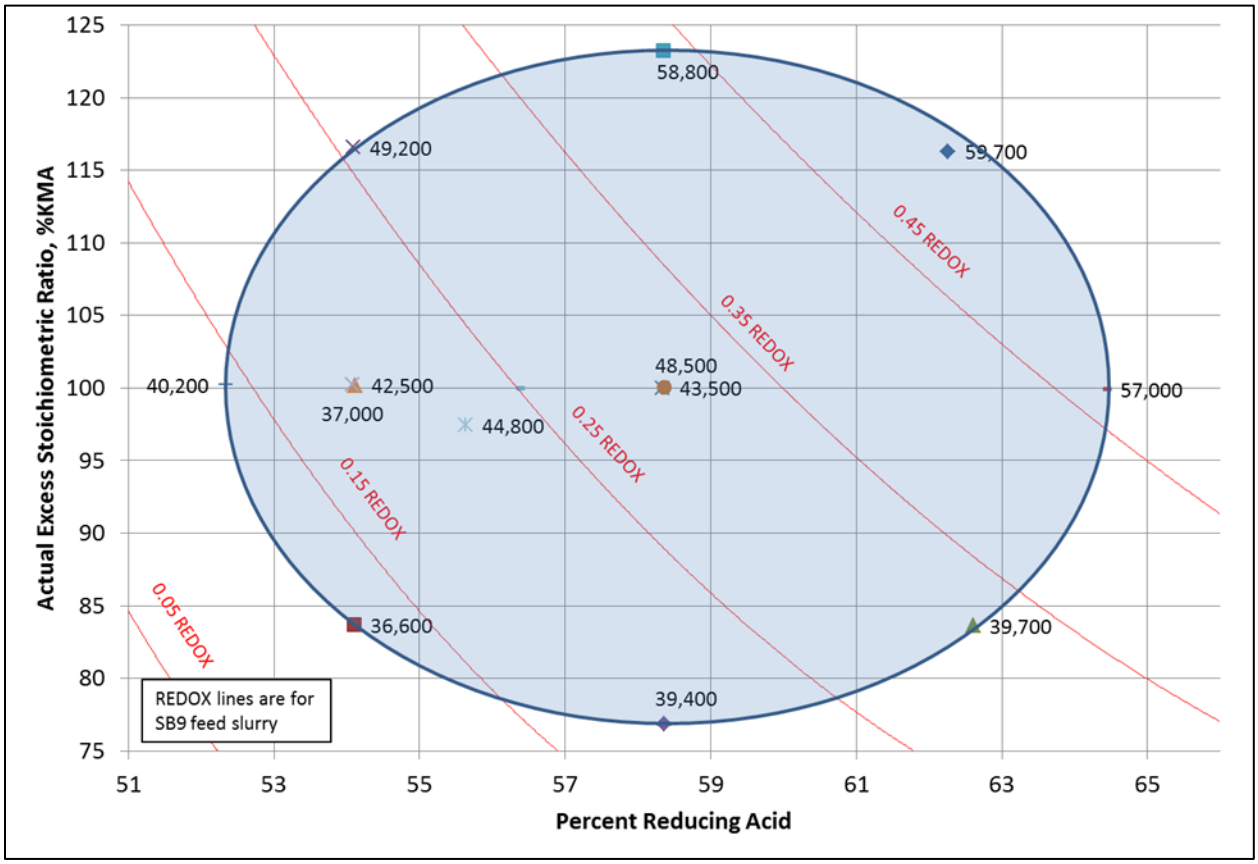

Figure 3-10. SRAT Product Glycolate Trends, mg/kg

The least concentrated organic anion is formate. Due to the improvements in the caustic quench method, the following can be concluded about formate (Figure 3-11):

- A small amount of formate (an impurity in glycolic acid) was generated in most of the runs at the highest and lowest acid stoichiometry. The glycolic acid can contain formate as an impurity, but this was below detection limits.

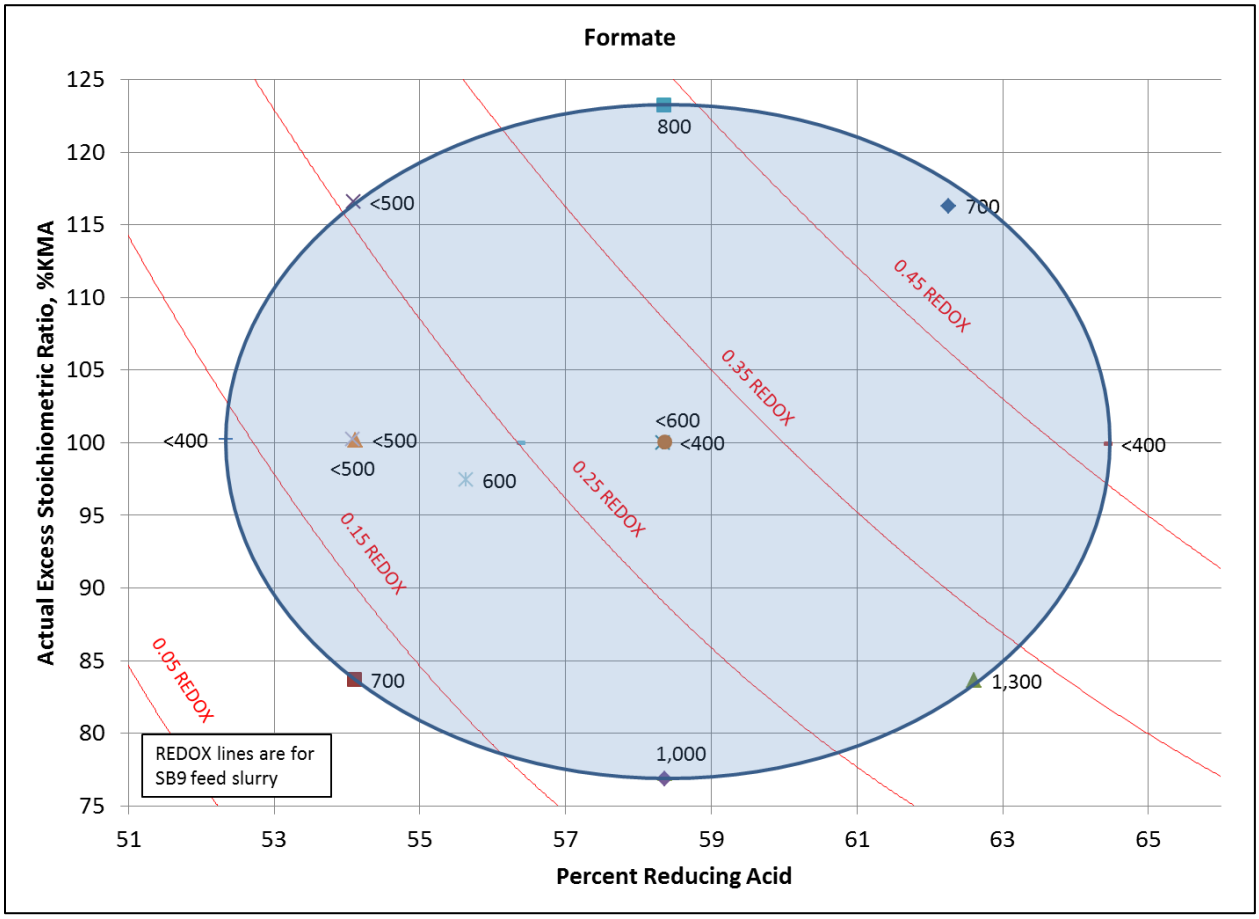

Figure 3-11. SRAT Product Formate Trends, mg/kg

The only oxidizing anion is nitrate. The following can be concluded about nitrate (Figure 3-12):

- Nitrate increases both with increased acid stoichiometry and decreased PRA. The nitrate concentration is roughly parallel to the red REDOX lines. This is expected as producing the desired REDOX is essentially balancing glycolate and nitrate.

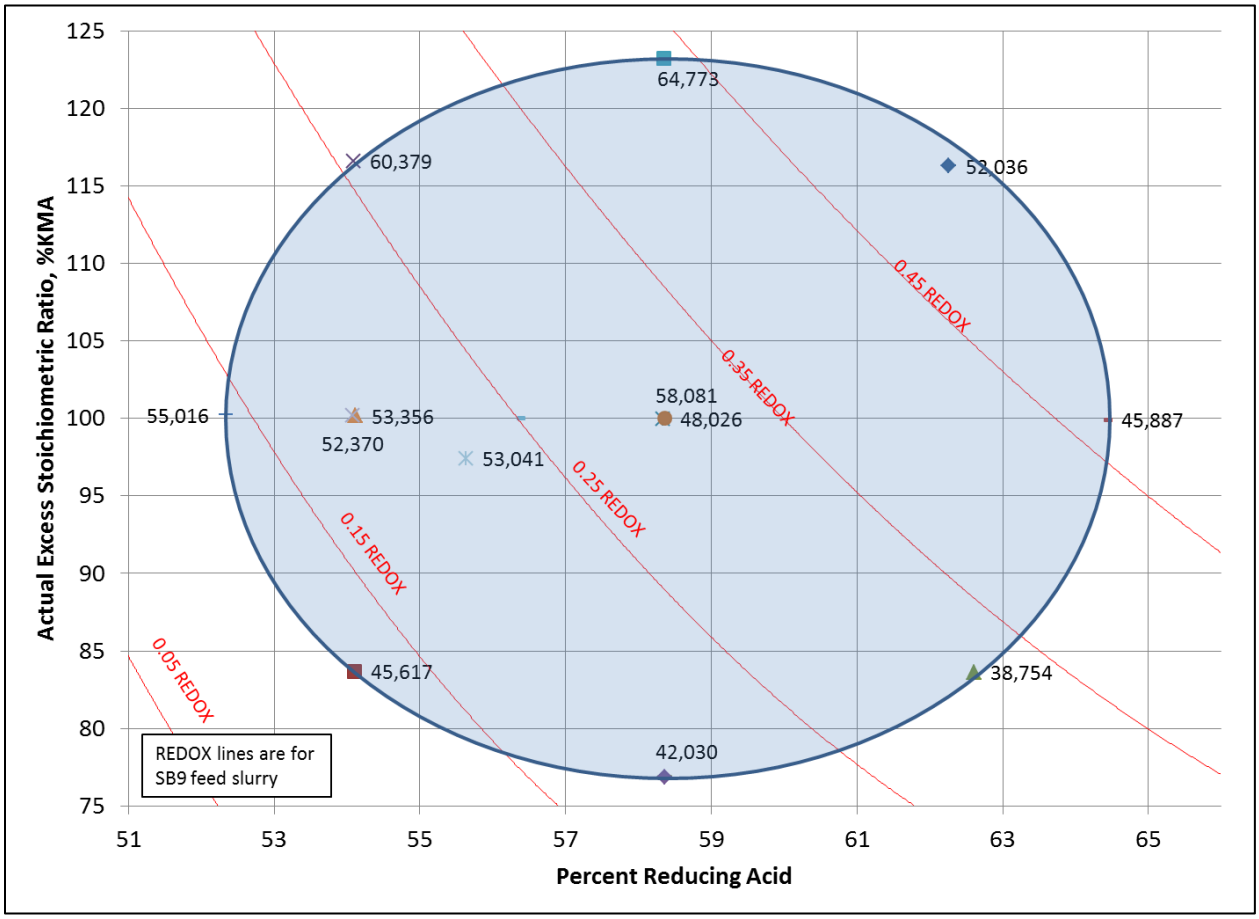

Figure 3-12. SRAT Product Nitrate Trends, mg/kg

3.1.5 Offgas Generation (Task 1i-1j in TTR[1])

The SRAT and SME offgas profiles were very similar for all runs. For all runs except NG62 (the coupled flowsheet run), the incoming nitrite, nitrate, carbonate and oxalate were identical so it isn't surprising that the offgas profiles looked similar. The NG60 offgas profile during the end of acid addition and the first ten hours of conflux is shown in Figure 3-13. Note that most of the reactions are complete within three hours after acid addition, although there was a surge of reactions as the SRAT reflux valve was opened at approximately 4 hours after acid addition.

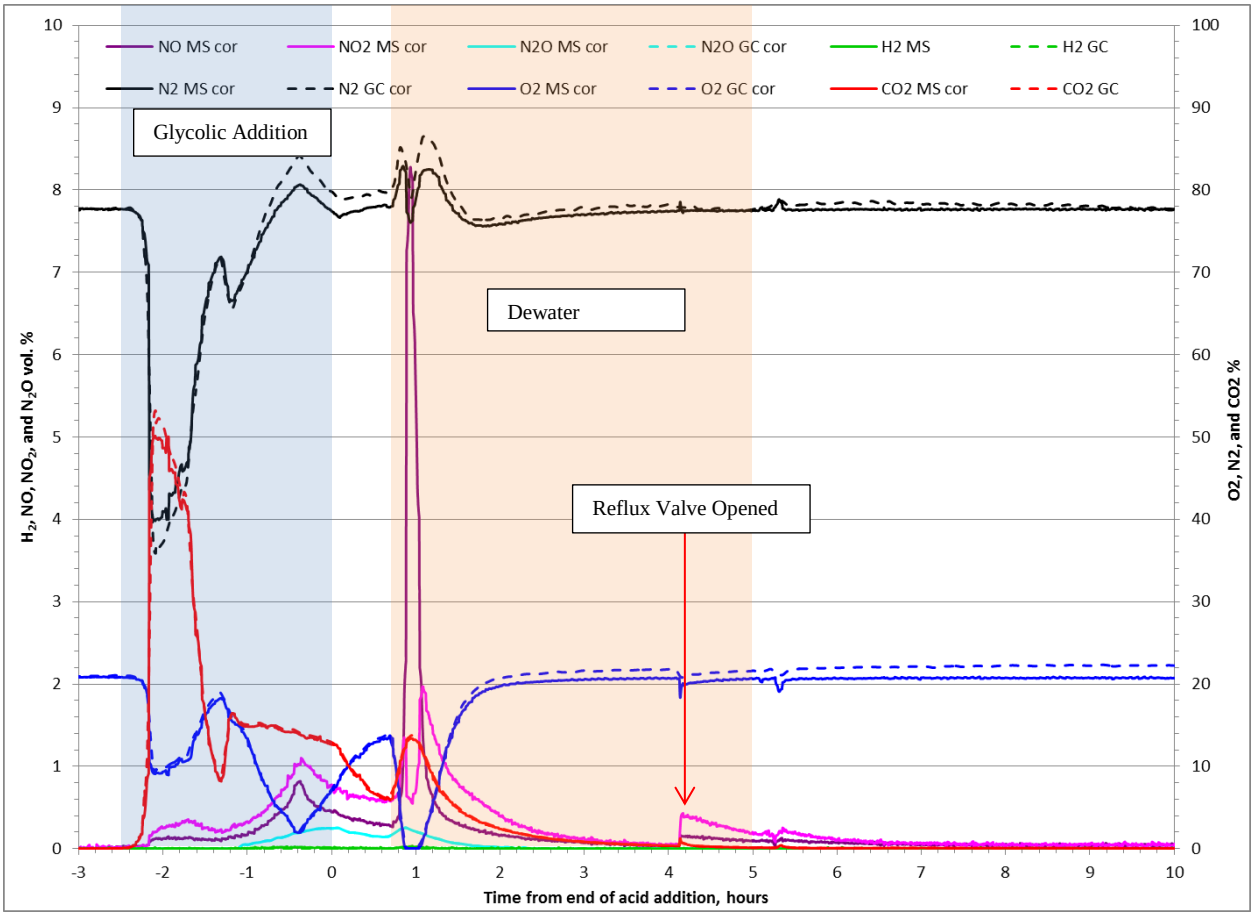

Figure 3-13. Offgas Profile for NG60, volume %

The species of highest concentration in the offgas is nitrogen. Nitrogen (N_2) is nonreactive and is not generated during processing. The expected concentration of nitrogen in the air/helium purge is 77.7% but increases and decreases due to generation of other gases or consumption of oxygen.

Oxygen usually has the second highest concentration at an expected concentration of 20.8% in the air/helium purge. During the period from late in glycolic acid addition to early in SRAT dewater, oxygen is consumed, especially in the oxidation of NO to NO_2. The N_2/O_2 ratio (Figure 3-14) should be about 3.7. During this SB9 nitric-glycolic acid flowsheet testing, a lower scaled purge of 93.7 scfm was used due to the low hydrogen generation. In periods where this ratio is much higher than 3.7 indicates oxygen is being consumed. There are two large peaks for the N_2/O_2 ratio, the first being the very end of acid addition when the O_2 concentration dropped to 2 volume %. The second occurred at the beginning of boiling, when no oxygen was detected. During both peaks, the NO concentration increases sharply due to insufficient oxygen to oxidize all of the NO to NO_2.

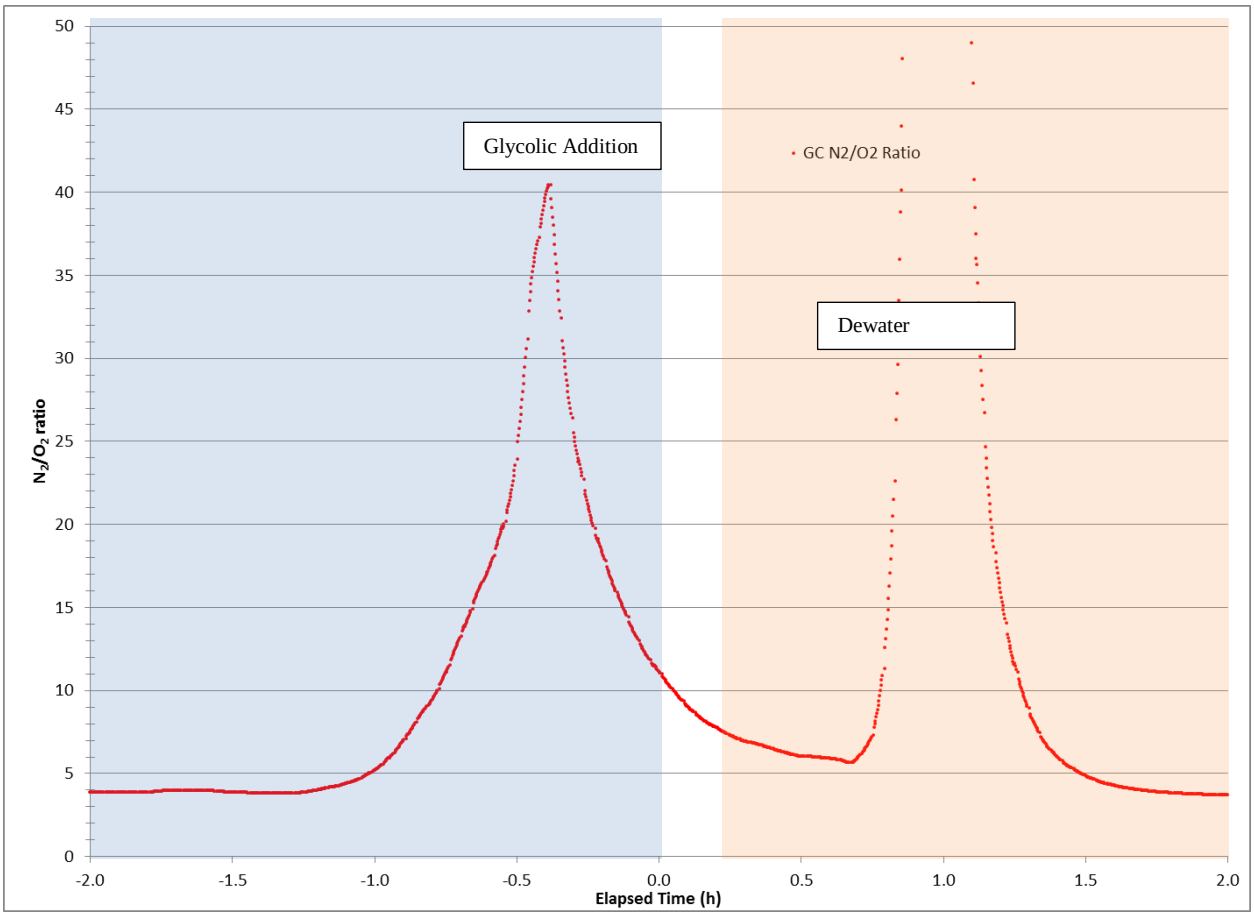

Figure 3-14. Run 60 N_2/O_2 ratio, End of Acid Addition, Beginning of Boiling

Hydrogen, the oxides of nitrogen, carbon dioxide, and HMDSO will each be discussed in a separate section. The moles of each gas produced are integrated and reported. A graph summarizing this data for NG60 is included in Figure 3-15. The offgas data was corrected to include other gases not analyzed by the GC and MS. Where available, data from all analyzers was reported for each component. In NG60, the agreement between the three analyzers was excellent.

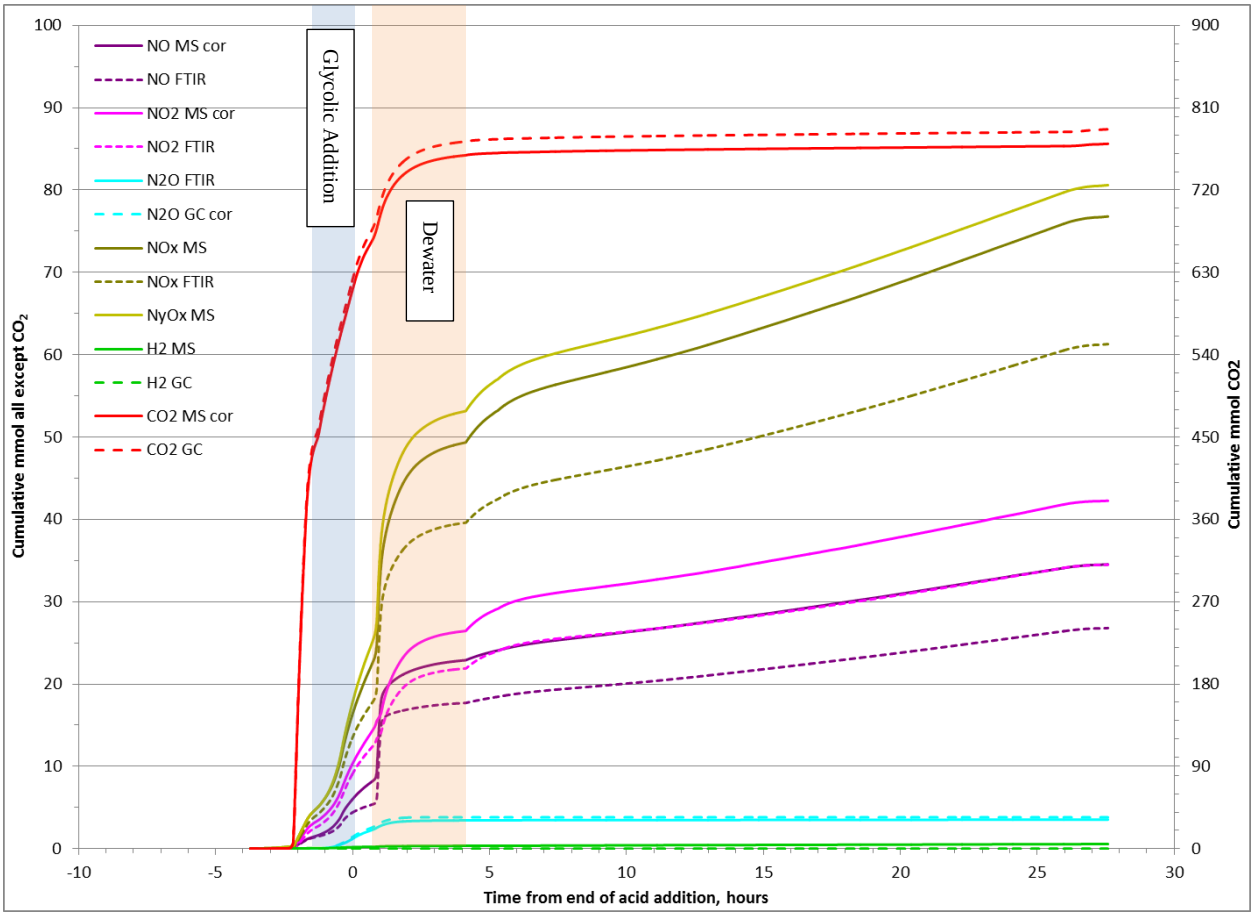

Figure 3-15. NG60 Cumulative Offgas Generation for NO, NO_2, N_2O, NO_x, N_yO_x, H_2, and CO_2

The offgas profiles of all runs are collected in Appendix C.

3.1.5.1 Hydrogen

Hydrogen is generated in nitric-glycolic acid processing. However the hydrogen concentration is almost always below the 0.006 volume % quantification limit of the GC. The GC data is presented in this section as the MS has trouble quantifying low masses at low concentrations. The MS data is included in Appendix C. In runs where hydrogen was detected but was below the quantitation limit, the results will be reported. In runs where no hydrogen was detected, the results will be reported as less than the quantitation limit. In runs NG52 and NG54, where significant hydrogen was quantified due to thick rheology, fouling, and excessive rod temperatures, a note will be added saying the hydrogen data was collected at rods temperatures in excess of DWPF steam coils. The rod temperature and hydrogen data for NG 52 and NG54 are shown in Figure 3-16. Note that the programming for the LabVIEW computer program was modified to prevent these temperatures in future testing with simulants and actual waste. Peak hydrogen generation data are summarized in Table 3-20. The SRAT cycle hydrogen concentration profile is shown in Figure 3-17.

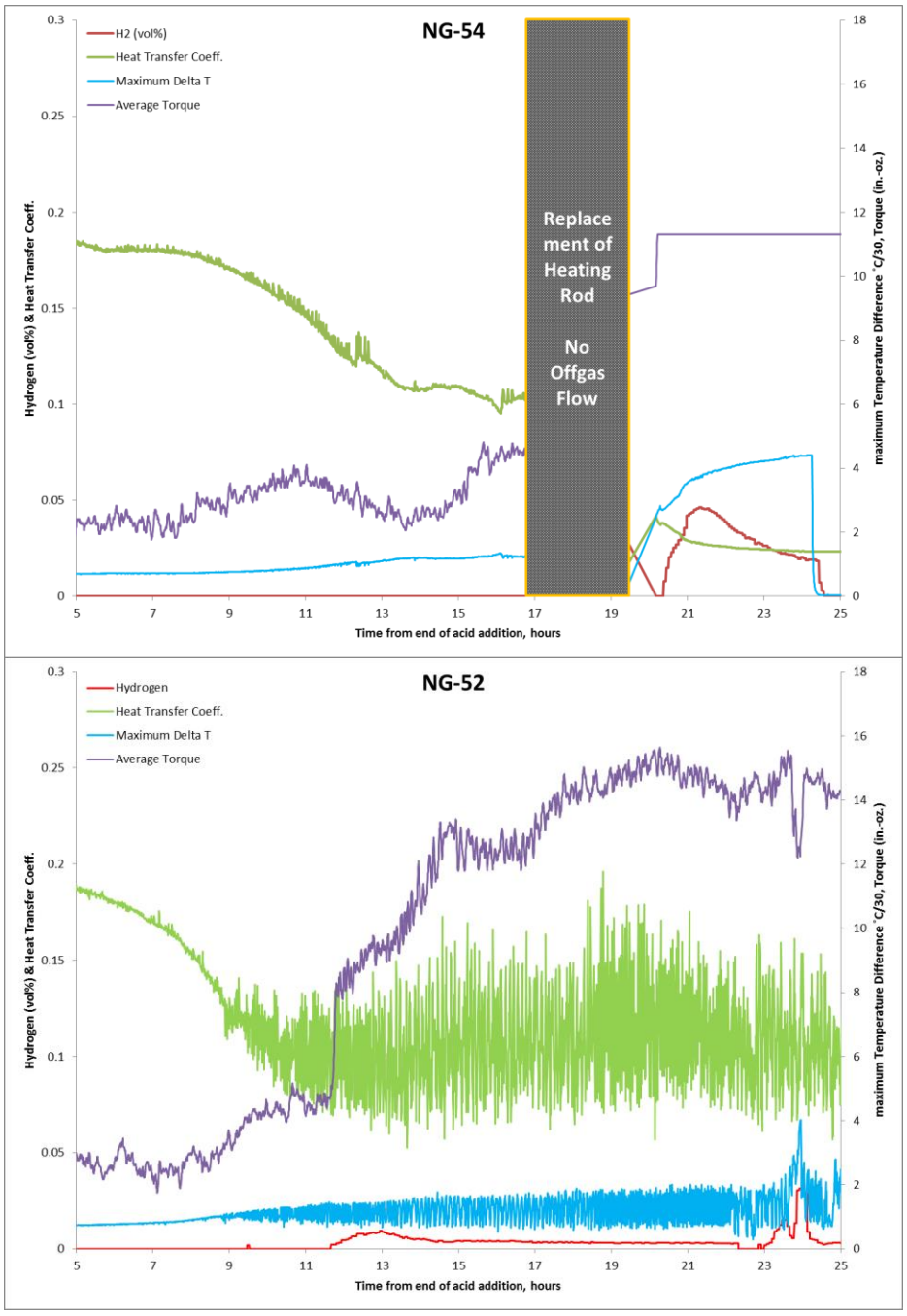

Figure 3-16. NG52, NG54 High Rod Temperature, ˚C and Hydrogen Concentration, Volume %

Table 3-20. GC Hydrogen Peak Concentration, Generation Rates

	KMA	PRA	H_2 Peak mmol/min, SRNL Scale	H_2 Peak lb/hr, DWPF Scale	H_2 Peak vol %	H_2 Total mmol, SRNL Scale
51	83.7	54.1	<0.0018	<0.0037	<0.006	N/A
52*	116	62.3	0.0048	0.0098	0.032	0.6
53	83.6	62.6	0.0005	0.0010	0.003	0.4
54*	117	54.1	0.0075	0.0155	0.049	1.5
55	100	58.3	0.0004	0.0009	0.003	0.3
55A	100	58.4	0.0004	0.0008	0.002	0.3
56	100	52.3	0.0004	0.0008	0.003	0.2
57	99.9	64.4	0.0005	0.0010	0.003	0.5
58	76.9	58.4	<0.0018	<0.0037	<0.006	N/A
59	123	58.4	<0.0018	<0.0037	<0.006	N/A
60 SRAT	100	54.1	<0.0018	<0.0037	<0.006	N/A
61 SRAT	100	54.1	<0.0018	<0.0037	<0.006	N/A
62 SRAT	97.4	55.6	0.0007	0.0014	0.004	0.9
60 SME	100	54.1	<0.0007	<0.0023	<0.006	N/A
61 SME	100	62.3	<0.0008	<0.0028	<0.006	N/A
62 SME	97.4	62.6	0.0005	0.0014	0.005	0.1

* Hydrogen data generated while heating rod temperatures exceeded 160 ˚C.

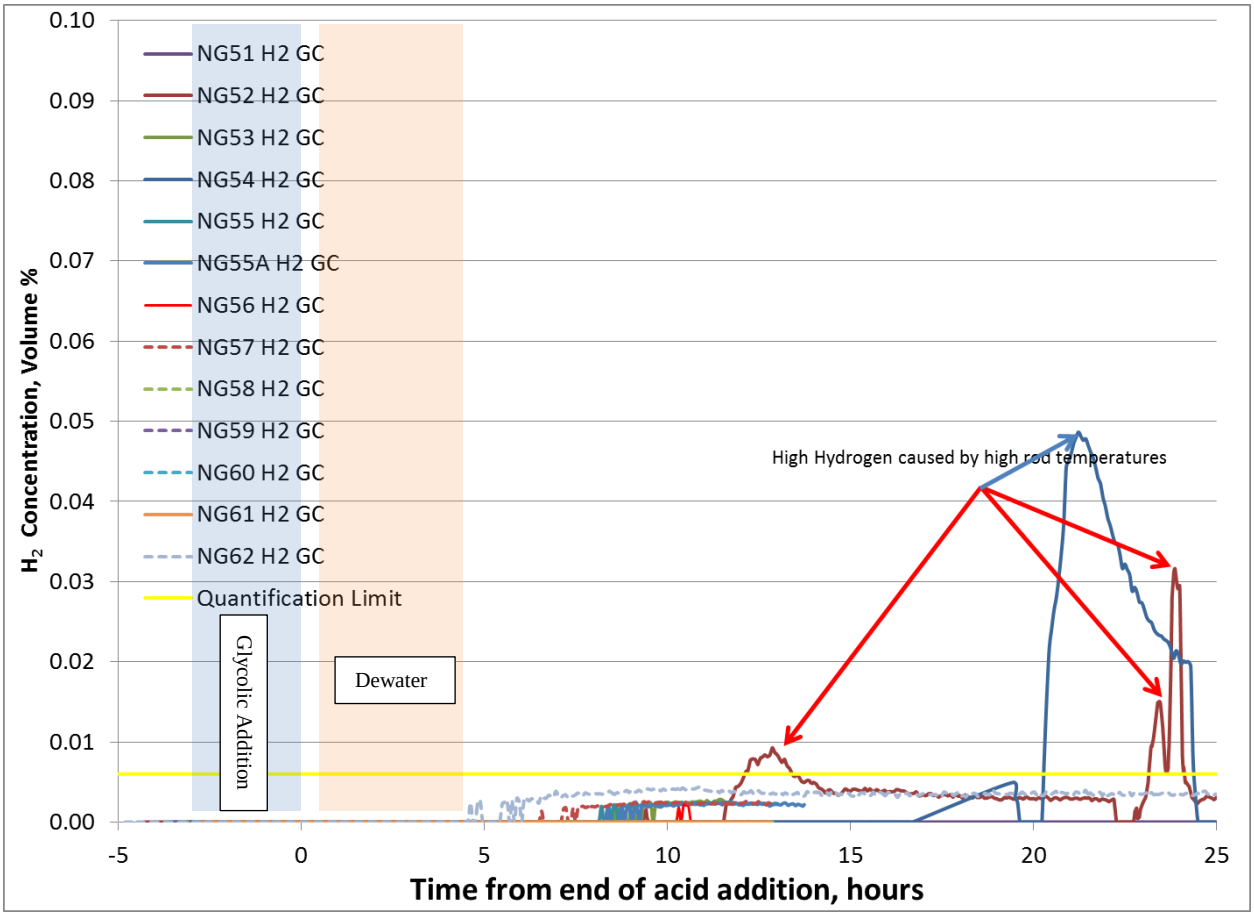

Figure 3-17. SRAT Cycle Hydrogen Concentration All Runs, Volume %

Note that hydrogen was not quantified by the GC during the NG60 andNG61 SME cycles.

3.1.5.2 Carbon Dioxide

The CO_2 peak occurred during acid addition in all runs due to the destruction of carbonate. In the high acid stoichiometry runs, because more nitric acid is added, the CO_2 peak is during nitric acid addition. In the low acid runs, the CO_2 peak is during glycolic acid addition. There is a second smaller peak during acid addition likely resulting from the reduction of mercury. There is a third peak at boiling and then the CO_2 slowly decreases throughout the rest of the SRAT cycle. The SRAT profile for the SRAT cycles is shown in Figure 3-18.

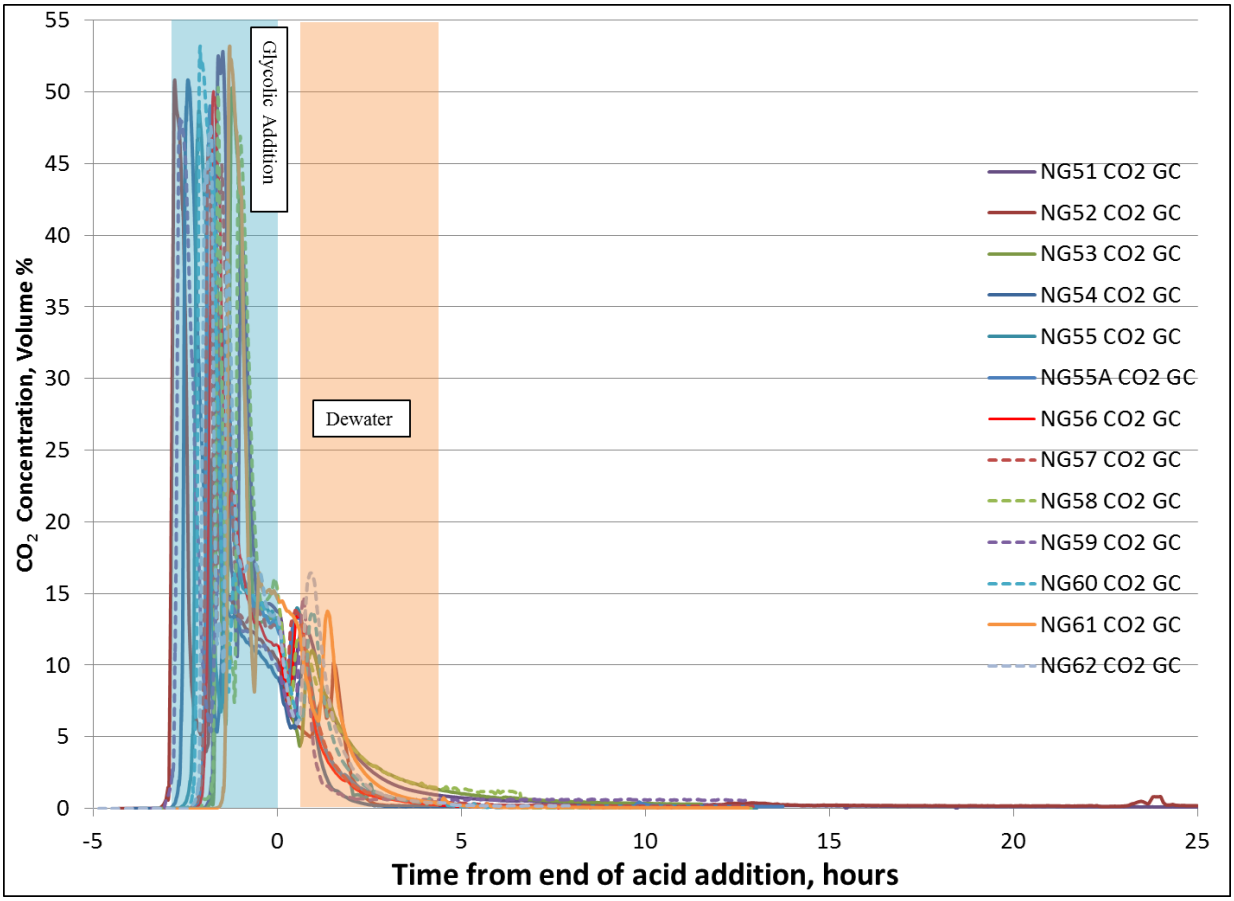

Figure 3-18. SRAT Cycle Carbon Dioxide Concentration All Runs, Volume %

Carbon monoxide was detected for brief periods during NG52 and NG54, the two runs that experienced rod fouling and high rod temperatures. No CO was detected during normal processing. Peak carbon dioxide generation data are summarized in Table 3-21. FTIR data was used where available.

Table 3-21. Carbon Dioxide Data All Runs

	CO_2 Peak mmol/min SRNL Scale	CO_2 Peak lb/hr	CO_2 Peak vol %, SRNL Scale	CO_2 Total mmol SRNL Scale
51 GC corrected	15.7	706	52.8	824
52 FTIR	15.2	684	50.8	756
53 FTIR	15.1	678	50.3	752
54 FTIR	15.6	701	50.8	737
55 GC corrected	14.2	636	48.7	701
55A GC corrected	14.9	671	49.0	743
56 FTIR	14.8	663	50.0	628
57 FTIR	14.0	631	46.4	719
58 GC corrected	14.7	662	50.3	802
59 FTIR	14.2	640	48.1	795
60 FTIR SRAT	16.3	733	53.2	745
61 FTIR SRAT	15.5	695	52.8	739
62 GC corrected SRAT	14.9	672	47.63	846
60 FTIR SME	0.069	4.9	0.676	50.4
61 FTIR SME	0.076	5.9	0.659	25.1
62 GC SME	0.091	6.1	0.920	12.8

3.1.5.3 Oxides of Nitrogen

Nitrite in the sludge decomposes primarily to NO_2, NO and N_2O. Although NO_2 is thought to be formed preferentially over NO (due to the reaction of NO and O_2 to form NO_2), NO_2 is scrubbed out in the offgas train as nitric acid. Therefore, measured concentrations of NO and NO_2 are generally comparable.

Nitrous oxide (N_2O) is an oxidant. N_2O concentration profiles for all runs are summarized in Figure 3-19. The peak concentration, peak mmol/min rates, peak lb/hr DWPF scale production rates and total mmol produced during the run are summarized in Table 3-22. Note that N_2O is generated during the period from late in glycolic acid addition to early in conflux. In higher acid runs, the N_2O generation period starts earlier (pH for destruction is achieved earlier) and ends earlier (nitrite is destroyed earlier). The lowest acid runs (NG51, NG53 and NG58) required the most time to destroy nitrite. However, even in these low-stoichiometry runs, nitrite destruction was still complete early in conflux. The high N_2O peaks after 13 hours in NG52 and NG54 were due to high rod temperatures.

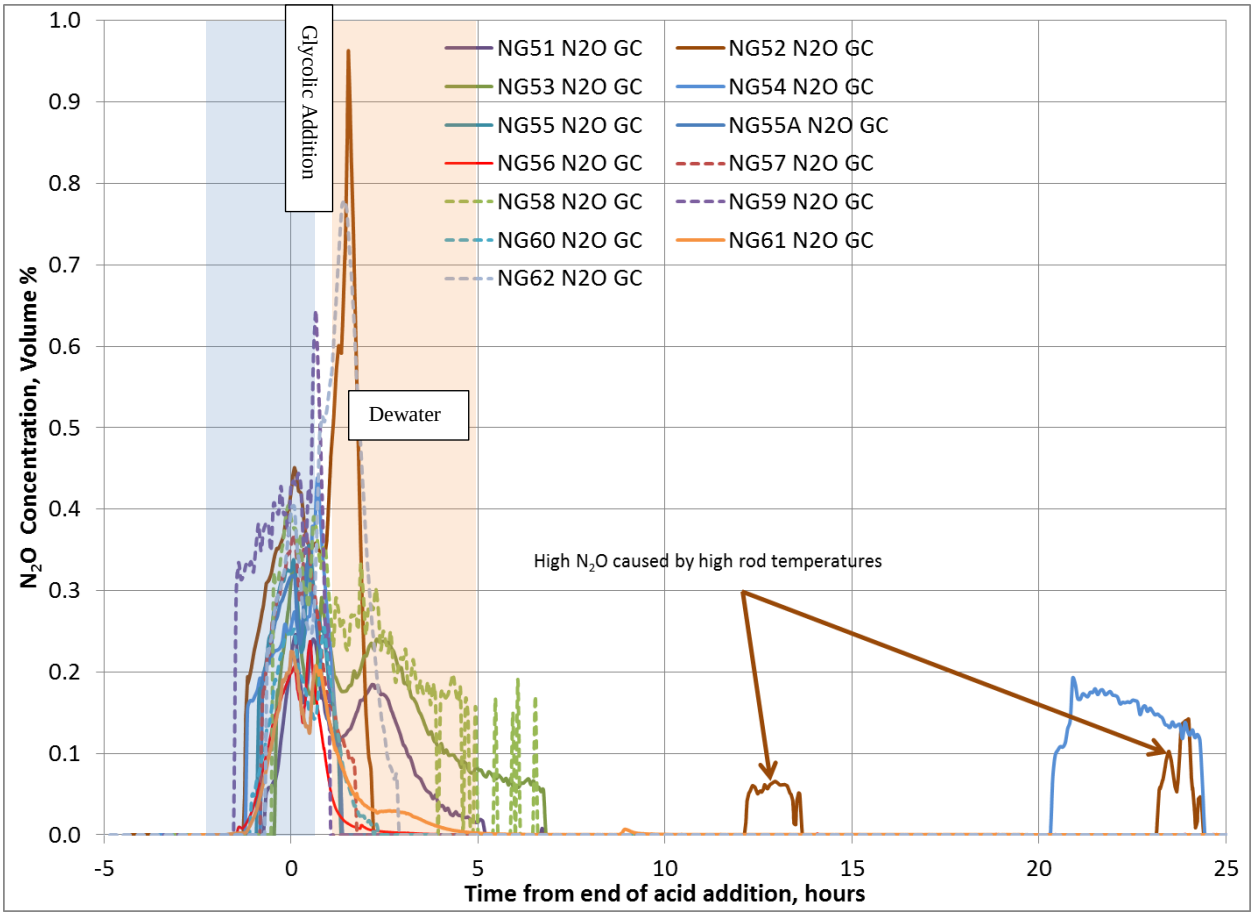

Figure 3-19. SRAT Cycle Nitrous Oxide Concentration All Runs, Volume %

Table 3-22. Nitrous Oxide Data All Runs

	N_2O Peak mmol/min SRNL Scale	N_2O Peak lb/hr, DWPF Scale	N_2O Peak vol %	N_2O Total mmol, SRNL Scale
51 GC	0.0360	1.62	0.25	5.63
52 FTIR	0.1481	6.66	1.003	15.28
53 FTIR	0.0395	1.78	0.26	8.90
54 FTIR	0.0605	2.72	0.392	8.77
55 GC	0.0529	2.38	0.36	4.92
55A GC	0.0546	2.45	0.33	4.68
56 FTIR	0.0333	1.50	0.24	2.90
57 FTIR	0.0567	2.55	0.36	4.70
58 GC	0.0613	2.76	0.40	12.04
59 FTIR	0.0682	3.07	0.458	4.93
60 SRAT FTIR	0.0339	1.52	0.233	3.53
61 SRAT FTIR	0.0317	1.43	0.23	3.65
62 SRAT GC	0.1235	5.55	0.78	12.75
60 SME FTIR	0.0003	0.02	0.003	0.03
61 SME FTIR	0.0001	0.01	0.001	0.03
62 SME GC	<0.0076	<0.51	<0.069	N/A

Nitric oxide (NO) is a second decomposition product of nitrite. The NO concentration profile is summarized in Figure 3-20. A table summarizing the NO peak concentration, peak mmol/min, peak lb/hr DWPF scale and total mmol for the run are summarized in Table 3-23. Note the NO is generated late in glycolic acid addition to early in conflux. In higher acid runs, the NO generation period starts earlier (pH for nitrite decomposition is achieved earlier) and ends earlier (nitrite is destroyed). The lowest acid runs (NG51, NG53 and NG58) had the longest time to nitrite destruction; however nitrite destruction was still complete early in conflux.

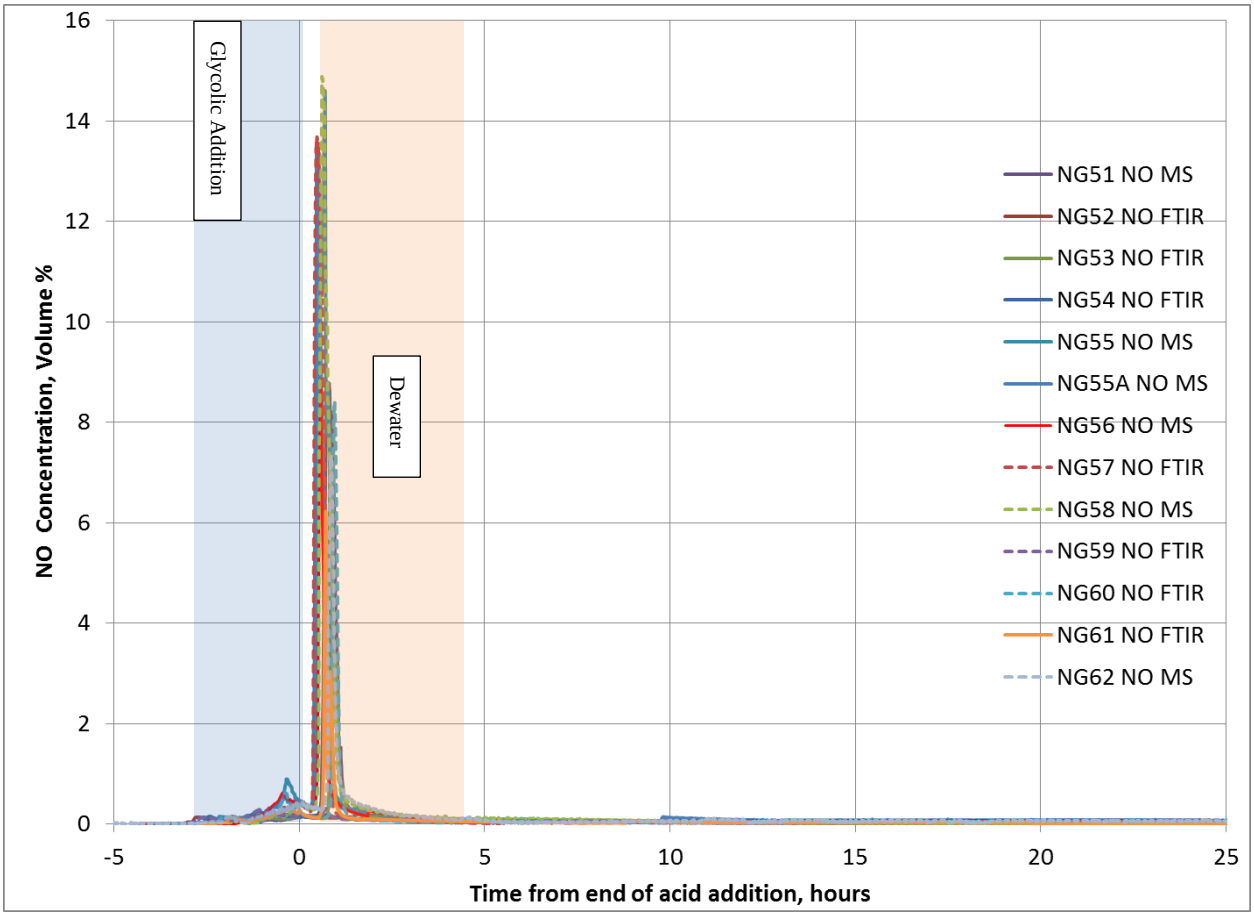

Figure 3-20. SRAT Cycle Nitric Oxide Concentration All Runs, Volume %

Table 3-23. Nitric Oxide Peak Data All Runs

	NO Peak mmol/min, SRNL Scale	NO Peak lb/hr, DWPF Scale	NO Peak vol %	NO Total mmol, SRNL Scale
51 MS	1.235	37.9	8.78	35.2
52 FTIR	0.040	1.2	0.218	17.9
53 FTIR	0.625	19.2	4.68	19.3
54 FTIR	0.046	1.4	0.247	10.0
55 MS	2.273	69.7	14.60	58.5
55A MS	2.259	69.2	13.36	53.3
56 FTIR	1.316	40.3	8.94	27.6
57 FTIR	2.443	74.9	13.68	54.4
58 MS	2.336	71.6	14.88	54.3
59 FTIR	0.046	1.4	0.309	14.9
60 SRAT FTIR	1.215	37.3	8.42	26.7
61 SRAT FTIR	0.830	25.5	6.23	16.3
62 SRAT MS	1.204	36.9	7.34	42.2
60 SME FTIR	0.003	0.1	0.03	0.7
61 SME FTIR	0.002	0.1	0.02	1.5
62 SME MS	0.004	0.2	0.04	0.5

Nitrogen dioxide (NO_2) is a third nitrite decomposition product. The NO_2 concentration profile is summarized in Figure 3-21. A table summarizing the NO_2 peak concentration, peak mmol/min, peak lb/hr DWPF scale and total mmol for the run are summarized in Table 3-24. Note the NO_2 is generated late in glycolic acid addition to early in conflux. In higher acid runs, the NO_2 generation period starts earlier (pH for decomposition is achieved earlier) and ends earlier (nitrite is destroyed earlier). The lowest acid runs (NG51, NG53 and NG58) had the longest time to nitrite destruction; however, nitrite destruction was still complete early in conflux.

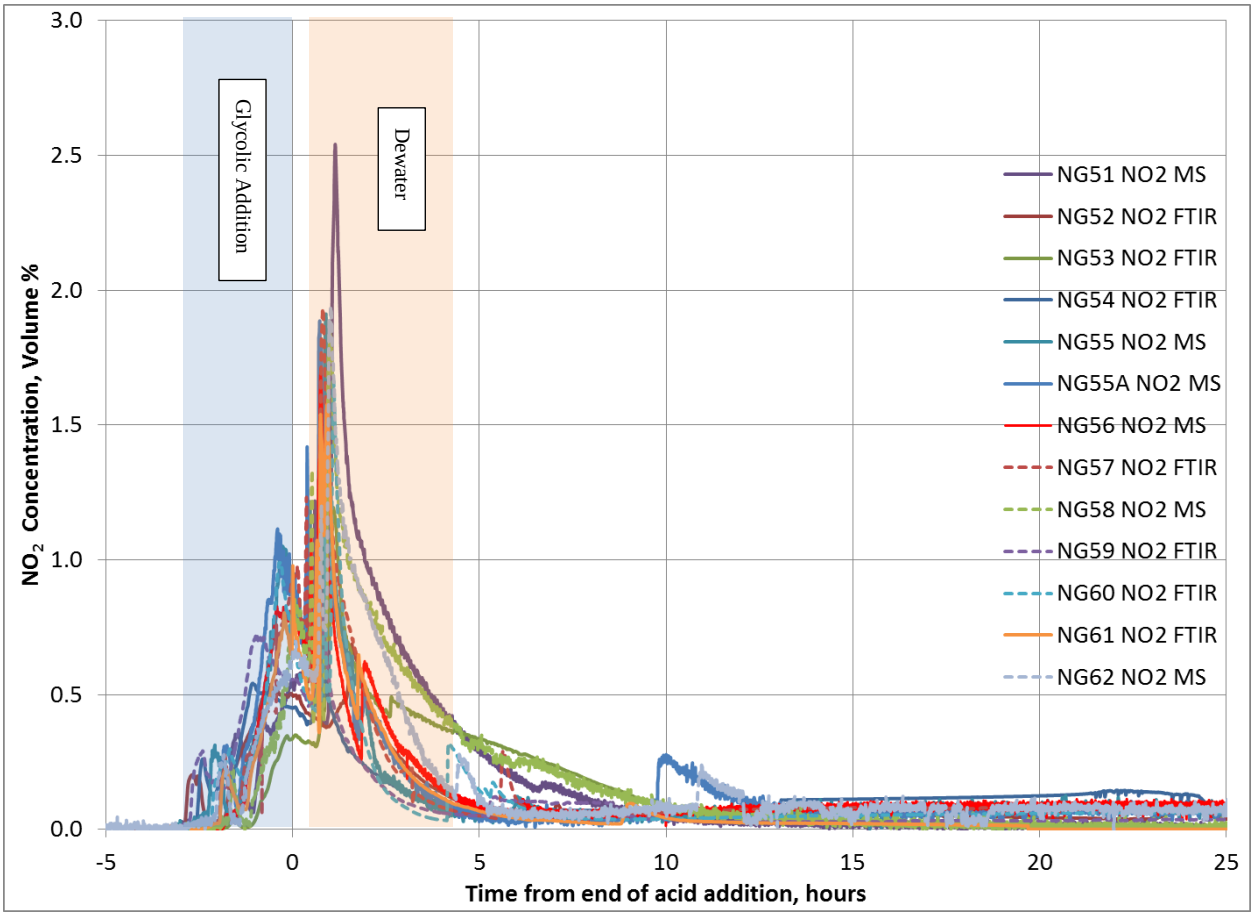

Figure 3-21. SRAT Cycle Nitrogen Dioxide Concentration All Runs, Volume %

Table 3-24. Nitrogen Dioxide Data All Runs

	NO_2 Peak mmol/min, SRNL Scale	NO_2 Peak lb/hr, DWPF Scale	NO_2 Peak vol %	NO_2 Total mmol, SRNL Scale
51 MS	0.326	15.3	2.54	46.0
52 FTIR	0.101	4.8	0.688	32.7
53 FTIR	0.159	7.5	1.19	35.4
54 FTIR	0.098	4.6	0.633	23.7
55 MS	0.260	12.2	1.91	39.6
55A MS	0.274	12.9	1.89	46.7
56 FTIR	0.194	9.1	1.43	31.9
57 FTIR	0.275	12.9	1.93	43.0
58 MS	0.250	11.7	1.88	46.2
59 FTIR	0.135	6.4	0.899	30.5
60 FTIR	0.221	10.4	1.66	34.4
61 FTIR	0.206	9.7	1.58	27.7
62 MS	0.302	14.2	1.94	55.5
60 SME FTIR	0.002	0.2	0.02	0.5
61 SME FTIR	0.001	0.1	0.01	0.6
62 SME MS	0.006	0.4	0.06	0.5

3.1.6 Ammonia (Task 1m in TTR[1])

The SRAT and SME ammonia scrubbers are designed to scrub ammonia from the offgas. Ammonia is scrubbed from the offgas to prevent the formation of ammonium nitrate (an explosive hazard) solids in the offgas piping. Ammonia can be generated during SRAT and SME processing and is released to the offgas when the ammonia/ammonium equilibrium favors ammonia (slurry pH >7). If the SRAT and SME pH is acidic, the ammonia is retained in the slurry as ammonium.

The two places to look for ammonia are the ammonia scrubber solution and the SRAT and SME products. The concentrations of ammonium in the scrubber solutions and the concentrations of ammonium in the SRAT and SME products are summarized in Table 3-25. Note that no ammonium was detected in the ammonia scrubber solutions. This indicates that if ammonium is being produced, the ammonia/ammonium equilibrium is preventing the release of ammonia to the offgas. Since, the typical SRAT/SME product is lower for nitric-glycolic acid flowsheet than the nitric-formic acid flowsheet, very little ammonia is expected to be absorbed in the ammonia scrubber. Note that a low concentration of ammonium was detected in runs NG61 and NG62. Since the slurry pH was acidic, no detectable ammonium was absorbed by the scrub solution. It is also interesting that the runs that lasted longer, runs NG61 and NG62, produced more ammonium. Processing at higher boilup rates has the advantage of shorter processing times, which gives less time for anion destruction and ammonia generation.

Table 3-25. Ammonium in Ammonia Scrubber Solution and SRAT and SME Products, mg/L

	NG51	NG52	NG60	NG61	NG62
Post Acid Scrub Solution	NA	NA	<5	<5	<5
Post SRAT Scrub Solution	NA	NA	<5	<5	<5
Post SME Scrub Solution	NA	NA	<5	<5	<5
Post SRAT Slurry	<50	<50	<5	6.26	14.2
Post SME Slurry	NA	NA	<5	6.39	11.5
Post SRAT Slurry pH	7.45	4.36	5.00	4.93	5.93
Post SME Slurry pH	NA	NA	4.43	4.94	6.09

The result is that little ammonia is produced during SRAT and SME simulant testing and the ammonia is retained as ammonium by the slurry since it is acidic. The main purpose of the scrubbers in the nitric-glycolic flowsheet is to scrub NO_2 as nitric acid, and scrub mercury and other particles from the offgas. Controlling the pH of the SMECT solution is not necessary for retaining ammonium so a neutral pH target for the scrub solution should lead to less dissolution of mercury in the SMECT. Ammonia was detected in the condensate samples from the SB9 shielded cells qualification run. There was no ammonia scrubber in the shielded cells run. The ammonia concentration was 17.7 mg/L in the MWWT, 12.7 mg/L in the post SRAT FAVC and ranged from 9.9-24.1 in the SME condensate.

3.1.7 Mercury (Additional Task b in TTR[1])

The recovery of mercury in the MWWT has been extremely poor in DWPF. During this testing, mercury stripping and recovery were quantified for each run. In an attempt to increase the mercury recovery, all runs maintained an agitator speed of 700 rpm. In addition, all runs except NG61 used design basis boilup.

The MWWT is not an ideal decanter with slow liquid flows allowing time for the mercury to coalesce. Instead, it is a busy vessel where NOx is scrubbed, mercury dissolved, other reactions are occurring, and water is continually flowing (dropping) during conflux. A photo of the MWWT during dewater is shown in Figure 3-22.

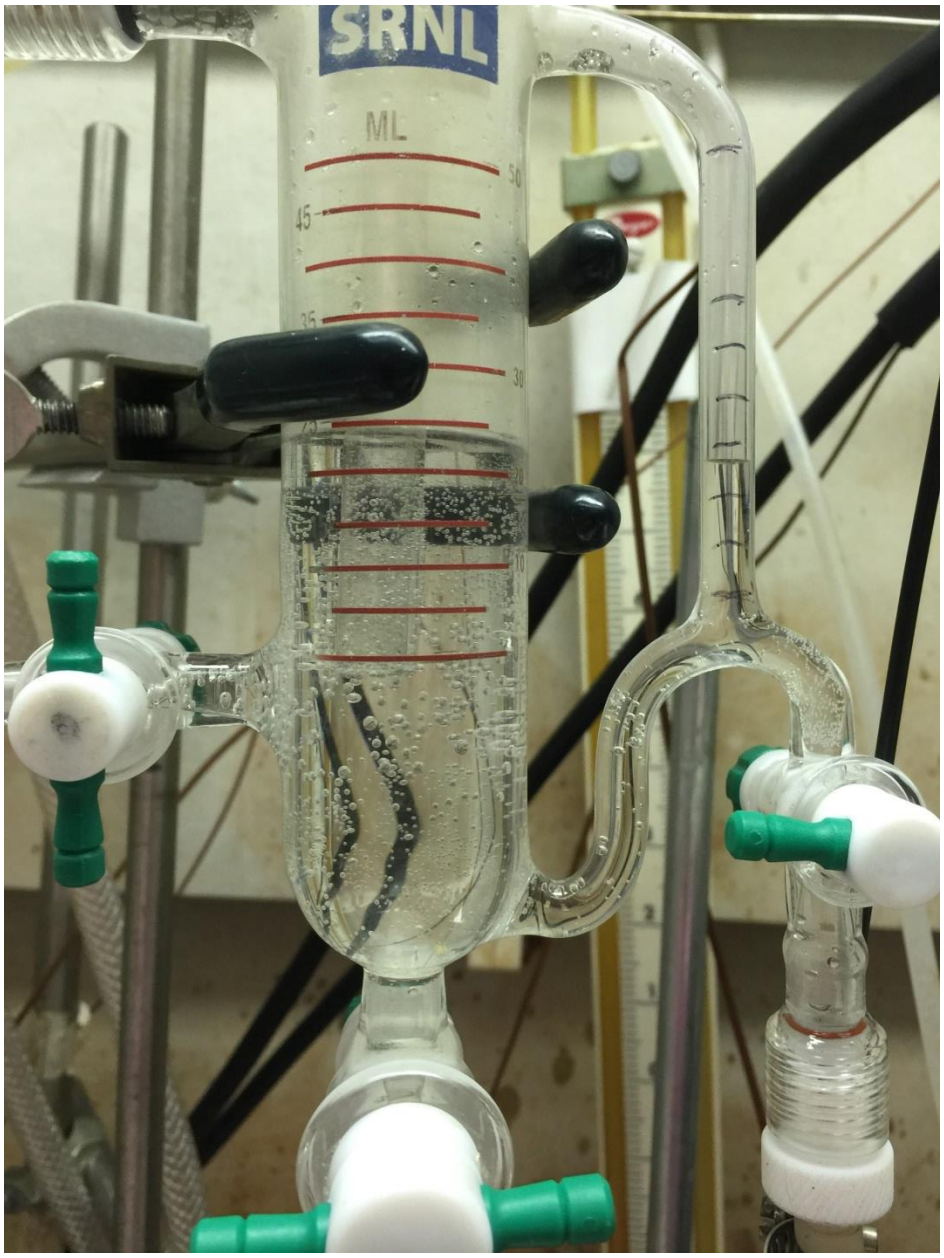

Figure 3-22. MWWT during SRAT Dewater

In each of the thirteen experiments, approximately 14.7 g of mercuric oxide (equivalent to 13.6 g of mercury) was added to target a mercury concentration of 2.48 wt% total solids basis in the sludge simulant. One goal of the SRAT cycle is to reduce the mercury loading by steam stripping the mercury to less than 0.45 wt % total solids basis in the SRAT product. In order to reach this SRAT product mercury target, steam stripping (time at boiling or conflux) is planned for approximately 36 hours at a scaled boilup rate of 5,000 lb/hr condensate or 72 hours at a scaled boilup rate of 2,500 lb/hr, assuming it takes 750 g of steam to strip 1 g elemental Hg.

SRAT slurry samples were pulled throughout the SRAT cycle. Mercury is only stripped during boiling. During dewater, the stripping rate is expected to be constant but the mercury concentration increases due to evaporation of water. So although mercury is being stripped (between 0 and 5 hours for 5000 lb/hr scaled

steam flow or between 0 and 10 hours for 2500 lb/hr scaled steam flow), the expected mercury concentration increases from about 3300 mg/kg to 4200 mg/kg. Once dewater is complete, the mercury concentration is expected to decrease linearly until SRAT boiling is complete (targeting a final mercury concentration of 1125 mg/kg or 0.45 wt %). A graph of the mercury concentration versus time at boiling for Runs NG60, NG61 and NG62 is summarized in Figure 3-23. The projected mercury trend is added for the design boilup runs (NG60 and NG62, purple line for 5000 lb/hr scaled steam flow). The projected mercury trend is added for the prototypic boilup run (NG61, orange line for 2500 lb/hr scaled steam flow).

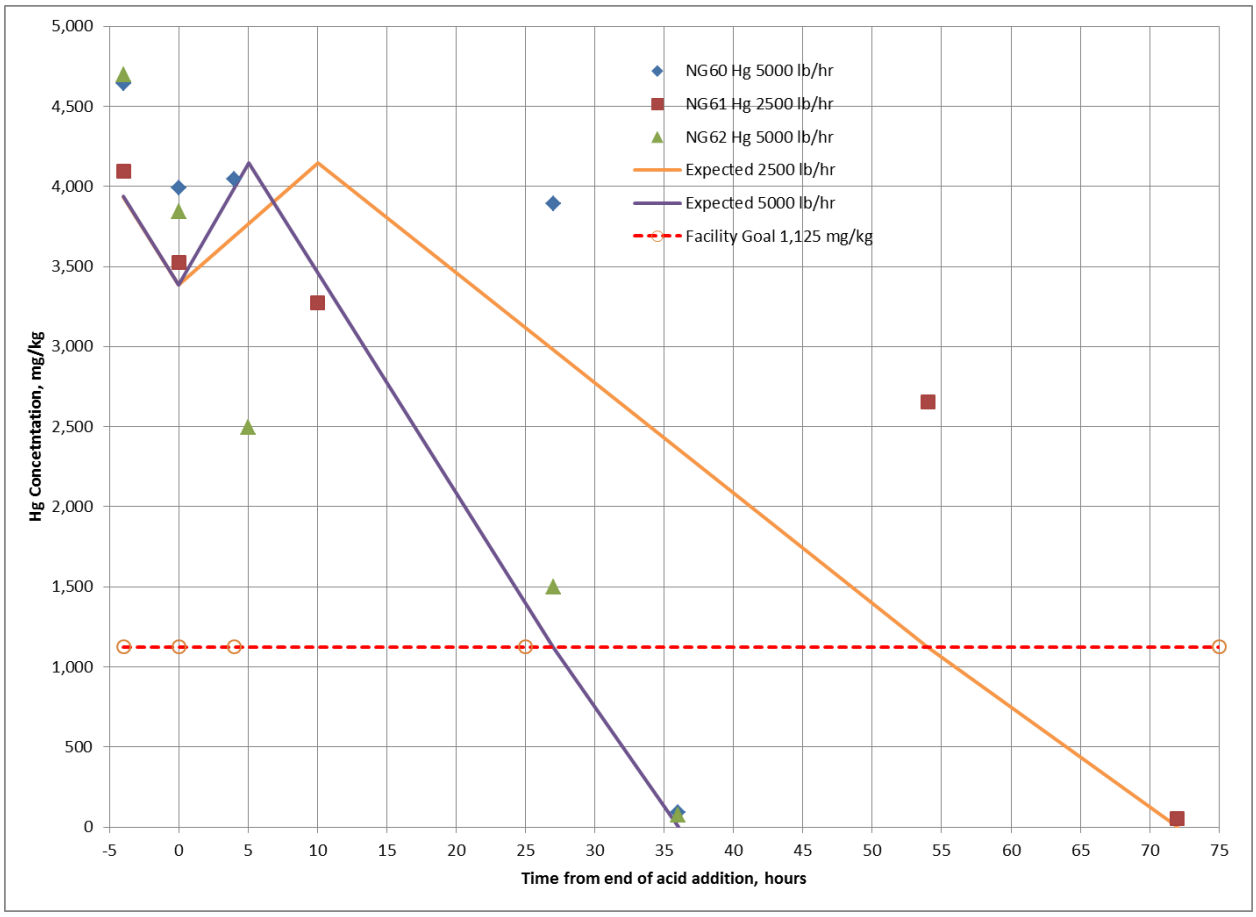

Figure 3-23. Mercury Concentration in NG 60, NG61 and NG62 SRAT Cycles

At the completion of each SRAT cycle, the MWWT contents were drained to a sample bottle. The aqueous liquid in the sample bottle was transferred to a second sample bottle, leaving the mercury (and a small amount of water) in the first sample bottle, which was placed in a desiccator for at least a week. The dried mercury was weighed. The mercury added, the MWWT collected mercury, the % mercury recovery, the measured mercury in the SRAT product, and the calculated mercury from each run is summarized in Table 3-26. The mercury in the SRAT product was calculated assuming any mercury not collected in the MWWT is still in the SRAT product.

Table 3-26. Mercury Added, recovered, and calculated mercury concentration in SRAT product

Run	Boilup Rate, lb/hr DWPF Scale	Mercury Oxide Added, g	Hg Added, g	Mercury collected MWWT, g	% Recovered in MWWT	Measured Hg in SRAT Product		Calculated Hg In SRAT Product, mg/kg
						mg/kg*	wt % TS	
NG51	5000	14.66	13.58	4.17	30.7	170	0.055	2,719
NG52	5000	14.66	13.58	6.83	50.3	1,610	0.610	1,358
NG53	5000	14.66	13.58	5.38	39.6	270	0.090	3,724
NG54	5000	14.66	13.58	5.91	43.5	#	#	4,127
NG55	5000	14.66	13.58	10.98	80.8	213	0.062	3,122
NG55A	5000	14.61	13.53	7.82	57.8	82	0.041	1,305
NG56	5000	14.66	13.58	11.00	81.0	432	0.140	1,682
NG57	5000	14.67	13.59	8.28	60.9	135	0.044	1,161
NG58	5000	14.66	13.58	7.32	53.9	64	0.021	4,380
NG59	5000	14.66	13.58	11.16	82.2	195	0.104	3,153
NG60	5000	14.65	13.57	10.03	73.9	269	0.105	2,430
NG61	2500	14.66	13.58	3.10	22.8	274	0.102	2,942
NG62	5000	14.66	13.58	3.97	29.2	108	0.042	632

* Aqua Regia digestion of entire sample followed by ICP-AES analysis for Hg
# Sample mass not recorded – concentration cannot be calculated

The mercury recovery was much higher than expected. A typical mercury recovery for SRNL testing is ~30%. In these runs, the mercury recovery was as high as 82% in the MWWT. Note the difference in mercury collection between runs NG60 and NG61, with the only difference being the boilup rate. Run NG60 had 3x higher mercury recover than NG61 (lower boilup rate). This may demonstrate the importance of high steam flow on mercury recovery. It is expected that agitation speed is key to improved mercury recovery, although this was not varied in these runs. Good mixing and high boilup rates should work together to disperse the mercury more uniformly and should lead to better steam stripping. One other surprise was the lower mercury recovery in NG62, the coupled run with added PRFT and SEFT simulants. Little testing has been done with PRFT and SEFT and more testing is recommended to determine the repeatability of the lowered mercury recovery and better understand mercury speciation under the coupled flowsheet.

Elemental mercury is the assumed form of mercury collected in the MWWT. If other forms or other impurities are present, they could change the mercury mass post desiccation. The mercury from runs NG51 and NG52 were completely digested and analyzed by ICP-AES. The results are reported in Table 3-27. Si was the only metal impurity reported above 10 mg/kg level, (likely antifoam or an antifoam degradation product) at 25.1 and 28 mg/kg. The sample collected from the MWWT was measured and reported as 1.23 E6 mg/kg Hg (15% 1 sigma uncertainty) and was therefore determined to be primarily elemental mercury.

Table 3-27. Impurities in NG51 and NG52 MWWT Mercury, mg/kg

	BLANK		NG51 MWWT Mercury		NG52 MWWT Mercury	
Element	**Result**	**Uncertainty**	**Result**	**Uncertainty**	**Result**	**Uncertainty**
Ag	< 0.735	(N/A %RSD)	3.77	(13.8 %RSD)	< 0.726	(N/A %RSD)
Al	< 1.52	(N/A %RSD)	1.44	(110 %RSD)	3.84	(13.6 %RSD)
B	< 0.53	(N/A %RSD)	< 0.483	(N/A %RSD)	< 0.524	(N/A %RSD)
Ba	< 0.083	(N/A %RSD)	< 0.076	(N/A %RSD)	< 0.082	(N/A %RSD)
Ca	< 0.119	(N/A %RSD)	0.336	(10 %RSD)	0.387	(13 %RSD)
Cd	< 0.144	(N/A %RSD)	< 0.131	(N/A %RSD)	< 0.142	(N/A %RSD)
Ce	< 2.29	(N/A %RSD)	< 2.09	(N/A %RSD)	< 2.26	(N/A %RSD)
Co	< 0.19	(N/A %RSD)	< 0.173	(N/A %RSD)	< 0.187	(N/A %RSD)
Cr	< 0.083	(N/A %RSD)	< 0.076	(N/A %RSD)	< 0.082	(N/A %RSD)
Cu	10.9	(11 %RSD)	5.82	(14.3 %RSD)	0.761	(115 %RSD)
Fe	< 0.096	(N/A %RSD)	1.85	(10.3 %RSD)	5.53	(10.3 %RSD)
K	< 12.1	(N/A %RSD)	< 11	(N/A %RSD)	< 11.9	(N/A %RSD)
La	< 0.332	(N/A %RSD)	< 0.303	(N/A %RSD)	< 0.328	(N/A %RSD)
Li	< 0.16	(N/A %RSD)	< 0.146	(N/A %RSD)	< 0.158	(N/A %RSD)
Mg	< 0.051	(N/A %RSD)	< 0.046	(N/A %RSD)	< 0.05	(N/A %RSD)
Mn	< 0.206	(N/A %RSD)	< 0.204	(N/A %RSD)	< 0.204	(N/A %RSD)
Mo	< 0.663	(N/A %RSD)	< 0.604	(N/A %RSD)	< 0.655	(N/A %RSD)
Na	< 1.18	(N/A %RSD)	< 1.08	(N/A %RSD)	< 1.17	(N/A %RSD)
Nb	< 0.475	(N/A %RSD)	< 0.433	(N/A %RSD)	< 0.469	(N/A %RSD)
Nd	< 0.804	(N/A %RSD)	< 0.734	(N/A %RSD)	< 0.795	(N/A %RSD)
Ni	< 0.156	(N/A %RSD)	< 0.142	(N/A %RSD)	< 0.154	(N/A %RSD)
P	< 0.896	(N/A %RSD)	< 0.817	(N/A %RSD)	< 0.885	(N/A %RSD)
Pb	< 0.373	(N/A %RSD)	< 10	(N/A %RSD)	< 10	(N/A %RSD)
Re	< 0.51	(N/A %RSD)	< 0.465	(N/A %RSD)	< 0.504	(N/A %RSD)
S	< 0.677	(N/A %RSD)	< 0.618	(N/A %RSD)	< 0.669	(N/A %RSD)
Si	6.2	(26.5 %RSD)	25.1	(10.3 %RSD)	28	(10.5 %RSD)
Sn	< 2.72	(N/A %RSD)	< 2.48	(N/A %RSD)	< 2.69	(N/A %RSD)
Sr	< 4.9	(N/A %RSD)	< 4.47	(N/A %RSD)	< 4.84	(N/A %RSD)
Ti	< 0.156	(N/A %RSD)	< 0.143	(N/A %RSD)	< 0.154	(N/A %RSD)
V	< 0.261	(N/A %RSD)	< 0.238	(N/A %RSD)	< 0.258	(N/A %RSD)
Zn	< 0.326	(N/A %RSD)	< 0.297	(N/A %RSD)	< 0.322	(N/A %RSD)
Zr	< 0.227	(N/A %RSD)	< 0.207	(N/A %RSD)	0.364	(23 %RSD)

In some of the later SRAT-only runs, the SRAT product slurry was carefully poured out in an attempt to recover any unstripped elemental mercury. In NG61, a run with poor mercury recovery, 6.22 g of elemental mercury was recovered from the SME product. This confirms the poor mercury recovery in this run. Contrast this to NG55, a run with excellent mercury recovery where only 1.22 g of mercury was recovered from the SRAT product. This suggests that the rate limiting step for mercury removal is physical and not chemical.

A mass balance was completed for all the runs and the results are summarized in Table 3-28.

Table 3-28. Mercury Mass Balance

Run	Elemental Hg Added, g	Mercury collected MWWT, g	Mercury Collected SRAT Product, g	Mercury * in Empty Kettle, g	Total Out, g	% Hg Balance
NG51	13.58	4.17	0.37	NA	4.54	33.4%
NG52	13.58	6.83	4.00	NA	10.83	79.7%
NG53	13.58	5.38	0.59	NA	5.97	44.0%
NG54	13.58	5.91	NA	NA	5.91	43.5%
NG55	13.58	10.98	0.42	1.09	12.50	92.0%
NG55A	13.53	7.82	0.28	NA	8.10	59.9%
NG56	13.58	11.00	0.96	0.87	12.83	94.5%
NG57	13.59	8.28	0.29	NA	8.57	63.1%
NG58	13.58	7.32	0.14	NA	7.46	54.9%
NG59	13.58	11.16	0.75	NA	11.91	87.7%
NG60	13.57	10.03	0.70	NA	10.73	79.1%
NG61	13.58	3.10	0.70	6.22	10.02	73.8%
NG62	13.58	3.97	0.33	NA	4.30	31.7%

* In some of the runs the SRAT contents were poured out slowly, leaving elemental Hg behind. This Hg was weighed and the mass included.

The impact of acid stoichiometry and percent reducing acid was one of the objectives of this testing. A graph showing the concentration of mercury in the SRAT products is included as Figure 3-24. The higher acid stoichiometry led to higher mercury recovery. The two high acid runs with low Hg recovery were NG52 and NG54, both with very thick rheology which likely hindered steam stripping. Note that the highest acid stoichiometry run (NG59) had similar recovery to the mid acid runs but had to be processed at 20 wt % total solids target to eliminate the problems with high rheology. This suggests that processing the slurry at the optimum acid stoichiometry and total solids should lead to higher mercury recovery.

One other note pertinent to mercury recovery occurred in NG55. The SRAT chiller water level dropped below the low level and the pump automatically shut off. During a period of about 30 minutes, there was no cooling water flow to the SRAT condenser and the SRAT condenser cooling water exit temperature increased to about 98 ˚C. During this time the ammonia scrubber served as the condenser and the volume of the scrubber liquid increased by about 100 g. At the completion of processing, a comment mentioned that mercury beads were identified in the ammonia scrubber. This was not seen in any of the other runs without the high condenser temperature. A high condenser temperature in DWPF is expected to lead to less mercury collection in the MWWT and more mercury collected in the SMECT.

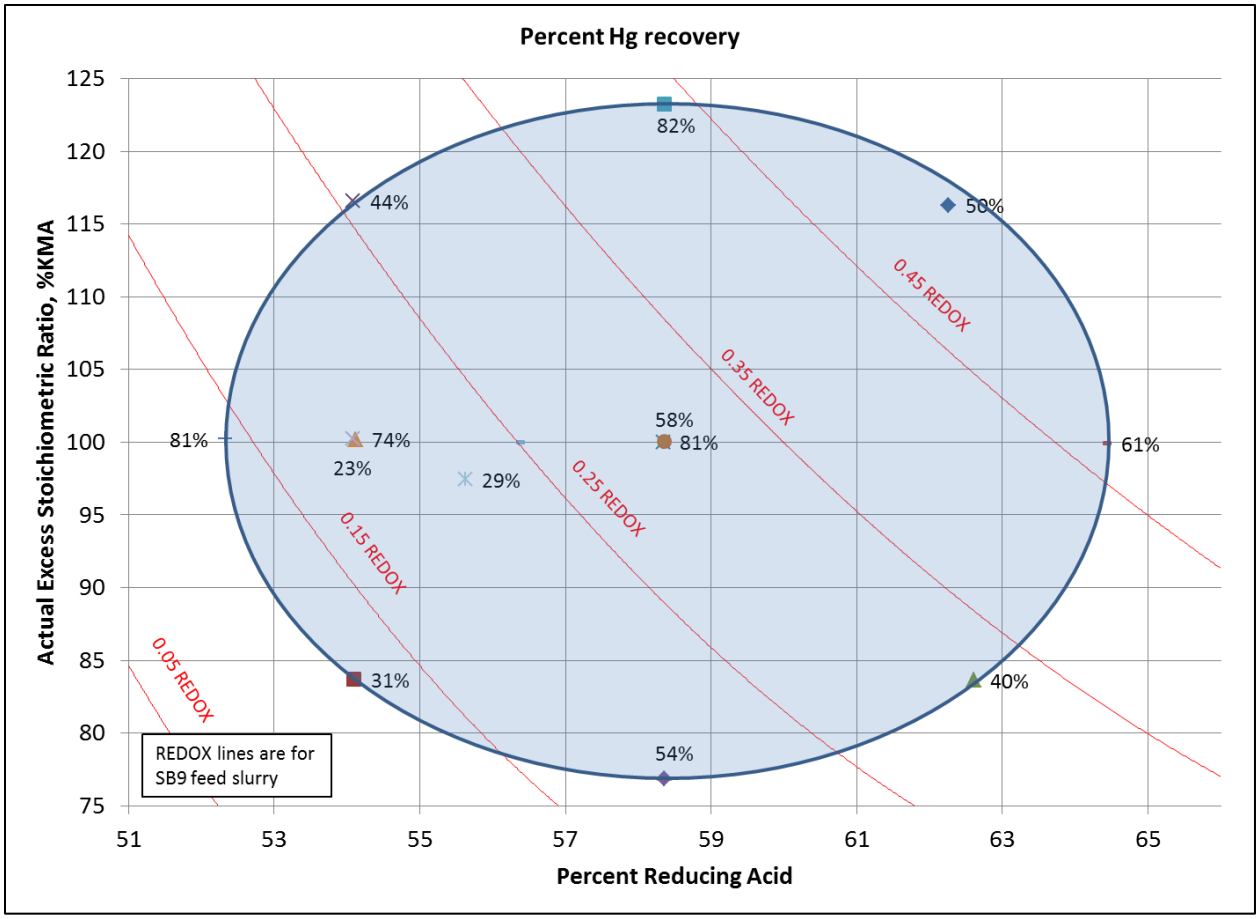

Figure 3-24. Percent Mercury Recovery as a Function of KMA and Percent Reducing Acid

3.1.8 REDOX

REDOX is a measure of the oxidation potential of the glass, as measured as $Fe^{2+}/\Sigma Fe$. A glass that is too oxidizing will evolve more oxygen from the melt pool leading to foaming. A glass that is too reducing may shorten the melter life. Typically a REDOX of about 0.09-0.33 (without bubbling in melter) would be targeted. REDOX results are typically reported with an uncertainty of ±0.1, as there is variability in measuring REDOX.

Runs NG51-59 were designed to produce a wide REDOX target by varying the percent reducing acid. The REDOX targets varied from about 0.09 to 0.5 for Runs NG51-59. Runs NG60-62 all had a REDOX target of about 0.2.

The acid calculation spreadsheet result for PRA and %KMA (using the actual mass of nitric and glycolic acid added) are summarized in columns 2 and 3 in Table 3-29. Based on this data, the acid calculation spreadsheet prediction of the glass REDOX is included in column 4 of Table 3-29. The REDOX was calculated using the concentration of anions and Mn in the SRAT or SME product. For SRAT products, the mass of frit to achieve a waste loading of 38% and the mass of water to add or remove to target a SME product of 48 wt% total solids was calculated. The concentration of the anions and Mn were recalculated using the mass of frit and water. The resulting anion and Mn concentrations were used to calculate REDOX,

The REDOX data is furthest from the target for the highest acid stoichiometry runs. A graph showing the data for all runs is summarized in Figure 3-25.

REDOX can be calculated using the interim REDOX prediction.[20]

$$\frac{Fe^{2+}}{\Sigma Fe} = 0.2358 + 0.1999*(2[F] + 4[C] = 6[G] + 4[O] - 5[N] - 0[Mn])*45/T \qquad \text{Equation 7}$$

[F] = formate (mol/kg feed)
[C] = coal (carbon) (mol/kg feed)
[O] = oxalate (soluble and insoluble) (mol/kg feed)
[G] = glycolate (mol/kg feed)
[N] = nitrate + nitrite (mol/kg feed)
[Mn] = manganese (mol/kg feed)
T = Total Solids (wt %)

The REDOX was also measured. This data is summarized in column 5 of Table 3-29.

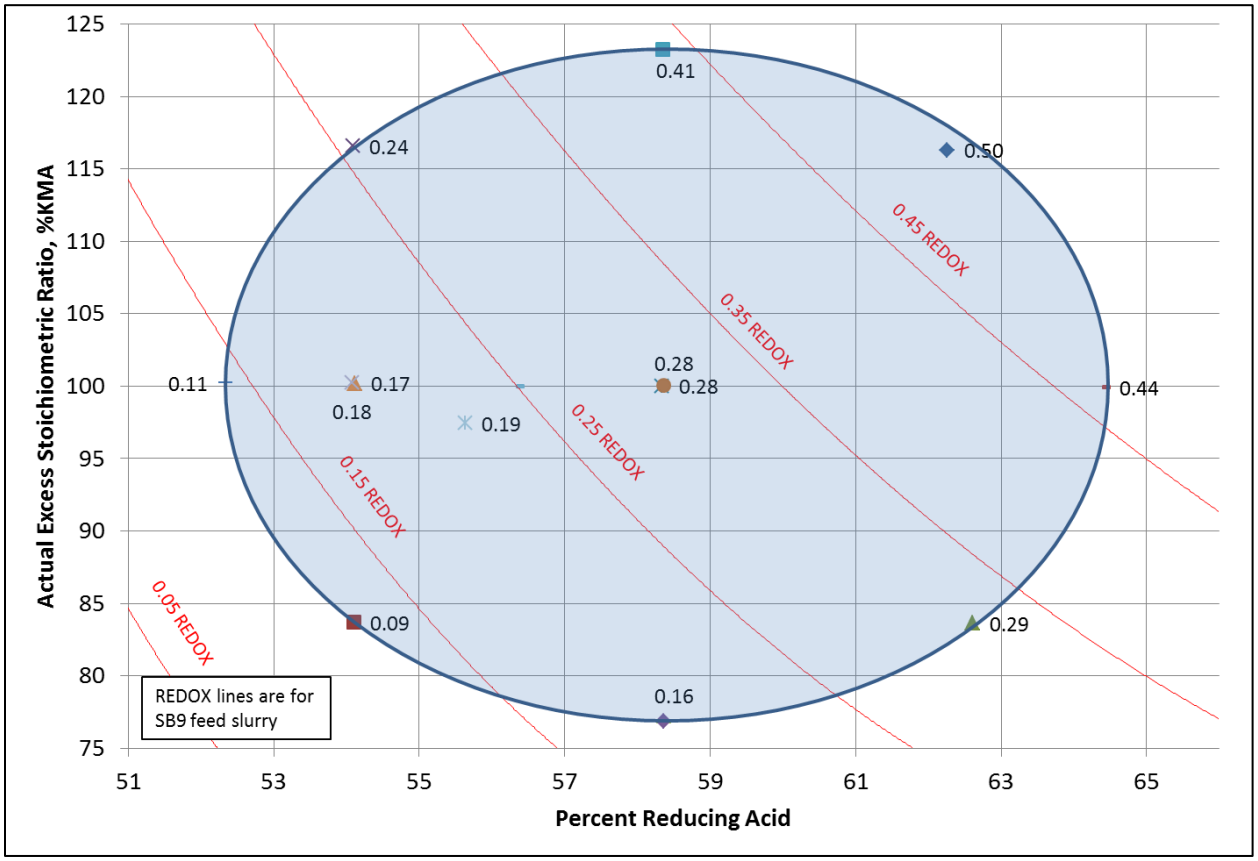

Figure 3-25. Predicted REDOX based on SRAT or SME Product Composition

The glass was prepared for REDOX measurement by two ways. Since the slurry was lower in sodium than the actual waste, additional sodium hydroxide was added in order to produce a lower viscosity glass. The sodium hydroxide was a replacement for the insoluble sodium that was not included in the SB9A sludge. For the SRAT only runs, the SRAT product was combined with frit 803 to produce a 38% waste loading slurry. After adding sodium hydroxide, the waste loading was 41.0-43.1%The melter feed was dried, melted, and the resulting glass was analyzed for Fe^{+2} and Fe^{+3}, allowing the REDOX to be calculated. For runs NG61-62, the SME products (made with frit 803) were combined with additional frit to produce a 38%

waste loading slurry. Sodium hydroxide was added to replace the insoluble sodium. The melter feed was dried, melted, and the resulting glass was analyzed for Fe^{+2} and Fe^{+3}, allowing the REDOX to be calculated. The results are summarized in the last column of Table 3-29.

Table 3-29. REDOX data for all runs (shaded data excluded from REDOX database)

Run number	Acid Calc Predictions Using Actual Masses			Anion Prediction	Measured Frit 803
	PRA	% KMA	REDOX, $Fe^{2+}/\Sigma Fe$	REDOX, $Fe^{2+}/\Sigma Fe$	REDOX, $Fe^{2+}/\Sigma Fe$
NG51	54.1	83.7	0.12	0.18	0.06, 51.2% rsd, n=2
NG52	62.3	116.3	0.52	0.41	0.62, 0.3% rsd, n=3
NG53	62.6	83.6	0.31	0.34	0.57, 8.1% rsd, n=3
NG54	54.1	116.6	0.26	0.11	0.19, 26% rsd, n=3
NG55	58.3	100.0	0.31	0.23	0.29, 17% rsd, n=3
NG55A	58.4	100.0	0.30	0.15	0.34, 42% rsd, n=6
NG56	52.3	100.2	0.14	0.08	<0.03, NA, n=2
NG57	64.4	99.9	0.46	0.47	0.53, 3.2% rsd, n=3
NG58	58.4	76.9	0.18	0.29	0.04, 3.4% rsd, n=2
NG59	58.4	123.2	0.44	0.20	0.58, 18% rsd, n=2
NG60	54.1	100.2	0.19	0.13	0.11, 41% rsd, n=3
NG61	54.1	100.2	0.19	0.08	<0.03, NA, n=6
NG62	55.6	97.4	0.22	0.17	0.09, 37% rsd, n=6

One potential uncertainty in the feed preparation is that it is easy to over oxidize the feed during drying or during glass melting. For most of the runs, the glass REDOX was lower than the predicted REDOX. But overall, despite extending the study past normal operating regions, the chemistry equations used to calculate the percent reducing acid and the method used to calculate the REDOX both worked well in simulant testing. The products from these runs will be used in a full evaluation that will be documented separately. The data from the REDOX measurements is included in Appendix E.

3.1.9 Rheology (Task 1k in TTR[1])

Rheological measurements were performed for each SRAT and SME product in order to observe the effects of acid stoichiometry and solids content on yield stress and consistency. As has been described previously, sludge simulant is best described as a Bingham plastic, which exhibits a linear relationship between shear stress and shear rate as described in Equation 8

$$\tau = \mu_{simulant}\gamma + \tau_0 \qquad \text{Equation 8}$$

where τ is the measured shear stress, $\mu_{simulant}$ is the consistency of the simulant, γ is the applied shear rate, and τ_0 is the yield stress of the simulant. Due to the linear nature of the shear stress-shear rate relationship of the simulant, product yield stresses and consistencies can be calculated by regression of the linear range of shear stress data as a function of shear rate. This data was acquired for each SRAT and SME product using a rheometer. The shear stress applied to each product was monitored as a function of shear rate through "spin-up" and "spin-down". Shear stress data for SRAT products were recorded at shear rates between 0 and 600 s^{-1}, while similar data for SME products were recorded at shear rates between 0 and 300 s^{-1}. Plots generated from the raw rheometer data are given in Appendix B.

3.1.9.1 SRAT and SME Rheological Data

Table 3-30 gives the measured yield stresses and consistencies of each SRAT and SME product in units of Pa and cP, respectively. For a Bingham plastic, consistency and yield stress are calculated by plotting sheer stress versus sheer rate and fitting the data to a straight line over the range that is most linear (labeled in tables as "Linear Fit Range (1/s)" The data are given as an average over two runs and reported with the appropriate %RSD. Results calculated from "spin-up" and "spin-down" data are given separately in order to observe possible changes in the product rheology after spin up (e.g. solids settling). Additionally, the range of shear rate data used to calculate the yield stress and consistency of each product is given. For convenience, acid stoichiometry, wt% total solids, and wt% insoluble solids are given for each product, as are the DWPF design bases for each type of product.

Table 3-30. Rheological Properties of SRAT and SME products

Run	KMA	% TS	% IS	Yield Stress, Pa (%RSD)		Consistency, cP (%RSD)		Range (1/s)
				Up	Down	Up	Down	
SRAT Products								
Design Basis[4]	**---**	**18-25**	**---**	**1.5-5.0**		**5.0-12.0**		**---**
NG51	83.7	30.8	19.3	1.0 (8.6)	0.5 (3.8)	9.5 (10.6)	6.9 (1.6)	100-300
NG52	116.3	26.4	14.2	11.5 (2.1)	12.4 (0.9)	32.7 (0.7)	30.3 (1.7)	100-300
NG53	83.6	29.9	17.5	0.5 (48.5)	0.4 (67.2)	9.0 (10.2)	7.0 (19.0)	100-300
NG54	116.6	27.7	14.9	11.7 (1.3)	12.7 (0.3)	28.3 (7.0)	26.3 (2.5)	100-300
NG55	100.0	34.2	19.1	1.7 (0.2)	1.7 (0.0)	10.5 (2.2)	10.4 (2.9)	100-300
NG55A	100.0	19.8	10.1	0.1 (6.0)	0.1 (2.7)	2.6 (2.8)	2.6 (0.6)	100-300
NG56	100.2	30.9	16.1	0.8 (0.7)	0.7 (0.4)	6.6 (0.4)	6.6 (1.0)	100-300
NG57	99.9	31.0	16.6	0.5 (1.0)	0.4 (0.4)	5.1 (2.6)	5.1 (2.8)	100-300
NG58	76.9	29.8	17.4	0.6 (2.1)	0.6 (1.0)	5.6 (0.9)	5.7 (0.7)	100-300
NG59	123.2	18.7	8.5	9.7 (0.9)	8.8 (0.8)	17.0 (1.4)	17.5 (0.3)	100-300
NG60	100.2	25.7	12.9	0.3 (0.1)	0.2 (0.7)	3.7 (0.5)	3.7 (0.2)	100-300
NG61	100.2	26.9	14.3	0.4 (1.1)	0.4 (0.7)	4.0 (0.9)	4.0 (0.9)	100-300
NG62	97.4	25.9	12.2	0.2 (4.2)	0.2 (0.9)	3.3 (0.7)	3.3 (0.6)	100-300
SME Products								
Design Basis	**---**	**40-50**	**---**	**2.5-15.0**		**10.0-40.0**		**---**
NG60	100.2	46.0	33.7	4.1 (1.5)	4.6 (5.6)	19.0 (1.6)	20.8 (3.7)	75-150
NG61	100.2	37.1	27.4	0.6 (2.2)	0.4 (1.1)	4.9 (1.4)	5.2 (1.3)	25-100
NG62	97.4	37.2	25.8	0.7 (10.9)	1.0 (12.5)	16.7 (19.7)	10.8 (9.5)	25-100

It seems that acid stoichiometry plays a large role in the determination of sludge rheological properties. Runs with the highest acid stoichiometry (NG52 = 116.3% KMA, NG54 = 116.6% KMA, and NG59 = 123.2% KMA) offer the highest yield stresses (12.4 Pa, 12.7 Pa, and 9.7 Pa, respectively) and consistencies (32.7 cP, 28.3 cP, and 17.5 cP, respectively). Furthermore, loading of solids appears to have an effect on rheological properties. Run NG55 (100% KMA) exhibits a total solids loading of 34.2% and a consistency of approximately 10 cP. However, NG55A (also 100% KMA) exhibits a total solids loading of 19.8% and a consistency of only 2.6 cP. These data suggest that acid stoichiometry and solids loading are tunable parameters that control the final sludge consistency and yield stress and are inherently linked in the processing stage. If a higher acid stoichiometry is desired, one may simply reduce the amount of water removed during processing to maintain desired rheological properties. A visual representation of these trends is shown in Figure 3-26.

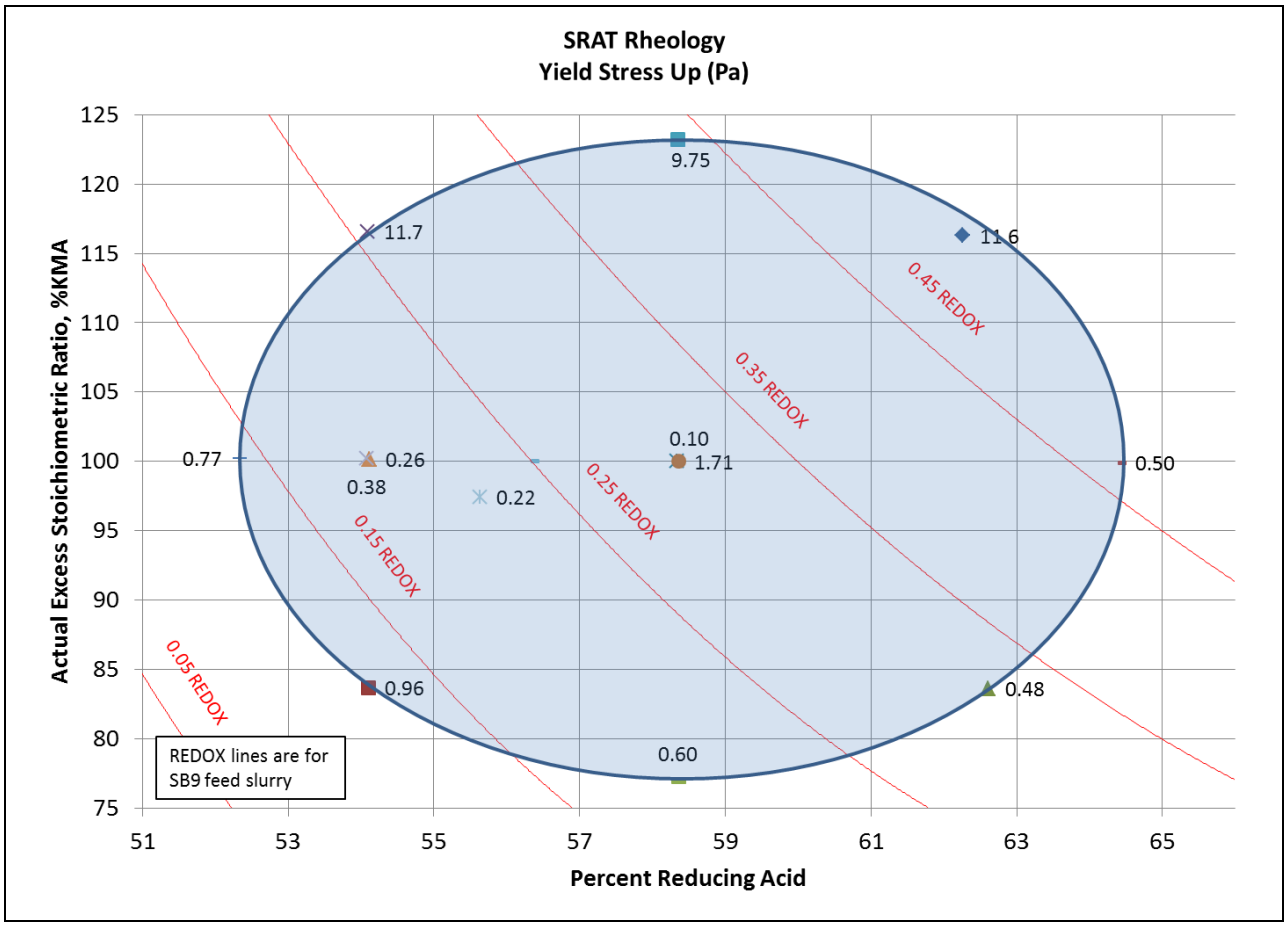

Figure 3-26. Rheology Yield Stress for SRAT Products

As expected, SME products seem to be significantly thicker than their corresponding SRAT products. Consistencies of NG60, NG61, and NG62 increase from 3.7, 4.0, and 3.3 cP (SRAT products) to 20.8, 5.2, and 16.7 cP (SME products). Similarly, yield stresses increase from SRAT to SME processing, increasing from 0.3, 0.4, and 0.2 Pa (SRAT products) to 4.6, 0.6, and 1.0 Pa (SME products). The sharp increase in NG60 rheological properties from SRAT to SME processing (relative to the same smaller increases seen in NG61 and NG62) is likely caused by the high total solids loading (46% relative to 37%) achieved in the SME cycle.

3.1.9.2 First-Principles Interpretation of Rheological Data

Common models for slurry viscosity (such as Einstein's equation and a multitude of variations) suggest that the plastic viscosity (consistency) of sludge simulant may be approximated by a polynomial relationship to the volume fraction of solids in the slurry, as is shown Equation 6:

$$\mu_{plastic} = f(\varphi_{IS}) \approx c_1 \varphi_{IS} + c_2 \qquad \text{Equation 9}$$

where $\mu_{plastic}$ is the consistency of the slurry, φ_{IS} is the volume fraction of insoluble solids in the slurry, and c_1 and c_2 are empirically-determined constants. It can be shown that φ_{IS} is related to the weight fraction of insoluble solids, ω_{IS}, by the expression given in Equation 10:

$$\varphi_{IS} = \omega_{IS} \frac{\rho_{slurry}}{\rho_{IS}} \qquad \text{Equation 10}$$

where ρ_{slurry} is the average density of the slurry and ρ_{IS} is the average density of the insoluble solids. It should be noted that, for a given sludge batch, ρ_{slurry} and ω_{IS} are expected to be linearly related to the weight fraction of total solids in the slurry, ω_{TS}, according to Equations 11 and 12:

$$\rho_{slurry} = c_3\omega_{TS} + c_4 \quad \text{Equation 11}$$

$$\omega_{IS} = c_5\omega_{TS} + c_6 \quad \text{Equation 12}$$

It follows that the consistency can be modeled as a non-linear function of ω_{TS} and ρ_{IS}, such that

$$\mu_{plastic} = f(\varphi_{IS}) = f(\omega_{TS}, \rho_{IS}) \quad \text{Equation 13}$$

However, ρ_{IS} is not easily determined, and is therefore not quantified experimentally. It becomes necessary, then, to express ρ_{IS} as a function of other measureable factors. It can be shown that ρ_{IS} can be calculated from the slurry and supernatant densities as well as the weight fraction of insoluble solids:

$$\rho_{IS} = \frac{\omega_{IS}\rho_{slurry}\rho_{sup}}{\rho_{sup} - (1-\omega_{IS})\rho_{slurry}} \quad \text{Equation 14}$$

where ρ_{sup} is the density of the supernatant phase. The empirical relationship of ω_{TS} to ω_{IS} and ρ_{slurry} has already been discussed (see Equations 11 and 12). Similarly, ρ_{sup} is expected to be related to the weight fraction of dissolved solids such that:

$$\rho_{sup} = c_7\omega_{DS} + c_8 \quad \text{Equation 15}$$

where ω_{DS} is the weight fraction of solids dissolved in the supernatant phase (mass solids per mass supernatant). ω_{DS} can be conveniently expressed as a function of ω_{TS} and ω_{IS}, as shown in Equation 16:

$$\omega_{DS} = \frac{\omega_{TS} - \omega_{IS}}{1 - \omega_{IS}} \quad \text{Equation 16}$$

where, as discussed previously, ω_{IS} can be calculated empirically from ω_{TS}. By combining each of these Equations (9 through 16), one may derive an expression for plastic viscosity that exhibits a non-linear dependence on ω_{TS} that can be calculated after fitting experimental data of ρ_{slurry}, ρ_{sup}, and ω_{IS}. Table 3-31 provides the data that was fit to derive a relationship between $\mu_{plastic}$ and ω_{TS} for SB9 simulant. Note that data from both nitric-formic and nitric-glycolic experiments are used, as no distinction for acid selection is made in the simple model described above.

Table 3-31. SB9 Data Used for Rheological Model Fitting

Run	Acid	wt% TS	wt% IS	wt% DS	ρ_{slurry} (g/mL)	ρ_{sup} (g/mL)	φ (Calculated)	Consistency (cP)
NG51	glycolic	30.8	19.3	14.2	1.2165	1.0958	0.104	9.5
NG52	glycolic	26.4	14.2	14.3	1.1798	1.0971	0.077	32.7
NG53	glycolic	29.9	17.5	15	1.2176	1.0922	0.080	9
NG54	glycolic	27.7	14.9	15.1	1.1792	1.097	0.085	28.3
NG55	glycolic	34.2	19.1	18.6	1.2465	1.1255	0.104	10.5
NG55A	glycolic	19.8	10.1	10.8	1.1432	1.0728	0.042	2.6
NG56	glycolic	30.9	16.1	17.6	1.2368	1.1202	0.074	6.6
NG57	glycolic	31	16.6	17.2	1.2383	1.115	0.074	5.1
NG58	glycolic	29.8	17.4	15	1.228	1.094	0.073	5.6
NG59	glycolic	18.7	8.5	11.2	1.1334	1.0779	0.038	17
NG60	glycolic	25.7	12.9	14.7	1.1495	1.0977	0.088	3.7
NG61	glycolic	26.9	14.3	14.7	1.2013	1.0976	0.062	4
NG62	glycolic	25.9	12.2	15.6	1.1966	1.0999	0.045	3.3
NG60 SME	glycolic	46	33.7	18.6	1.3775	1.1256	0.189	19
NG61 SME	glycolic	37.1	27.4	13.4	1.3118	1.0856	0.123	4.9
NG62 SME	glycolic	37.2	25.8	15.4	1.2911	1.0959	0.126	16.7
SB9-1	formic	22.7	13.7	10.4	1.1796	1.067	0.045	8.1
SB9-10	formic	24.2	13.6	12.2	1.0722	1.077	0.140	10.5
SB9-11	formic	24.7	12.9	13.5	1.1326	1.0848	0.090	7.8
SB9-2	formic	24.3	13.9	12.1	1.1952	1.0736	0.041	15
SB9-3	formic	24.4	13.7	12.3	1.1309	1.0818	0.098	8.7
SB9-4	formic	22.8	13	11.3	1.167	1.0736	0.054	9.1
SB9-5	formic	24.3	13.5	12.5	1.1717	1.069	0.052	7.8
SB9-6	formic	24.9	12.5	14.2	1.1817	1.0802	0.043	8.4
SB9-7	formic	21.6	11	11.9	1.1712	1.0831	0.037	4.8
SB9-8	formic	21.3	11.2	11.4	1.1211	1.0765	0.075	5.6
SB9-9	formic	27.4	13.9	15.6	1.2131	1.1035	0.053	5.3
SB9-1 SME	formic	45.7	38.1	12.3	1.3787	1.0736	0.205	24.8
SB9-10 SME	formic	45	36.5	13.4	1.1535	1.0754	0.319	51.6
SB9-11 SME	formic	47.2	37.4	15.7	1.3801	1.0971	0.213	38.9
(SME) SB9-2	formic	47.5	39.2	13.7	1.41	1.0863	0.211	41.6
(SME) SB9-3	formic	47.6	38.9	14.2	1.395	1.0959	0.222	35.8
(SME) SB9-4	formic	41.6	34.3	11.1	1.2498	1.0809	0.240	20
(SME) SB9-5	formic	46.6	37	15.2	1.2556	1.083	0.270	31.2
(SME) SB9-6	formic	48.9	38.9	16.4	1.337	1.0978	0.256	38.5

By using linear, least-squares fits of the data above, empirical values for c_1-c_8 can be calculated. Results of these fits are shown in Table 3-32.

Table 3-32. Best Fit Constants for Rheological Modelling

Fit Equation	Slope	Intercept	R^2
$\mu_{plastic} = c_1\varphi_{IS} + c_2$	136.7661	-0.0420	0.6498
$\rho_{slurry} = c_3\omega_{TS} + c_4$	0.7662	0.9810	0.7205
$\omega_{IS} = c_5\omega_{TS} + c_6$	1.0741	-0.1342	0.9689
$\rho_{sup} = c_7\omega_{DS} + c_8$	0.6504	0.9988	0.8519

Figure 3-27 gives the consistency in cP vs. the weight fraction of total solids in SB9 simulant SRAT/SME products, as well as the expected relationship derived above (shown in red).

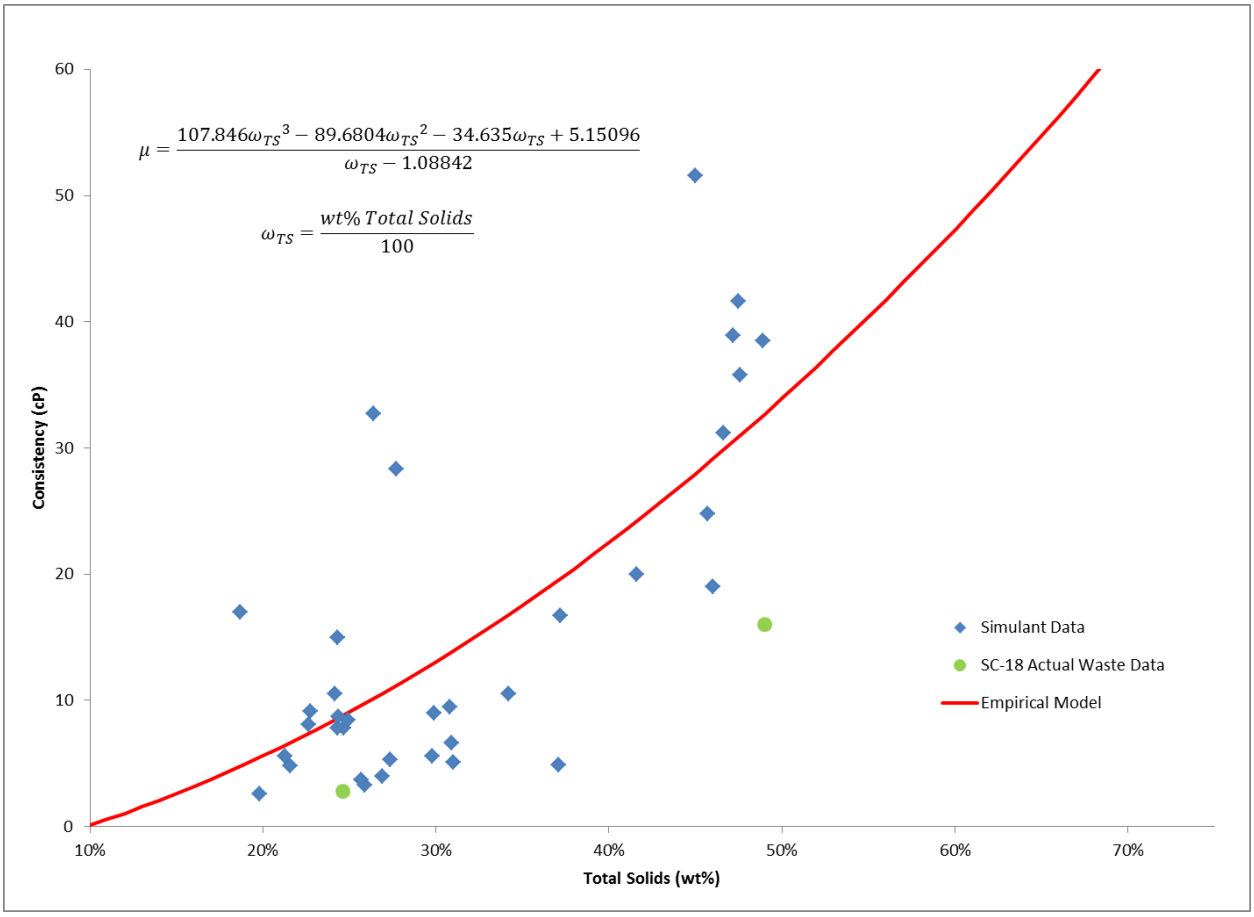

Figure 3-27. Plot of Consistency vs. Weight Fraction of Total Solids

Interestingly, the trend exhibited by the empirical model suggests that consistency increases nonlinearly with increasing total solids, which is the behavior noted in previous sludge batches. Such a model has the capacity to explain the "sudden increase" seen in consistency at very high total solids concentrations. The fit model allows an estimation of maximum total solids achievable to remain below maximum design basis consistencies during SRAT and SME consistencies. Using calculated consistencies based on the empirical model, it appears that total solids limits of 28 wt% and 53 wt% should be assumed for processing during SB9 SRAT and SME cycles in order to restrict slurry consistencies to values below 12 and 40 cP, respectively. The measured SB9 actual waste SRAT consistency was 2.8 cP (24.8 wt % total solids) and SME product consistency was 16.0 cP (49.0 wt% total solids)Both of these consistency values are lower than the empirical model predictions, which would be expected for a low acid stoichiometry run.

Although the semi-empirical model derived here explains some behavior previously noted in the sludge consistency dependence on total solids weight fraction, it suffers from a few drawbacks including a lack of dependence on acid stoichiometry (which appears to have a measureable influence on SRAT/SME product consistency). Additional testing focusing on rheological research is recommended to further understand the order of relationship between insoluble solid volume fraction and consistency, the influence of acid stoichiometry, and determination of similar trends in real waste vs. simulated waste.

3.1.10 Condensate (Antifoam Degradation Products, Additional Task f in TTR[1])

Condensate samples were pulled from the SRAT dewater sample, the post SRAT MWWT contents, the ammonia scrub liquid and the post SRAT FAVC. In DWPF, these samples would have all collected in the

SMECT. Many of the anions and cations are not detectable and are not reported in the tables. It will be noted in a note below each table which analytes are below detection limit.

The SRAT dewater samples are the largest volume and account for ~99% of the condensate volume in the sludge-only SRAT cycles, and about half for the combined SRAT and SME sludge-only cycles. In coupled processing, the SRAT dewater sample is a smaller volume fraction. The condensate samples were analyzed for anions and cations. The results are summarized in Table 3-33. Note that the two significant components were nitrate and silicon. The nitrate is scrubbed from the offgas and the silica is likely an antifoam degradation product. The absence of the other metals and anions is indicative of little or no carryover of the SRAT contents into the condensate. If the silica is present as TMS, the TMS concentration is 2.75 times the Si concentration. If the silica is present as HMDSO, the HMDSO concentration is 2.89 times the Si concentration. One interesting observation is the low nitrate concentration in the high acid stoichiometry runs (NG52, NG54, and NG59). This may result in lower dissolution of mercury in the MWWT and SMECT and higher recovery of elemental mercury.

Table 3-33. SRAT/SME Dewater, mg/L (except density, which is kg/L at 20 ˚C)

Sample ID	Ca	Mn	Na	Si	Nitrate	Density
NG51	<1.00	<1.00	2.83	135	5,905	1.0007
NG52	<1.00	<1.00	1.87	151	533	0.9976
NG53	<1.00	<1.00	1.45	79.4	7,185	1.0013
NG54	<1.00	<1.00	1.04	116	1,665	0.9983
NG55	<1.00	1.29	4.75	26.6	4,055	0.9997
NG55A	1.09	1.48	6.40	284	12,300	1.0055
NG56	1.08	<1.00	3.13	57.0	3,050	0.9991
NG57	1.24	<1.00	5.29	137	5,075	1.0002
NG58	1.11	<1.00	4.92	60.4	6,670	1.0013
NG59	1.07	<1.00	2.97	123	2,600	0.9989
NG60-Post SRAT	<1.00	<1.00	3.98	1,230	<100	0.9971
NG60-Post SME	<1.00	<1.00	2.61	562	<100	0.9971
NG61-Post SRAT	<1.00	3.03	10.0	574	<100	0.9971
NG61-Post SME	1.26	5.45	14.4	1,340	<100	0.9971
NG62-Post SRAT	<1.00	<1.00	2.33	265	<100	0.9971
NG62-Post SME	<1.00	<1.00	2.42	327	<100	0.9971

Note: Al, Ba, Cu, Fe, K, Li, Ni, S, Sn, Ti <1.00; Cr, Zn <0.1; P <10.0; F^-, Cl^-, NO_2^-, SO_4^{2-}, $C_2O_4^{2-}$, HCO_2^- <100

The scrubber solution is used in experiments to allow the differentiation of anions scrubbed in the scrubber. The scrubber solution samples were analyzed for anions and cations. The results are summarized in Table 3-34. Note that the two significant components were nitrate and silicon. The nitrate is scrubbed from the offgas and the silicon is likely an antifoam degradation product. The absence of other metals and anions is indicative of little or no carryover of the SRAT contents into the condensate. If the silica is present as TMS, the TMS concentration is 2.75 times the Si concentration. If the silicon is present as HMDSO, the HMDSO concentration is 2.89 times the Si concentration on a mass basis.

Table 3-34. Scrub Solution, mg/L (except density, which is kg/L at 20 ˚C)

Sample ID	Na	Si	Nitrate	Density
NG51	3.14	31.2	12,500	1.0054
NG52	3.53	177	9,715	1.0029
NG53	1.16	16.2	9,705	1.0029
NG54	1.19	60.6	4,395	0.9999
NG55	1.83	27.6	11,450	1.0053
NG55A	1.21	1.46	5,090	1.0000
NG56	1.33	1.22	5,595	1.0006
NG57	1.44	4.51	4,235	0.9996
NG58	1.26	8.19	6,145	1.0006
NG59	1.33	25.0	8,520	1.0018
NG60-Post SRAT	3.87	17.4	4,060	0.9995
NG60-Post SME	3.66	84.1	10,800	1.0038
NG61-Post SRAT	3.24	16.1	83,200	1.0039
NG61-Post SME	3.47	221	13,300	1.0057
NG62-Post SRAT	3.19	195	6,710	1.0010
NG62-Post SME	NA	NA	NA	NA

Note: Al, Ba, Ca, Cu, Fe, K, Li, Mn, Ni, S, Sn, Ti <1.00; Cr, Zn <0.10; P <10.0; F^-, Cl^-, NO_2^-, SO_4^{2-}, $C_2O_4^{2-}$, HCO_2^- <100

The MWWT solution samples (submitted after elemental mercury is removed) are small volume (~30 mL) and would not account for generated condensate volume in DWPF. These samples were analyzed for anions and cations. The results are summarized in Table 3-35. Note that the MWWT is washed by the condensate that is produced throughout the SRAT cycle (5,000 lb/hr condensate generation is 600 gallons condensate per hour). The resulting solution had trace concentrations of Al, Ca, Fe, K, Mn, Ni, and S in some of the samples. This is likely the result of a small carryover from the SRAT. The two significant components were nitrate and silicon.

Table 3-35. MWWT Solution, mg/L (except density, which is kg/L at 20 ˚C)

Sample ID	Al	Ca	Cr	Fe	K	Mn	Na	Ni	S	Si	Nitrate	Density
NG51	1.27	1.32	<0.100	1.31	1.01	<1.00	7.09	<1.00	<1.00	168	996	0.9979
NG52	<1.00	1.04	0.13	<1.00	13.06	<1.00	4.92	<1.00	<1.00	687	121	0.9973
NG53	<1.00	1.02	<0.100	<1.00	<1.00	<1.00	3.88	<1.00	<1.00	156	540	0.9977
NG54	<1.00	<1.00	<0.100	<1.00	<1.00	<1.00	4.23	3.33	<1.00	31.9	585	0.9978
NG55	<1.00	<1.00	<0.100	<1.00	<1.00	1.03	5.34	<1.00	<1.00	7.88	<100	0.9973
NG55A	<1.00	1.09	<0.100	<1.00	<1.00	2.51	7.49	<1.00	<1.00	8.36	<100	0.9972
NG56	1.34	1.24	<0.100	<1.00	<1.00	<1.00	5.53	<1.00	<1.00	9.99	132	0.9975
NG57	1.24	1.92	0.10	1.41	<1.00	4.05	14.26	<1.00	<1.00	6.49	261	0.9977
NG58	1.09	3.81	0.10	<1.00	<1.00	<1.00	6.93	<1.00	<1.00	12.0	2,425	1.0010
NG59	<1.00	<1.00	<0.100	<1.00	<1.00	<1.00	2.42	<1.00	<1.00	8.21	196	0.9981
NG60-Post SRAT	<1.00	1.31	0.11	<1.00	<1.00	5.43	12.62	<1.00	1.02	7.55	<100	0.9973
NG61-Post SRAT	1.80	1.65	0.11	1.31	1.01	5.63	17.56	<1.00	<1.00	7.61	612	0.9978
NG62-Post SRAT	<1.00	<1.00	<0.100	<1.00	13.06	<1.00	5.86	<1.00	<1.00	12.2	<100	0.9972

Note: Ba, Cu, Li, Sn, Ti <1.00; Zn <0.10; P <10.0; F^-, Cl^-, NO_2^-, SO_4^{2-}, $C_2O_4^{2-}$, HCO_2^- <100

The Post SRAT and Post SME FAVC samples are very small volume (~10 mL) and account for <1% of the condensate volume. These samples were analyzed for anions and cations. The results are summarized

in Table 3-36. The FAVC sample is very high in nitrate and silicon. The highest nitrate concentration was in run NG57, which is equivalent to 21.2 wt % or 3.60 M.

Table 3-36. FAVC Solution, mg/L (except density, which is kg/L at 20 ˚C)

Sample ID	Al	Ca	Cr	Na	S	Si	Nitrate	Density
NG51	<1.00	<1.00	<0.100	1.13	<1.00	27.1	90,950	1.0490
NG52	<1.00	<1.00	<0.100	1.14	<1.00	171	74,450	1.0401
NG53	1.32	<1.00	<0.100	3.96	<1.00	28.5	124,500	1.0691
NG54	1.92	<1.00	<0.100	6.31	1.14	31.7	121,500	1.0675
NG55	2.40	<1.00	<0.100	6.19	<1.00	13.7	112,500	1.0625
NG55A	1.86	<1.00	<0.100	5.51	<1.00	16.1	154,000	1.0844
NG56	1.78	<1.00	<0.100	4.69	<1.00	12.4	85,700	1.0484
NG57	2.09	1.22	<0.100	6.57	<1.00	24.9	223,000	1.1200
NG58	2.76	<1.00	<0.100	7.36	<1.00	14.4	131,500	1.0739
NG59	1.85	<1.00	0.11	5.57	<1.00	266	106,000	1.0588
NG60-Post SRAT	NA	NA	NA	NA	NA	NA	NA	NA
NG60-Post SME	NA	NA	NA	NA	NA	NA	NA	NA
NG61-Post SRAT	NA	NA	NA	NA	NA	NA	NA	NA
NG61-Post SME	<1.00	<1.00	<0.100	1.12	<1.00	294	13,850	1.0065
NG62-Post SRAT	1.40	1.36	<0.100	4.58	<1.00	24.8	144,000	1.0798
NG61-Post SME	5.25	2.04	<0.100	4.64	<1.00	228	55,400	NA

Note: Al, Ba, Cu, Fe, K, Li, Mg, Mn, Ni, Sn, Ti <1.00; Zn <0.10; P <10.0; F^-, Cl^-, NO_2^-, SO_4^{2-}, $C_2O_4^{2-}$, HCO_2^- <100

3.1.11 SME Cycles

Three SME cycles were completed, NG60-62. Two of the SME cycles were designed to be identical except for the boilup rate. Both were sludge-only SRAT cycles with no decon dewater phases and two process frit additions. The third SME cycle included sludge, PRFT, SEFT, six decon dewater phases and two process frit additions.

3.1.11.1 Waste Loading

The waste loading for all three SME cycles was targeted at 38%. The measured waste loading, calculated using calcined elemental composition of the SRAT and SME products, was higher for all three SRAT/SME runs. As a result, additional frit was added to SME product prior to vitrifying the waste and measuring REDOX. For elements that are in the slurry but not in the frit, the waste loading is calculated by dividing the SME product elemental composition by the SRAT product elemental composition. For lithium, the waste loading is calculated by dividing the SME product elemental composition by 2.787, the lithium concentration in frit 803. For boron, the waste loading is calculated by dividing the SME product elemental composition by 2.485, the boron concentration in frit 803Sodium and silica were not used in the calculation as there is Na and Si in both sludge and frit 803. The waste loading results are summarized in Table 3-37.

Table 3-37. Waste Loading Calculated from SRAT, SME, and Frit Elemental Composition

	Al	B	Ca	Cr	Fe	Li	Mg	Mn	Ni	S
NG60	42.30	39.10	37.60	42.20	43.00	37.60	44.80	42.30	35.90	37.60
NG61	40.70	35.90	35.80	47.60	41.30	41.70	41.70	40.50	35.00	36.10
NG62	45.10	37.40	36.60	48.60	43.60	45.60	43.90	44.60	36.30	40.00

3.1.11.2 Anion Destruction

Depending on the activity of the noble metals/mercury, the anion concentration can decrease due to continuing decomposition of glycolate and nitrate. The SME cycle anion destruction results are summarized in Table 3-38. The oxalate generation is significantly higher for NG61, the SRAT/SME cycle completed at half the design basis boilup (twice the boiling time), even though both had the same sludge, acid additions, etc.

Table 3-38. SME Cycle Anion Destruction

	NG60	NG61	NG62
Nitrate destruction	0.9%	1.2%	6.8%
Glycolate destruction	1.8%	4.4%	5.7%
Oxalate generation	6.7%	20.2%	0.1%
Formate generation	NA	NA	12%

3.2 Antifoam (Task 1n, Additional Task d in TTR[1])

The development of an antifoam strategy was one of the objectives of the SB9 nitric-glycolic acid flowsheet testing. An antifoam strategy was developed but led to excessive HMDSO peak at boiling. Additional testing[21] was completed to develop a strategy (run NG67 in Table 3-40) for reducing the HMDSO peak. The strategy developed adds 0.25 gallons of antifoam prior to each processing step and was demonstrated in NG67, a coupled SRAT and SME cycle. Similar quantities of antifoam were used in the shielded cells demonstration[7] of the nitric-glycolic acid flowsheet.

3.2.1 Antifoam Addition Strategy Recommended for SB9 Nitric-Glycolic Acid Processing

Based on the success of both controlling foaming and minimizing the HMDSO peak, the antifoam strategy used during simulant run NG67[21] (Table 3-40) should be used in DWPF for SB9 nitric-glycolic acid flowsheet. The success during the SB9 nitric-glycolic acid flowsheet in controlling foam with significantly lower mass of antifoam additions gives more confidence that it will work in DWPF. However, DWPF needs to remember that simulant testing is not conservative relative to foaming. The DWPF SRAT/SME surface flux is 44.21 lb/hr/ft^2 at a boilup rate of 5,000 lb/hr while the surface flux in the 4-L kettle is 2.90 lb/hr/ft^2 or fifteen times lower in DWPF. More antifoam or more frequent antifoam additions might be required in SB9.

3.2.2 Generation of Flammable Antifoam Degradation Products

Throughout SB9 nitric-glycolic testing, it was observed that the generation rates of flammable antifoam degradation products (ADPs) such as HMDSO, TMS, and propanal were elevated in the presence of glycolic acid, compared to similar testing performed under the nitric-formic flowsheet. Currently, the formation of these ADPs is thought to occur from the hydrolysis of antifoam 747 and subsequent degradation (shown in Figure 3-28).

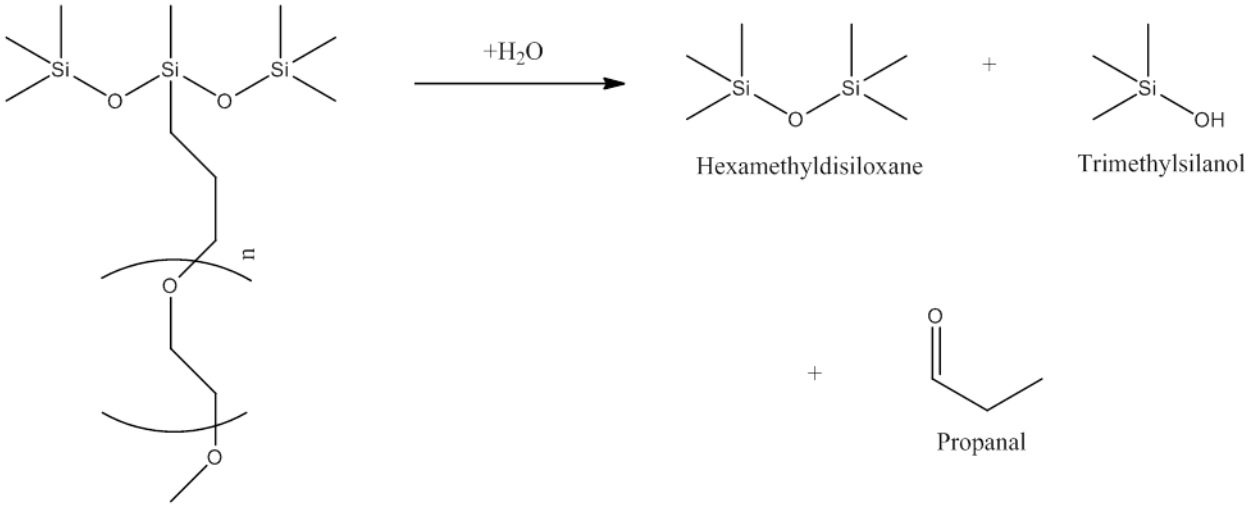

Figure 3-28. Hydrolysis of Polyelkyleneoxide-Modified Heptamethyltrisiloxane, a Main Ingredient of Antifoam 747

It is speculated that despite the relatively high boiling point of HMDSO (~100 °C), nearly all HMDSO is removed from the process vessel and tubing via offgas due to the low solubility of HMDSO in water (<1 mg/L). TMS exhibits a similarly high boiling point (~99 °C) but is expected to be present in process condensates due to its increased solubility in water (~995 mg/L). Propanal benefits from a reduced boiling point (~50 °C) and an increased water solubility (~200,000 mg/L), and is therefore expected to appear primarily in condensate samples throughout processing. Therefore, HMDSO is quantified in nitric-glycolic simulant runs exclusively by FTIR analysis of offgas process streams while TMS and propanal are quantified by Semi-Volatile Organics Analysis (SVOA) and Volatile Organics Analysis (VOA), respectively.

3.2.3 Production of HMDSO

Figure 3-29 gives the offgas HMDSO profile during SRAT processing for run NG60, a prototypical SRAT/SME run under the nitric-glycolic flowsheet. As summarized in Table 2-12, runs NG51-62 added four to six times as much antifoam prior to SRAT boiling compared to run NG67, which was used to formulate the SB9 antifoam strategy. It is clear that the largest emission of HMDSO occurs shortly after acid addition, achieving a peak HMDSO concentration of 968 ppm_v at approximately 0.95 hours after the completion of acid addition. A broader peak of lower magnitude occurs just before this maximum spike, reaching a local maximum concentration of 531 ppm_v at approximate 0.4 hours before the completion of acid addition.

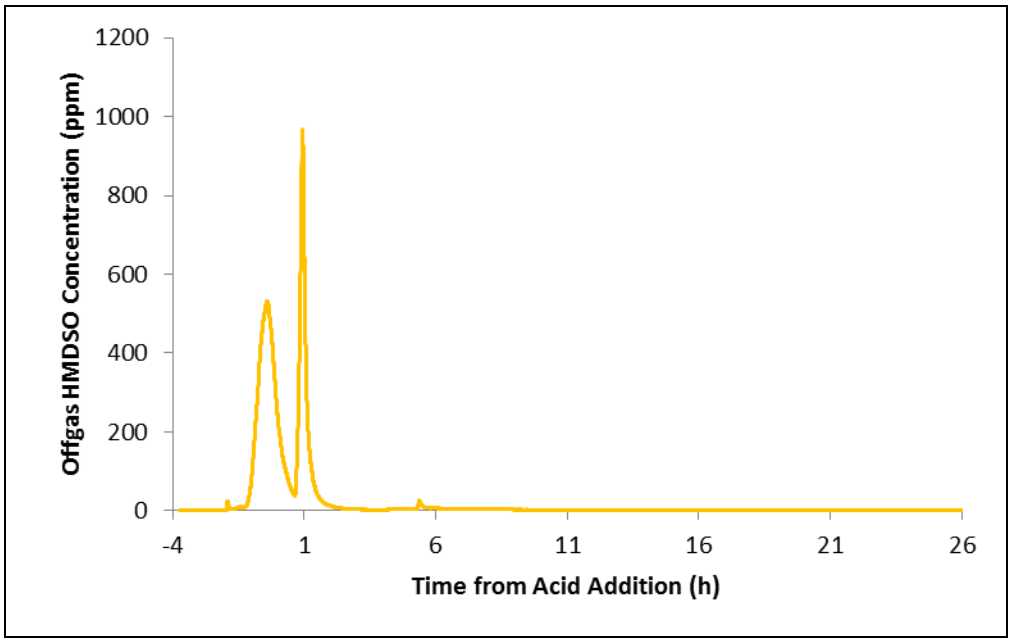

Figure 3-29. HMDSO Offgas Profile of NG60 SRAT Processing

Similarly, Figure 3-30 gives the offgas HMDSO profile during SME processing for run NG60. During SME processing, HMDSO concentrations remain significantly lower than those encountered during the SRAT cycle, with a maximum SME cycle HMDSO concentration of 117 ppm_v at the beginning of the second post-frit addition dewater step (~30.8 hours after acid addition). A similar (albeit lower) spike in HMDSO concentration is seen at the beginning of the first post-frit addition dewater step (~41 ppm_v at 28.3 hours after acid addition).

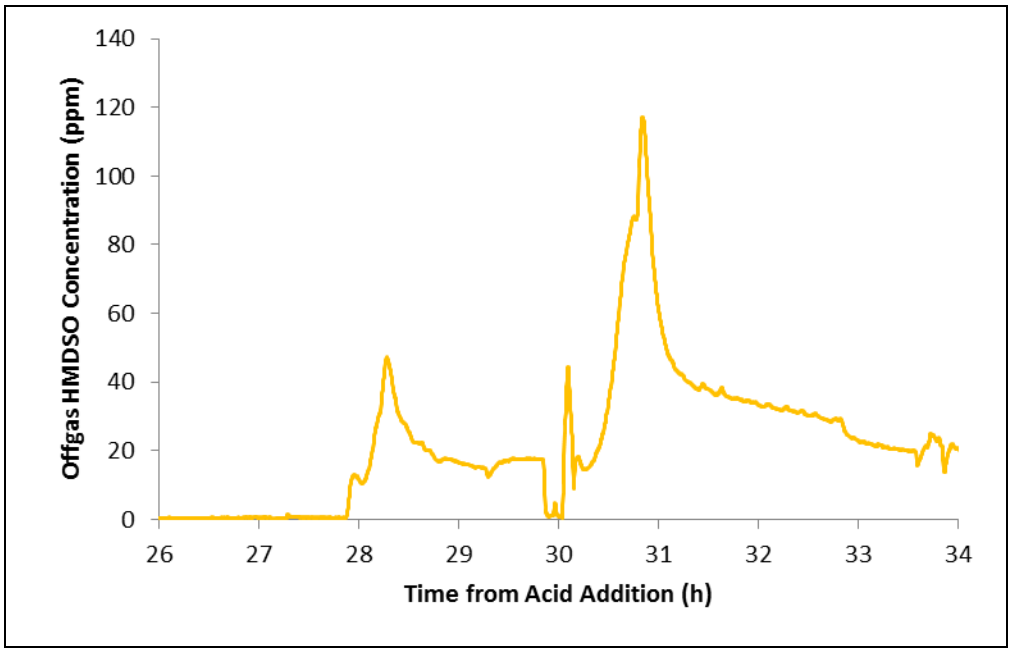

Figure 3-30. HMDSO Offgas Profile of NG60 SME Processing

In general, HMDSO offgas measurements exhibit similar behavior to that shown in Figure 3-29 and Figure 3-30 throughout all nitric-glycolic testing: The addition of antifoam causes a sharp increase in offgas HMDSO measured, with the largest spike immediately following the addition of antifoam and initiation of boiling in the SRAT cycle.

3.2.4 TMS and Propanal Production

Table 3-39 gives the condensate concentrations of TMS and propanal at various processing times and locations during NG60, 61, and 62. All units are reported as mg/L.

Table 3-39. Process Condensate Concentrations of TMS and Propanal for Runs NG60, NG61, and NG62

Time	Vessel	NG60		NG61		NG62	
		TMS (mg/L)	Propanal (mg/L)	TMS (mg/L)	Propanal (mg/L)	TMS (mg/L)	Propanal (mg/L)
SRAT Processing							
Post-Acid Addition	MWWT	4	<0.25	120	<0.25	<0.25	<0.25
Dewater	Dewater	3.5	<0.25	9.5	<0.25	10	<0.25
Post-SRAT							
SRAT Product	SRAT	<0.25	<0.25	<0.25	<0.25	<0.25	<0.25
MWWT Drain	MWWT	<0.25	<0.25	<0.25	<0.25	<0.25	<0.25
Scrubber Solution	Scrubber	1	<0.25	7	<0.25	5.8	<0.25
FAVC Condensate	FAVC	11	<0.25	11	<0.25	<0.25	<0.25
SME Processing							
1st Frit Dewater	Dewater	15	7.5	7.5	1	3.8	7.4
2nd Frit Dewater	Dewater	6.5	1	12	5	2.4	2.3
Post-SME							
SME Product	SME	<0.25	<0.25	<0.25	<0.25	<0.25	<0.25
Scrubber Solution	Scrubber	15	<0.25	12	0.5	7.6	<0.25
FAVC Condensate	FAVC	140	2	NA	NA	NA	NA

Interestingly, the majority of propanal observed in the condensate appears to occur during SME processing, with every SRAT cycle propanal measurement returning a less-than-detectable concentration of propanal (compared to concentrations >7 mg/L in the 1st frit dewater step in the SME cycle of NG60). While this might indicate a difference in degradation kinetics of antifoam or antifoam impurities, it is important to note that several physical differences exist between the SRAT and SME cycles that could cause such behavior (lower air purge rate in SME vs. SRAT, decreased salinity of SME condensates vs. SRAT condensates, condenser/scrubber inefficiencies, etc.).

3.2.5 TMS and HMDSO Production from Antifoam 747

Antifoam 747 is currently manufactured by Siovation as SiO-747. This particular antifoam is a blend of two commercial fluids produced by Momentive Performance Materials, Silwet-L77 (90 wt% of antifoam 747) and Y-17580 (10 wt% of antifoam 747). Table 3-40 gives the elemental composition of Silwet L-77 and Y-17580, as well as the expected elemental composition of antifoam 747 (based on 90 wt% composition of Silwet L-77).

Table 3-40. Elemental Mass Compositions of Silwet L-77, Y-17580, and Antifoam 747

Element	Silwet L-77	Y-17580	Antifoam 747
Carbon (wt%)	51.29	51.14	51.28
Hydrogen (wt%)	9.74	9.44	9.71
Oxygen (wt%)	27.24	30.39	27.55
Silicon (wt%)	11.73	9.03	11.46

Using the calculated elemental compositions of antifoam 747 described in Table 3-42, it is possible to predict the mass of silicon added per gram of antifoam 747 added (0.1146 g Si/g antifoam). In addition to this information, it is believed that only two-thirds of the added silicon is available to undergo transformation to HMDSO or TMS (assuming that silicon is primarily present as 1,1,1,3,5,5,5-heptamethyltrisiloxane derivatives like the one shown in Figure 3-28 and that no auxiliary transmetallation reaction pathways are available to methylate additional silicon). Combining all of this information, one may calculate the amount of "active" silicon added per mass of antifoam charged, according to the expression shown in Equation 17:

$$\hat{n}_{silicon,active} = \frac{2}{3} * 0.1146 \frac{g\ Si}{g\ antifoam} * \frac{1\ mol\ Si}{28.086\ g\ Si} * \frac{1000\ mmol}{1\ mol} = 2.72\ \frac{mmol\ Si_{active}}{g\ antifoam} \qquad \text{Equation 17}$$

Using this calculated value, recorded masses of antifoam added, measured concentrations of HMDSO (offgas) and TMS (condensates), and estimated volumes of condensate samples (assuming densities of 1 g/mL for condensate samples), it is possible to estimate the percentage of available, "active" silicon that undergoes transformation to HMDSO and TMS from each run. Table 3-41 gives the percent conversions of active silicon to HMDSO for several SRAT-only runs. Similarly, Table 3-42 gives the percent conversion of active silicon to HMDSO and TMS for the SRAT/SME runs NG60, NG61, and NG62.

Table 3-41. Percent Conversions of Active Silicon to HMDSO in SRAT-Only Runs

	NG52	NG53	NG54	NG56	NG57	NG59
Total Antifoam Added (g)	2.5485	2.0365	2.0022	1.7922	1.7883	2.0363
Total HMDSO Measured (mmol)	1.405	0.573	0.913	0.658	0.606	1.346
% of Active Si Converted to HMDSO	48.2*	20.7	33.6	37.9	34.8	48.6

*Calculated without mass of final antifoam addition and without integration of HMDSO data beyond 26.7 hours due to completion of SRAT cycle during elevated HMDSO production.

Table 3-42. Percent Conversions of Active Silicon to HMDSO and TMS in SRAT/SME Runs

	NG60	NG61	NG62*
Total Antifoam Added (g)	2.1923	2.1554	2.7978
Total TMS Collected (mmol)	0.265	NM	0.200
Total HMDSO Measured (mmol)	0.772	0.786	>0.069
% of Active Silicon Converted to TMS	4.4	NM	NM
% of Active Silicon Converted to HMDSO	25.9	26.8	>1.82

* FTIR was valved into run NG61 until complete, then valved into NG62, so NG62 data is incomplete

In addition to calculating the average consumption of active silicon over the course of an entire SRAT/SME run (as is shown in Table 3-44), the amount of HMDSO silicon generated as a function of time can be plotted against the time-dependent amount of antifoam added to the kettle in order to observe differences in apparent HMDSO reaction rates at various times during SRAT/SME processing. Figure 3-31 gives such data for run NG60. The amounts of active silicon added as antifoam are depicted as red step-changes, while

consumption of active silicon measured as HMDSO is shown in blue. The offgas profile of HMDSO (shown in orange) is also given to assist in identification of process events (e.g. SRAT cycle, SME cycle).

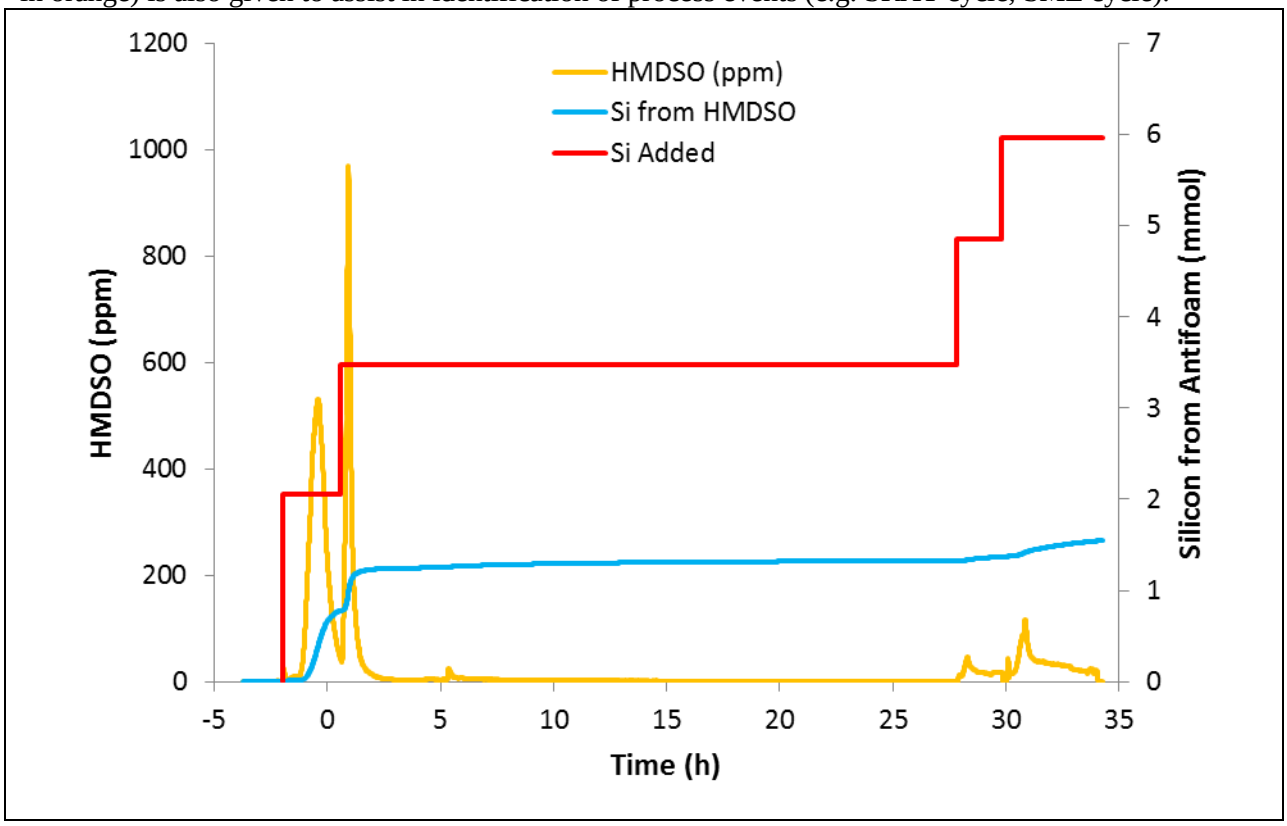

Figure 3-31. Active Silicon Addition and Consumption as a Function of Time in Run NG60

Interestingly, there appears to be a significant difference between the HMDSO generation rates of the SRAT and SME cycles. At the conclusion of the SRAT cycle in NG60 (~25 hours), approximately 40% of the added active silicon has been accounted for as measured HMDSO. However, by the conclusion of the SME cycle this percentage has dropped to ~27%. This suggests that antifoam degradation pathways that form HMDSO are more prevalent during SRAT processing than in SME processing. The effect of this apparent change in production rate of HMDSO on the production of other ADPs is unclear and should be investigated.

3.2.6 Foaming and Air Entrainment

The goal for this testing was to determine the minimum antifoam needed for processing the SB9 simulant. In hindsight, based on additional antifoam testing discussed in section 3.2.2, the original antifoam additions derived from the current nitric-formic acid flowsheet were too large, leading to HMDSO peaks that were too large for DWPF offgas flammability. However, the antifoam strategy used was effective in preventing foamovers during testing. Minimal antifoam additions were made during processing (Table 3-40). In early testing (NG51 and NG52), CO_2 generation created foam during nitric acid addition but in some of the runs, no antifoam was added throughout acid addition. In all runs, an antifoam addition was made just after acid addition was complete and just prior to boiling. In some of the runs, no additional antifoam was added throughout SRAT processing.

3.2.7 HMDSO Peak during SRAT and SME Processing

The FTIR software estimates both the concentration and uncertainty for each analysis. This is assumed to be a rectangular uncertainty for calculations of the HMDSO mmol/min. The uncertainty calculation is described below:

An uncertainty analysis was performed to place an upper bound (with 95% confidence) on the reported maximum HMDSO concentrations and generation rates for the runs where the FTIR was used. Several factors contribute to uncertainty in the HMDSO measurements and generation rates. The factors considered in this analysis include the following:

- Uncertainty in the air purge flowrate
- Uncertainty in the helium tracer flowrate
- Uncertainty in the helium concentrations in the Gas Chromatograph (GC) calibration gasses
- Uncertainty in the HMDSO concentration measurement by FTIR
- Uncertainty due to variance in GC measurements
- Bias due to drift in the calibration during the run

The MKS flow meter / flow controllers used for the flow rates of the air purge and helium tracer had tolerances of 2% of full scale and were tracked in the Measuring and Test Equipment (M&TE) program. The standards used to calibrate GC for concentration of hydrogen, helium, and other gasses have a NIST certification to 5% of the reported concentrations. The variance in the GC measurements is estimated from the data collected during the instrument calibration check. The bias due to the calibration drift is handled by processing the calibration of the GC in a manner to provide conservatively large hydrogen generation measurements. The pre- and post-run calibration-check information is compared, and the sets of calibration data are used that would maximize the instrument-measured hydrogen and nitrous oxide concentrations and minimize the helium tracer concentration.

Uncertainty can be applied to the observed helium concentrations and HMDSO concentration by using Equations 18 and 19. Equation 15 gives the calculation for C_{He} using a helium response factor (calculated from measured GC responses of calibration gas) and the helium GC response of interest (in terms of area units). The C_{HMDSO} is calculated by the FTIR software and returned with an approximate uncertainty according to ASTM D6348. Both C_{HMDSO} and C_{He} are expressed as mole fractions. $F_{SRNL\text{-}purge}$ is the target SRNL purge rate; and F_{air} and F_{He} are the flow rates of air and helium purges at lab scale. While the ratio ($F_{SRNL\text{-}purge}$ / (F_{air} + F_{He})) is by definition equal to 1 (the sum of the He and air flow rates are set to equal the SRNL purge rate), these terms allow accounting for the uncertainty in the He and air flow controllers.

$$C_{He} = area_{He}\left(\frac{C_{He}^{std}}{area_{He}^{std}}\right) \qquad \text{Equation 18}$$

The value calculated by Equation 16 is the SRNL-scale generation rate of HMDSO in mmol/min, calculated from the results for HMDSO concentration and uncertainty provided by FTIR analysis software. The helium tracer concentration is used to correct the offgas data for the unknown total offgas flowrate.

$$HMDSO_{(SRNL-scale)}(mmol/\min) = \frac{C_{HMDSO}}{C_{He}} * F_{He}(cm^3/\min) * \left(\frac{F_{SRNL-purge}}{F_{air}+F_{He}}\right) * \frac{mmol}{24.146 cm^3} \qquad \text{Equation 19}$$

The inputs were processed using the statistical package GUM Workbench[22] to propagate the uncertainty in the measurements to the calculated results. The expanded uncertainties are the half-widths of the two-sided

95% confidence intervals on the average analytical measurements for all data except HMDSO. For HMDSO, a rectangular distribution is assumed (any value within the rectangle is equally likely).

The peak HMDSO concentration, with uncertainty is summarized in Table 3-43. A graph showing the HMDSO concentration for all runs is shown in Figure 3-32. Graphs showing the HMDSO concentration for each run are included in Appendix D.

Table 3-43. SRAT and SME HMDSO Peak, ppm_v and mmol/min SRNL Scale

	SRAT				SME			
Run	**Antifoam Addition, g**	**ppm_v**	**SRNL Scale mmol/min**	**mmol/ min/g**	**Antifoam Addition, g**	**ppm_v**	**SRNL Scale mmol/min**	**mmol/ min/g**
NG51	0.7356	NA	NA	NA	NA	NA	NA	NA
NG52	0.763	1870±73	0.0277±0.00027	0.0363	NA	N/A	N/A	N/A
NG53	0.7565	810±36	0.0112±0.0011	0.0148	NA	N/A	N/A	N/A
NG54	0.7267	1230±50	0.0188±0.0018	0.0259	NA	N/A	N/A	N/A
NG55	0.5189	NA	NA	NA	NA	NA	NA	NA
NG55A	0.7658	NA	NA	NA	NA	NA	NA	NA
NG56	0.5146	1090±43	0.0161±00.0015	0.0313	NA	N/A	N/A	N/A
NG57	0.5169	970±42	0.0178±0.0018	0.0344	NA	N/A	N/A	N/A
NG58	0.7601	NA	NA	NA	NA	NA	NA	NA
NG59	0.7606	1780±67	0.0270±0.0025	0.0355	NA	N/A	N/A	N/A
NG60	0.5178	968±40	0.0145±0.0014	0.028	0.4074	117±5	0.00182±0.00017	0.0045
NG61	0.7549	807±35	0.00992±0.00096	0.0131	0.2163	17±0.9	0.00023±0.00002	0.0011
NG62*	0.7635	6.7±0.7	0.00010±0.00001	0.0001	0.3864	16±1.0	0.00025±0.00003	0.0006
NG63	0.6437	492±21	0.01176±0.00080	0.0183	NA	N/A	N/A	N/A
NG64	0.754	371±17	0.00926±0.00065	0.0123	NA	N/A	N/A	N/A
NG65A	0.1336	115±7	0.00313±0.00027	0.0253	NA	N/A	N/A	N/A
NG66	0.1236	297±16	0.00436±0.00047	0.0353	NA	N/A	N/A	N/A
NG67	0.1133	146±9	0.0041±0.0004	0.0362	0.1357	27.6±1.3	0.00028±0.00004	0.0021

* FTIR was not online during post-acid boil peak. The value shown is for maximum during use of the FTIR. FTIR was not used at time of expected maximum SRAT peak HMDSO,

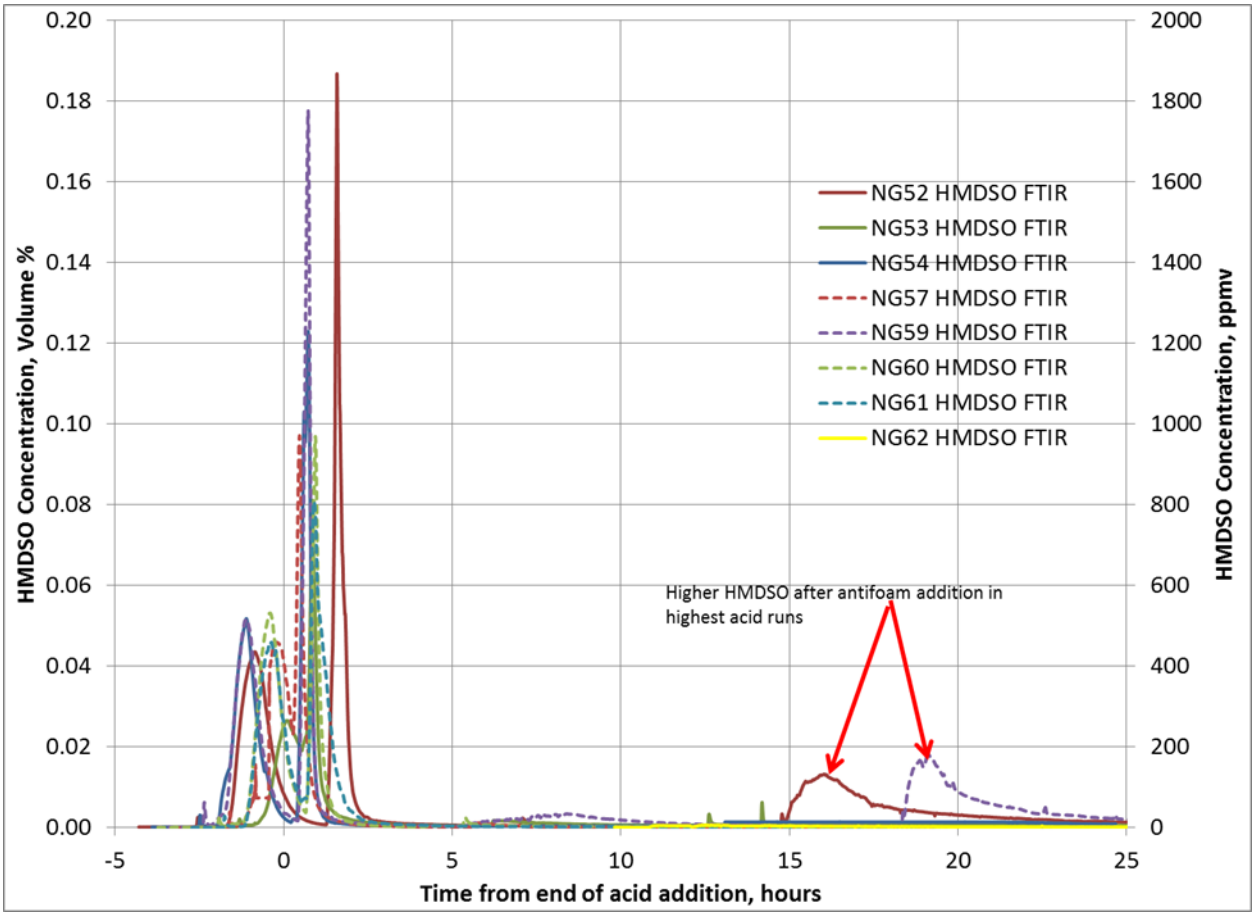

Figure 3-32. HMDSO Concentration Profile for Runs NG52, 53, 54, 57, 59, 60, 61 and 62

3.3 Comparison of SC-18 Shielded Cells Run and NG58 Simulant Run

Shielded cells experiment SC-18[7] was completed at conditions most similar to the NG58 SRAT cycle. The collected data by the control computer and the GC are compared in this section. A graph showing the location of SC-18 in the SB9 simulant matrix is included in Figure 3-33.

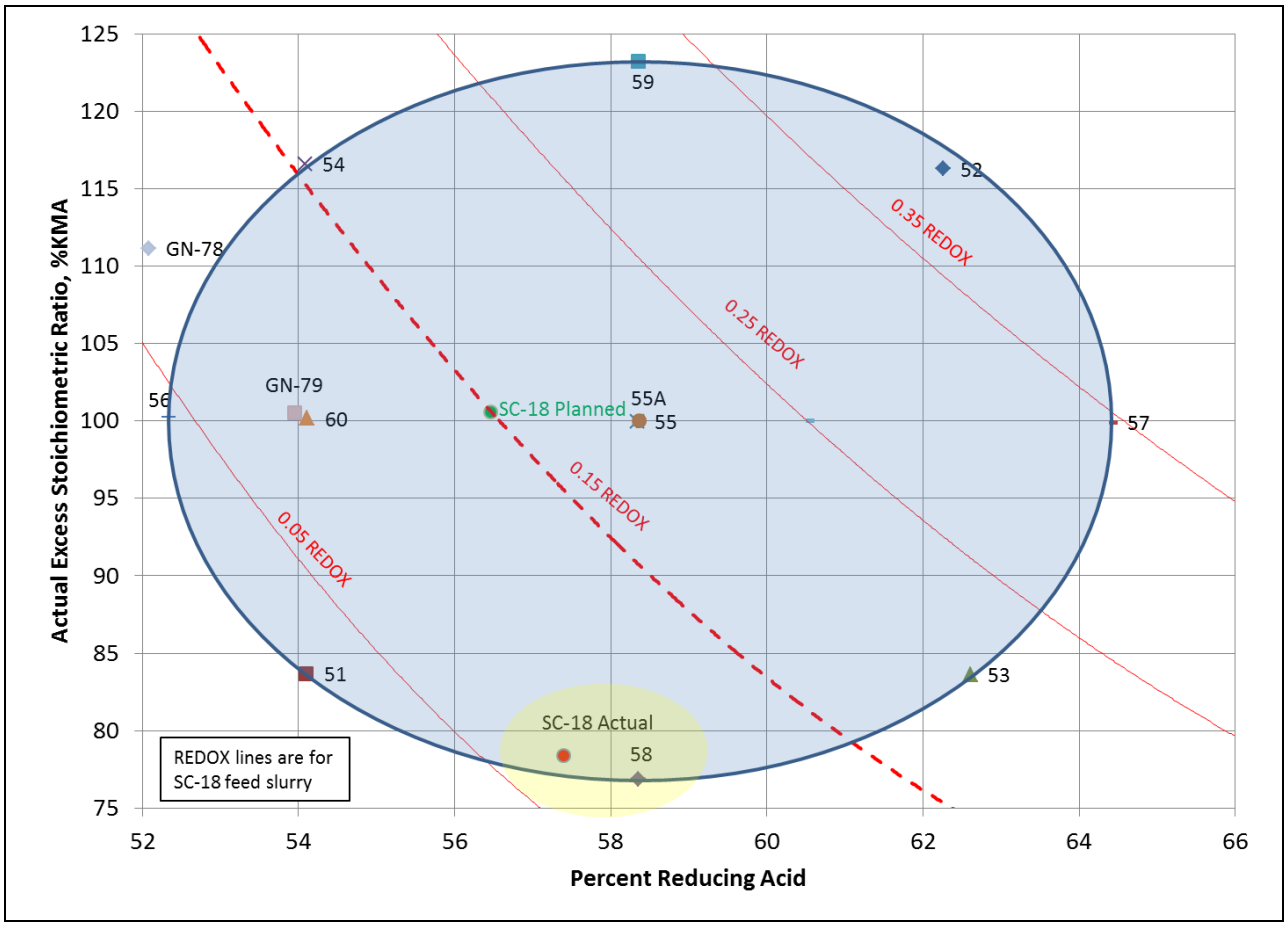

Figure 3-33. SB9 Nitric-Glycolic Acid Flowsheet Testing Window

Since rheology is the most important parameter for optimizing CPC processing for the nitric-glycolic acid flowsheet, the torque and rheology will be compared. The torque as measured by the mixer can be used to determine changes in resistance of the slurry to flow throughout the SRAT and SME processing. The measured torque for each run is the sum of the resistance of the shaft through the coupling plus the resistance due to the slurry. Since the torque due to the shaft resistance is different for each run, the torque for SC-18 was plotted on the left y-axis and the torque for NG58 was plotted on the right axis. Both runs had agitation speeds of 700 rpm. Both torque profiles have the same shape, starting with a high torque, decreasing during nitric addition/heating, staying relatively steading during glycolic acid addition, dropping by about 5 in-oz during initial dewater and then remaining steady throughout the rest of the SRAT cycle. The advantage of torque measurement is that it shows the changes throughout the SRAT and SME cycle at the processing temperature (rheology is impacted by temperature). The torque data is illustrated in Figure 3-34.

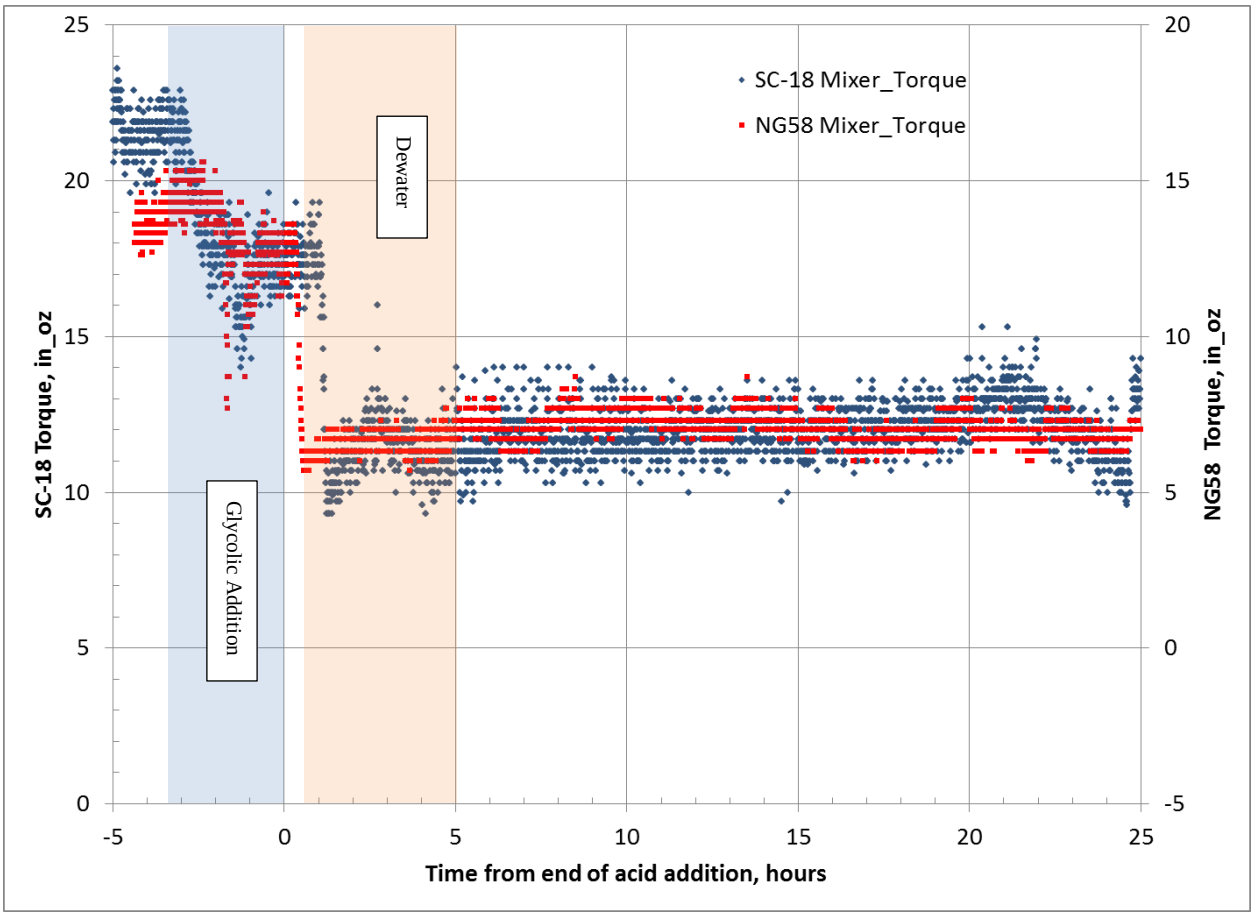

Figure 3-34. Torque Profile for Runs NG58 and SC-18, in-oz

Two rheograms were completed on the NG58 SRAT product and three rheograms were completed on the SC-18 SRAT product. Note that the NG58 SRAT product was 29.8 wt % total solids, more concentrated than the SC-18 SRAT product which was 24.6 wt % total solids. The NG58 and SC-18 were both thin rheological slurries with both the yield stress and consistency lower than design basis. The yield stress for the NG58 run was slightly higher than SC-18, likely due to it being more concentrated. The results are summarized in Figure 3-35. The NG58 SRAT product had a yield stress of 0.6 Pa and a consistency of 5.6 cP. The SC-18 shielded cells run had a SRAT product yield stress of 0 Pa and a consistency of 2.8 cP. Both SRAT products were rheologically thin, although the NG58 SRAT product was higher in total solids (30% versus 25% for SC-18) so would be expected to high a higher yield stress and consistency.

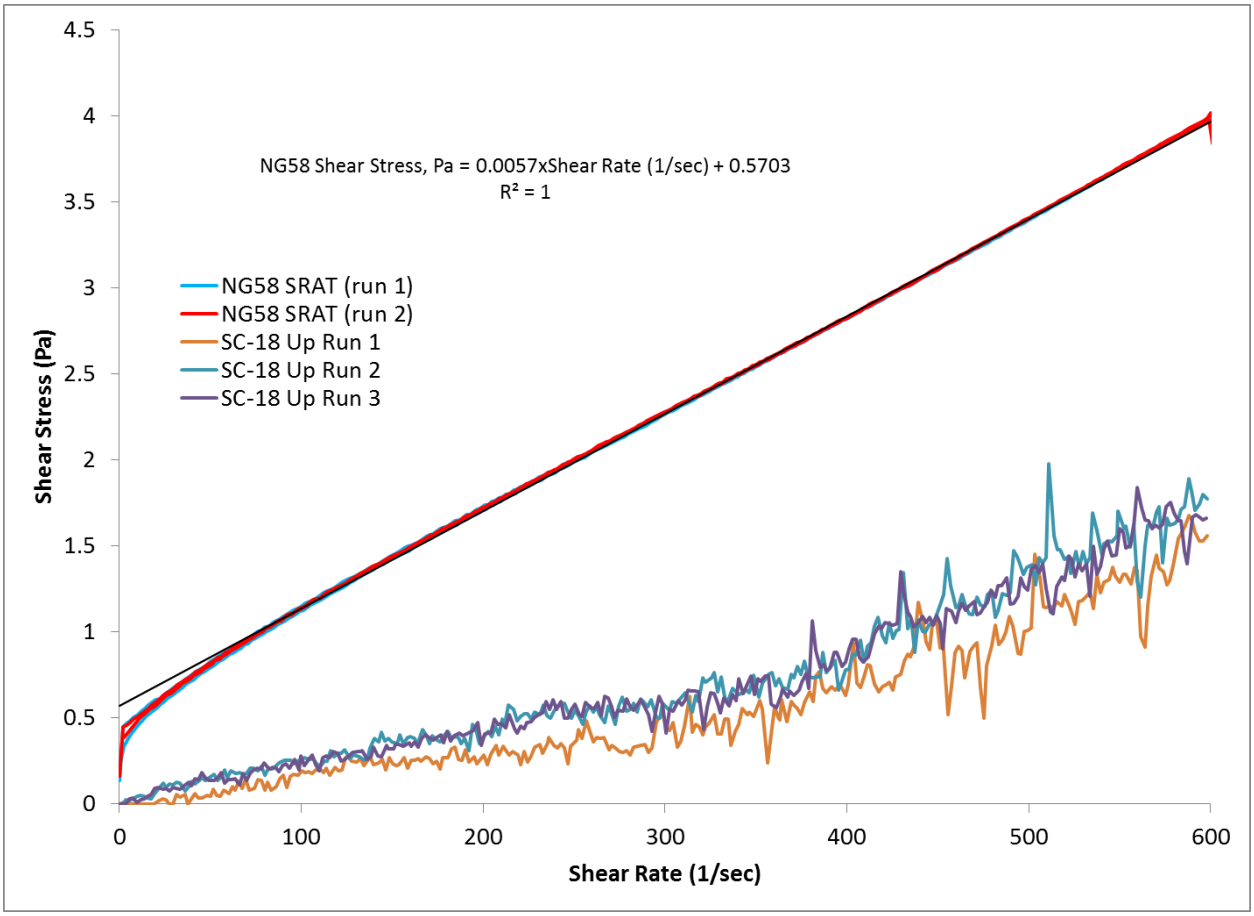

Figure 3-35. Rheology Profile for Runs NG58 and SC-18, Shear Stress (Pa) vs Shear Rate (1/sec)

Both runs SC-18 and NG58 had pH probe problems. In SC-18, the pH probe stopped functioning during glycolic acid addition. Samples pulled throughout the SRAT cycle were analyzed for pH in the cells after the completion of the SRAT cycle. Both sets of SC-18 pH data are shown in Figure 3-36. The post calibration check of the pH probe after NG58 had an offset of 0.8 pH units as it was checked in 4, 7 and 10 pH buffers. As a result, all pH readings were linearly adjusted by adding up to 0.8 pH units. The SRAT product was 6.9 for SC-18 and 7.75 for NG58. The resulting profiles for both runs look similar. The SRAT product pH is expected to be higher than other runs because of the low acid stoichiometry for both runs.

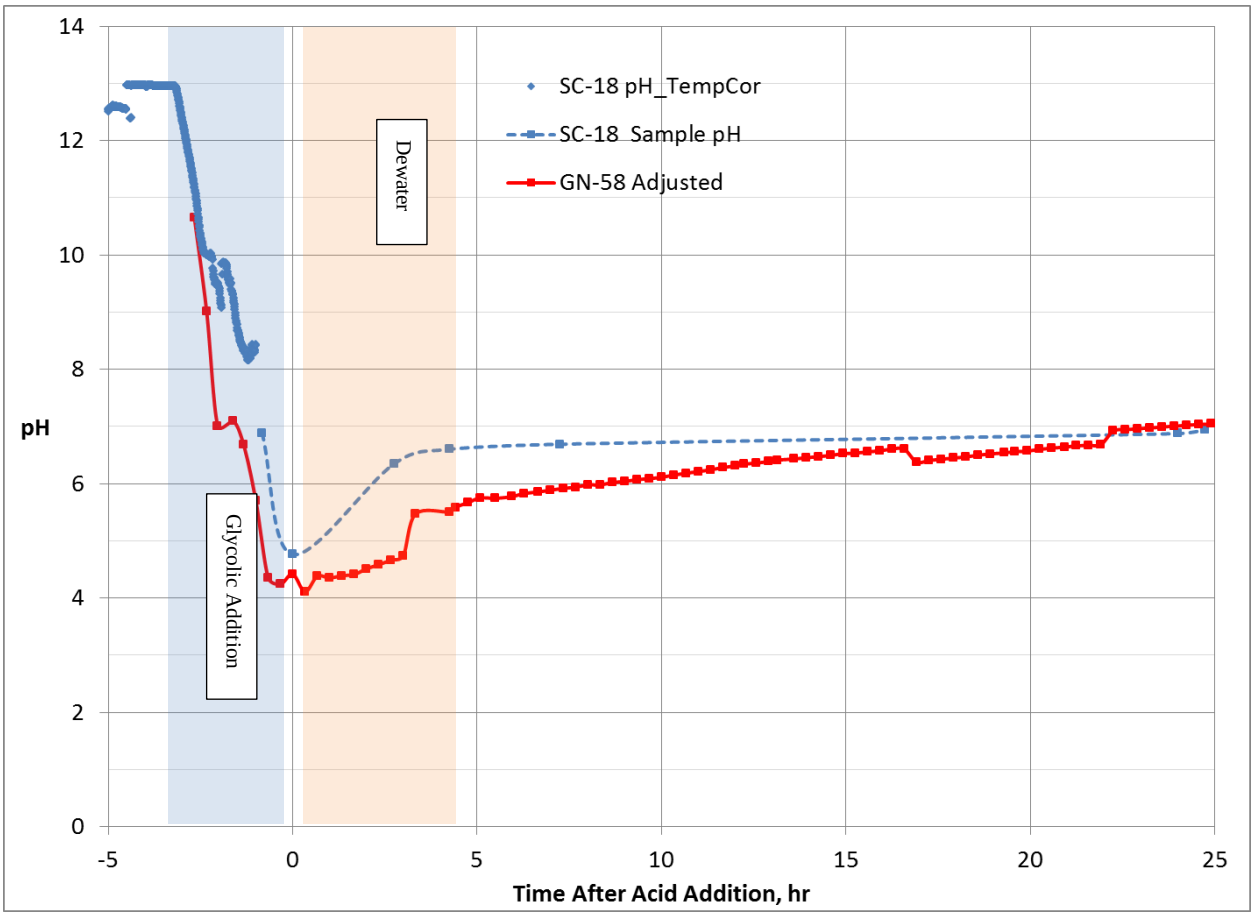

Figure 3-36. pH Profile for Runs NG58 and SC-18

Offgas profiles for three offgas species are included in this section, namely oxygen, carbon dioxide and nitrous oxide. A hydrogen profile is not included as hydrogen was below the quantification limit in both runs. In both runs, the oxygen concentration profiles are similar. During the glycolic acid addition, carbon dioxide and oxides of nitrogen are formed and dilute the oxygen concentration. The oxygen concentration begins to increase once acid addition stops and then drops again, becoming nearly depleted as boiling is initiated. About an hour after dewater begins, the oxygen concentration begins climbing and has recovered to essentially normal by about 10 hours into conflux. A graph showing the oxygen profile for both runs is included in Figure 3-37.

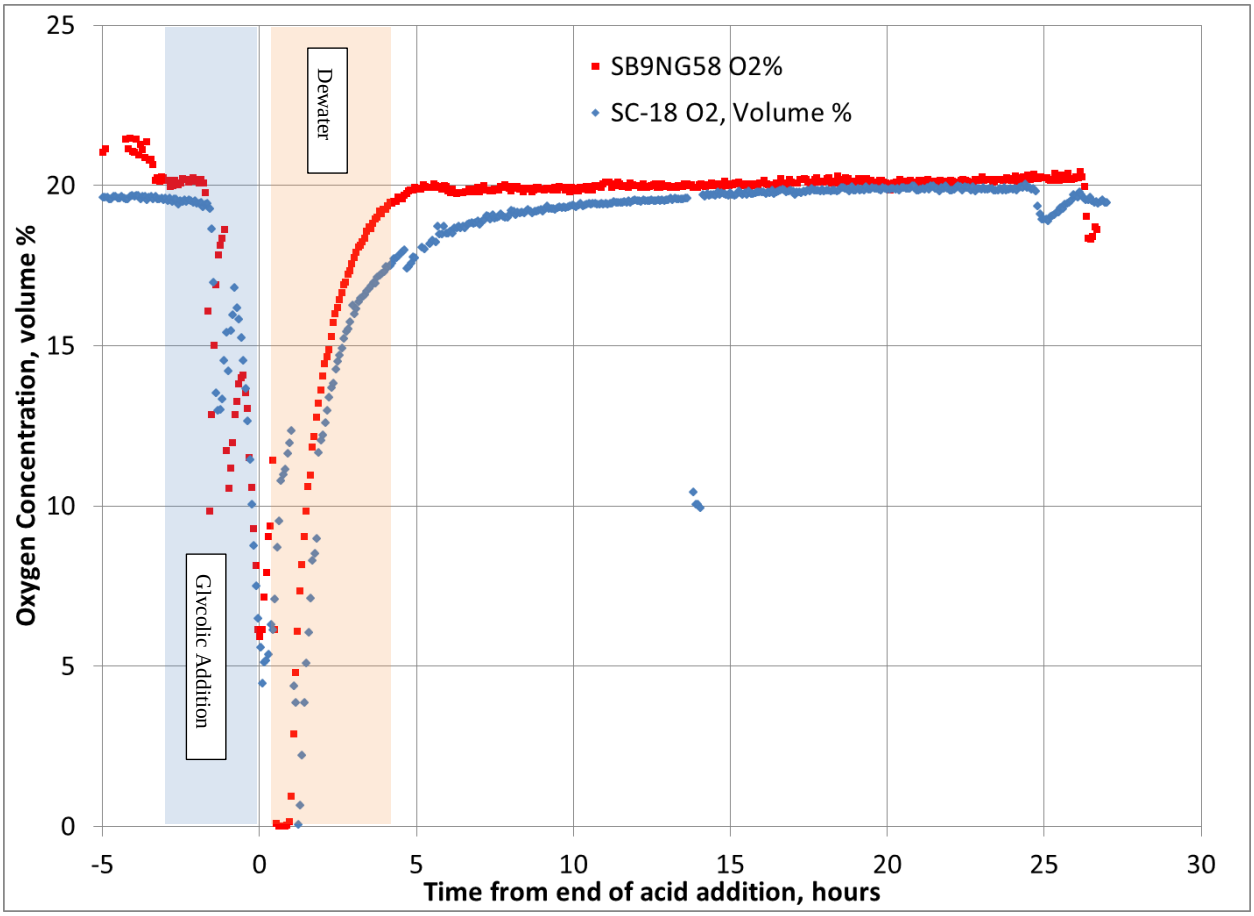

Figure 3-37. Oxygen Profile for Runs NG58 and SC-18, volume %

In both runs, the carbon dioxide concentration profiles are very similar. During the glycolic acid addition, carbon dioxide is formed as carbonate is destroyed and the CO_2 concentration peaks at 36 volume % for SC-18 and 50 volume % for NG58. The simulant is higher in carbonate (simulant TIC was 1,619 mg/kg, significantly higher than the SB9 actual slurry which was 1,140 mg/kg). The higher peak from the simulant experiment is expected. The CO_2 concentration increased again as boiling was initiated. The CO_2 concentration continues to decrease to essentially normal by about 7 hours into conflux. A graph showing the CO_2 profile for both runs is included in Figure 3-38. The peak carbon dioxide in the SRAT varied from 690 to 800 lb/hr at DWPF scale, significantly higher than the 342 lb/hr measured in the SC-18 shielded cells actual-waste demonstration. The peak carbon dioxide in the SME varied from 4.9-6.1 lb/hr, significantly lower than the 19 lb/hr measured in the SC-18 shielded cells run.

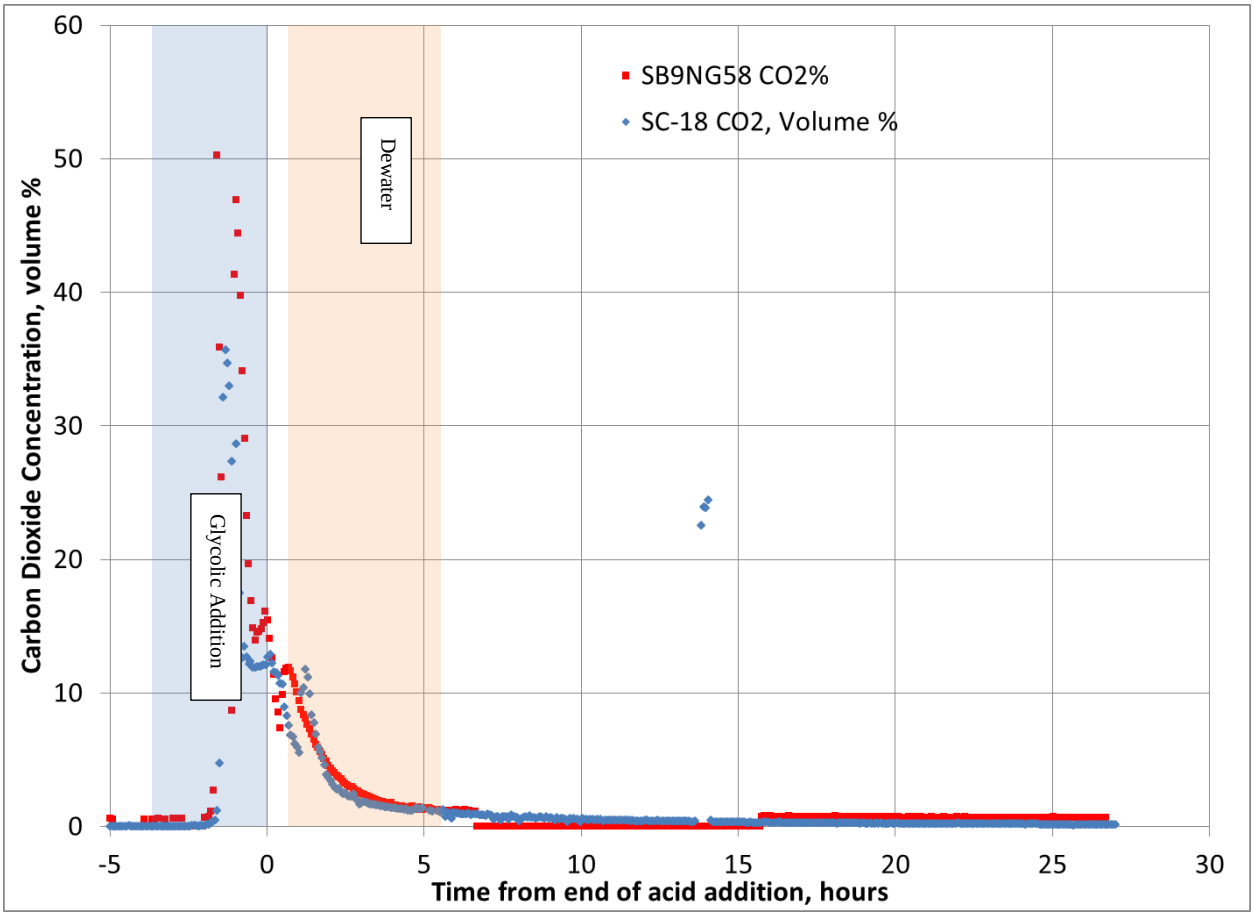

Figure 3-38. Carbon Dioxide Profile for Runs NG58 and SC-18, volume %

In both runs, the nitrous oxide concentration profiles are similar, although the N_2O quantification limit is much higher in the NG58 run. This led to the data dropping from about 0.15 to 0 at about 5 hours. Two things are noted here to explain the slower nitrite destruction and N_2O generation in NG58. First, the N_2O peak is higher for the shielded cells run (0.57 volume %) compared to 0.40 volume % for NG58 (a run using ruthenium nitrosyl nitrate). In SB9 nitric-formic acid flowsheet runs[11], testing using ruthenium chloride (SB9A-11A) led to an N_2O peak that was 29% of the N_2O peak from an identical run using ruthenium nitrosyl nitrate. Second, the nitrite destruction is probably a little slower in run NG58, likely due to the lower acid stoichiometry or higher starting nitrite concentration. A graph showing the N_2O profile for both runs is included in Figure 3-39. In simulant experiments, the nitrous oxide peak was 0.23 to 1.0 vol% in the SRAT and <0.069 vol% in the SME. The peak nitrous oxide in the SC-18 shielded cells run actual-waste demonstration was 0.57 vol% in the SRAT and 0.08 vol% in the SME.

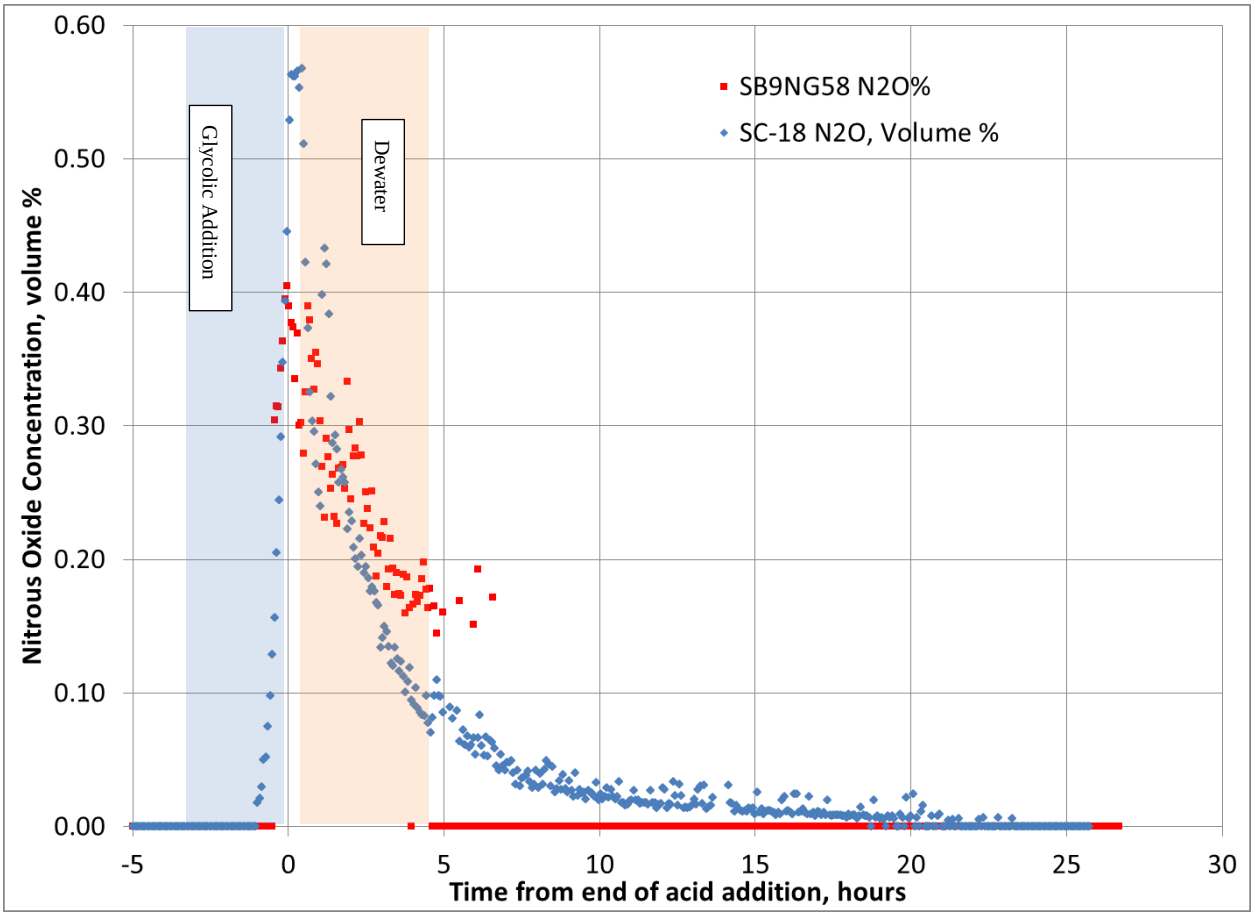

Figure 3-39. Nitrous Oxide Profile for Runs NG58 and SC-18, volume %

Nitrite was reduced during simulant experiments from 10,200 mg/kg in the sludge simulant to <500 mg/kg in the slurry and <100 mg/L in the supernate. Nitrite in the SC-18 SRAT and SME products were 304 and 380 mg/kg respectively.

The conclusion from this section is that the chemical profiles and resulting rheology are very similar in comparing NG58 and SC-18. The resulting rheology, offgas generation and pH profiles are all similar, which allows the prediction of SRAT and SME product anion concentration using the equations developed from simulant testing.

3.4 Analytical Methods (Additional Task e in TTR[1])

Two critical analytical methods for DWPF are the methods necessary for measuring the SRAT and SME products for anions and cations. The most variable in developing the nitric-glycolic acid flowsheet have been the ion chromatography method for anions and the REDOX method. These will both be discussed below.

3.4.1 Anion Methods

The DWPF laboratory uses a water dilution method to prepare samples for analysis by ion chromatography. Because this method is inadequate for the oxalate analysis, the DWPF laboratory also uses an HCl/HNO_3 digestion (oxalate prep method) to quantify oxalate.

The results from three analytical methods are discussed below. The water dilution method uses water to dilute a slurry sample. The caustic quench method adds 2 mL of 50 wt% sodium hydroxide to approximately 10 mL of slurry. In both water and caustic quench method, additional water is added and the samples are filtered prior to analysis. The caustic quench method was developed since the water dilution method works well for nitrate analysis but does not work well for glycolate or oxalate. A third method, filtering the slurry prior to analysis was also completed. Filtered sample results were converted to a slurry basis using equation x to put all results on a slurry basis.

For runs NG54, 55, 55A, 56 and 59 each SRAT product was analyzed twice using each method. For each of these runs, the SRAT product slurries were resubmitted and reanalyzed, giving two sets of caustic quench results for each run. A bar graph comparing analysis for nitrate, glycolate, oxalate and formate are summarized in Figure 3-40 and included in Appendix F. It should be noted that each of the reanalysis oxalate values were lower than the initial oxalate value for the caustic quench method.

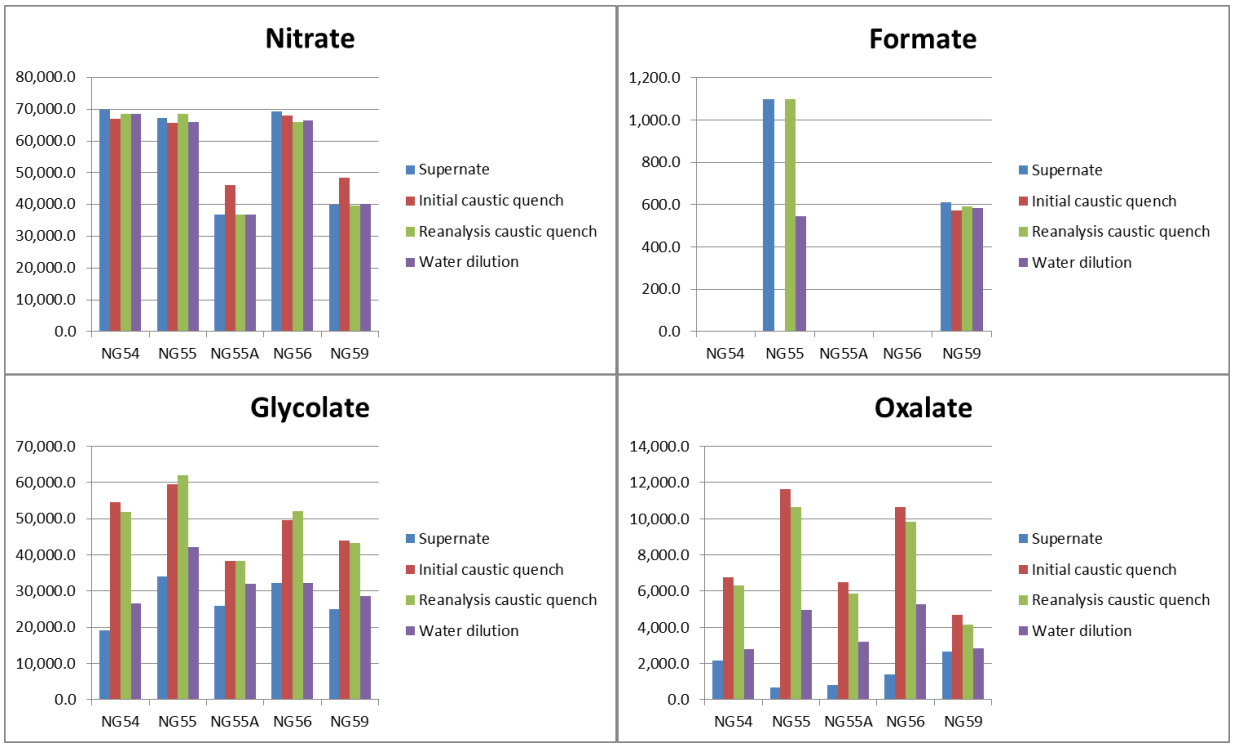

Figure 3-40. Comparison of SRAT Product Anion Measurements for Runs 54, 55, 55A, 56, and 59, mg/kg slurry basis

The caustic quench method has no impact on the nitrate analysis. However, for glycolate and oxalate, both significant in predicting REDOX, the caustic quench methods reports higher concentrations for both oxalate and glycolate. It is recommended that the caustic quench method is used for analyzing all SRAT and SME slurry samples for anions. It also can be used to replace the oxalate prep method.

3.4.2 REDOX Method (Additional Task c in TTR[1])

During this study, there were 72 attempted REDOX samples, with 35% of them having a problem where the lid popped off or the crucible foamed over during melting. In cases where the lid popped off, there is

likelihood that the REDOX sample will be over oxidized. Some of the glasses had noticeable red swirling within the glass (the matrix center point, NG-55-2 glass photo, is shown in Figure 3-41).

Nonhomogeneity makes it more difficult to accurately measure the REDOX. Sample to sample variation in the REDOX measurement (within the set of 13 runs) as measured by percent relative standard deviation (RSD) varied from 0.3 to 51.2% (averaging 23%) for nitric-glycolic acid runs. For the 11 nitric-formic acid runs, the REDOX percent relative standard deviation varied from 2 to 19% (averaging 9%). The nitric-glycolic acid runs crucible test glasses demonstrated less homogeneity and the resulting REDOX is more varied than the nitric-formic acid runs crucible test glasses. A follow-up study will be completed to finalize the REDOX model.

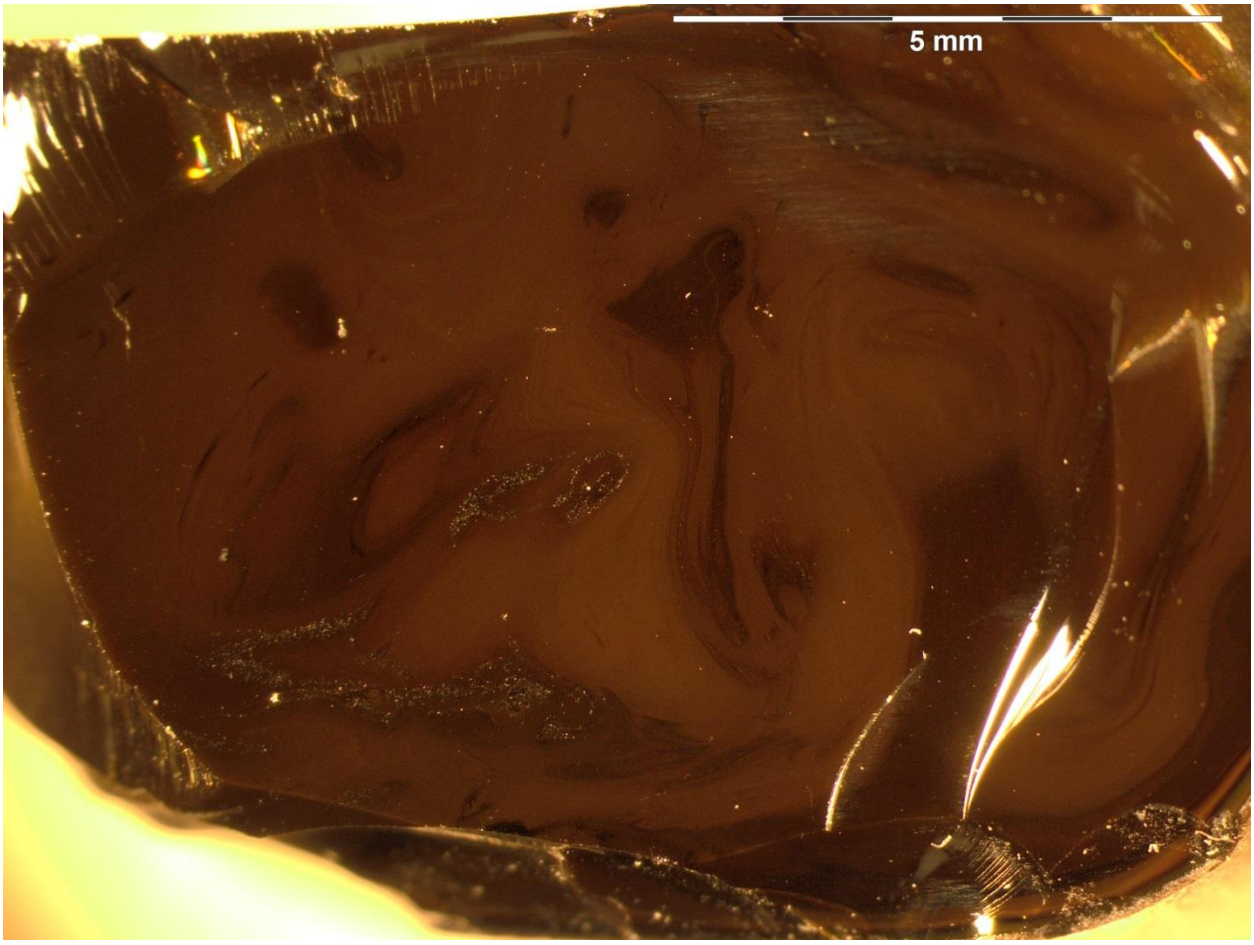

Figure 3-41. 1.25x magnification of NG55-2 glass sample prior to REDOX analysis

3.5 Optimum Processing for the Nitric-Glycolic Acid Flowsheet

The nitric-glycolic acid flowsheet offers huge improvements for DWPF processing. First it virtually eliminates that catalytic production of hydrogen, a flammable gas that requires air dilution during processing. Second, it greatly minimizes the production of ammonia (likely also catalyzed by noble metals). A third improvement is the steady pH throughout the second half of the SRAT cycle and the SME cycle, leading to rheologically thinner slurries and minimizing the adsorption of carbon dioxide (sodium carbonate) in the slurry. Fourth, the wide operating region for processing gives DWPF more flexibility in

choosing the acid stoichiometry, especially related to the stripping of mercury and collection of mercury in the MWWT. The conclusion is that DWPF should transition to the nitric-glycolic acid flowsheet to maximize safety and process flexibility as is planned.

Due to the eminent startup of the Salt Waste Processing Facility (SWPF) and its higher production rate for PRFT and SEFT, it is recommended that the steam flow used during processing should be increased to allow faster processing of slurries in the CPC, which may also improve mercury recovery.

3.5.1 Processing Recommendations

Based on simulant and actual waste testing, the following is recommended as the processing targets for the nitric-glycolic acid flowsheet in DWPF for SB9 after the transition is complete. Some of these targets may not be achievable based on current equipment configuration, safety basis or processing strategies. They are recommended to optimize processing (maximum throughput, maximum mercury recovery, and acceptable rheology). DWPF experience in processing with this flowsheet will lead to different processing targets that work best for the facility.

- Heat SRAT to boiling. Add 0.25 gallons of antifoam just prior to SRAT boiling (antifoam not needed until process gases are generated).
- Add PRFT material at maximum rate and continue processing until PRFT dewater phase is complete. Ramp down steam flow concurrently with ramping down PRFT addition.
- After cooling, pull sample and analyze SRAT receipt as is being done currently with the addition of the glycolate analysis.
- Complete acid calculation. Initially target 100% KMA or Hsu 104.5% acid stoichiometry. In subsequent batches, a higher acid stoichiometry may be preferable if 100% KMA doesn't increase MWWT mercury recovery. Analysis of the SRAT product for mercury is recommended to monitor the effectiveness of mercury stripping.
- Use glycolic chemistry equations to calculate the percent reducing acid to target a REDOX of 0.1 for argon bubbled melter and 0.2 for non-bubbled melter operations until REDOX evaluation and report are complete. Analysis of a pour stream sample for REDOX is recommended to ensure the REDOX target is being met.
- Add acid at high agitator speed if possible.
- Add nitric acid during heatup at a rate equivalent to 179 mol/min or 4.5 gpm for 50 wt% nitric acid.
- Antifoam may be needed during nitric acid addition. The HMDSO peak is highest during acid addition and the first two hours of boiling. Antifoam additions should be at least 3 hours apart to minimize the risk from "stacked" antifoam additions.[23] Add 0.25 gallons of antifoam when carbonate destruction begins (nitrogen concentration drops due to dilution and the SRAT pressure will increase by about 10 inwc). This is about half-way through nitric acid addition.
- Add glycolic acid at a rate equivalent to 179 mol/min or 4.0 gpm for 70 wt% nitric acid.
- Add 0.25 gallons of antifoam prior to SRAT boiling or as needed during glycolic acid addition to prevent foaming.
- Ramp steam flow to target boilup rate after SRAT boiling begins. Dewater and reflux at high agitator speed to improve mercury recovery if possible.
- Dewater to 25 wt % total solids in SRAT.
- Add SEFT material at maximum rate.
- Add 0.25 gallons of antifoam each 12 hours at boiling or sooner if needed.
- Continue adding SEFT until addition and dewater phase is complete. Ramp down steam flow concurrently with ramping down SEFT addition.
- Continue refluxing until conflux time has been reached.

- Cooldown, sample, and analyze SRAT product. Note nitrite concentration but nitrite does not need to be destroyed to transfer SRAT product to SME. A nitrite concentration above 2,000 mg/kg in the SRAT product is an indication of under addition of acid. The predicted REDOX should be checked to ensure the proper ratio of acids was added.
- Transfer SRAT product to SME heel.
- Add canister blast to SME, if required.
- Heat SME to boiling. Add 0.25 gallons just prior to SME boiling (antifoam not needed until process gases are generated). Ramp steam flow to minimize offgas surge. Cool when dewater is complete.
- Repeat until all canister blasts to SME and dewater is complete.
- Heat SME to boiling. Add 0.25 gallons just prior to SME boiling (antifoam not needed until process gases are generated). Ramp steam flow to minimize offgas surge. Cool when dewater is complete.
- Repeat until all process frit/water additions are completed and dewater target of 45 wt % total solids has been reached.

3.5.1.1 Increased Mercury Recovery:

- If possible, maintain a high steam rate to maximize mercury stripping. Testing with simulants at design basis boilup rate led to higher mercury collection than testing at 2,500 lb/hr. Since DWPF is designed to be the purge point for mercury recovery, maximizing the boilup rate may lead to higher mercury recovery in addition to shortening cycle time.
- If possible, operate SRAT during boiling at high agitation speed. Testing with simulants at higher agitation rate led to higher mercury collection. This might not be a good processing idea in the SME due to erosion by the frit. Better suspension of the elemental mercury is likely the reason for the improved recovery.
- Increase or eliminate the pH limit in the SMECT. Condensate generated in CPC processing is very acidic during the first few post acid addition hours of boiling. Eliminating the practice of adding nitric acid to the SMECT, except in the case of a foamover should minimize the dissolution of mercury in the SMECT.
- Transfer mercury from the MWWT to the mercury cell each batch. If mercury is left in the MWWT, it may be dissolved in subsequent batches during periods of high nitric acid generation.
- Consider processing changes to maximize mercury recovery. A study might identify processing changes without having to replace equipment
- Consider initiating a study to consider physical changes to the DWPF MWWT and condensers to improve mercury recovery. The poor decanter design and the hot operating temperature of the SRAT and SME condenser may be limiting mercury recovery. The removal of solids other than mercury from the SMECT and MWWT is difficult based on the current design.

3.5.1.2 Minimize Processing Time:

- Processing time is minimized by operating at maximum acid addition and steam flowrates and minimum acid stoichiometry.
- Process melter feed produced at minimum acid stoichiometry will minimize the offgas produced in the melter, leading to faster melting and fewer process upsets..
- Concentrate the SRAT and SME products to maximum extent without exceeding rheology limits to minimize use of melter for evaporation of water.

3.5.1.3 Increasing Boilup Rate

Increasing boilup rates in the CPC does have disadvantages. The primary disadvantage is foaming/entrainment of solids. Good processing techniques are recommended to minimize foaming/entrainment, and should be considered for implementation:

- Back off on boilup rate as boiling is approached after acid addition (there is a surge of offgas as boiling is initiated)
- Ramp up steam flow (instead of stepping up steam flow from 1000 to 2000 lb/hr for instance) once boiling is initiated will minimize the chance of a foamover (this should be automated to more quickly reach peak steam flowrate and eliminate shift to shift variations in processing)
- Ramp down steam flow coincident with ramping down PRFT or SEFT addition to prevent a surge of offgas steam when liquid flow is stopped without backing off on steam flow
- Use gas chromatographs to monitor offgas generation and note when offgas generation is increasing. The nitrogen and oxygen concentration will drop when CO_2 is being produced. The nitrogen concentration will drop and the oxygen concentration might drop to zero when the NO and NO_2 production is high.
- A good practice is to monitor SRAT foam level with camera during periods of significant offgas production and when it has been a long time since antifoam was added. Antifoam can be added as needed.
- Optimize the use of antifoam. Batch additions of antifoam are not the optimum delivery method. A slow, continuous antifoam addition during processing would limit the mass of antifoam needed, maximize the antifoam effectiveness and eliminate the addition of dilution water to flush in the antifoam.
- Develop a better method for controlling foam. A more chemically stable antifoam or a nonchemical foam control method would help to decrease processing time in the CPC.
- Consistent processing is the key to maximum productivity in any chemical processing plant. This means using the same volume of sludge, PRFT, and SEFT for each batch, which will lead to the same nitric and glycolic addition, the same dewater volume, the same conflux time, etc. When possible, PRFT and SEFT should be used in all batches to minimize the upsets and changes in chemistry, particle size, rheology, and foaming, especially from the addition of PRFT.

3.5.2 Operating Window(Additional Task h in TTR[1])

Since negligible catalytically generated hydrogen is produced throughout SRAT and SME processing, the CPC operating window is determined primarily by slurry rheology. Slurry rheology will change from sludge batch to sludge batch as the rheology of the sludge changes. The SB9 operating window with sludge simulants tested to date is approximately from 75% KMA to 123% KMA. Testing has been completed up to 200 % KMA[12] but these higher acid stoichiometry windows produce very thick slurries and would have to be processed at lower total solids in the SRAT and SME products to be feasible. For SB9 runs with KMA ≤100%, the SRAT products were processable up to about 30 wt % total solids. For SB9 runs with KMA greater than 100%, the SRAT products were processable up to about 20 wt % total solids. In the high KMA runs, processing at higher total solids led to thick rheological slurry, fouling of rods, and mixing problems. The antifoam strategy has only been tested to 110% KMA. Note that the three regions in the graph were determined based on simulant testing and DWPF experience in processing with this flowsheet may lead to different processing targets that work best for the facility.

Assuming a REDOX window of 0.09-0.33, the operating window (based on simulant testing) is shown graphically in Figure 3-42.

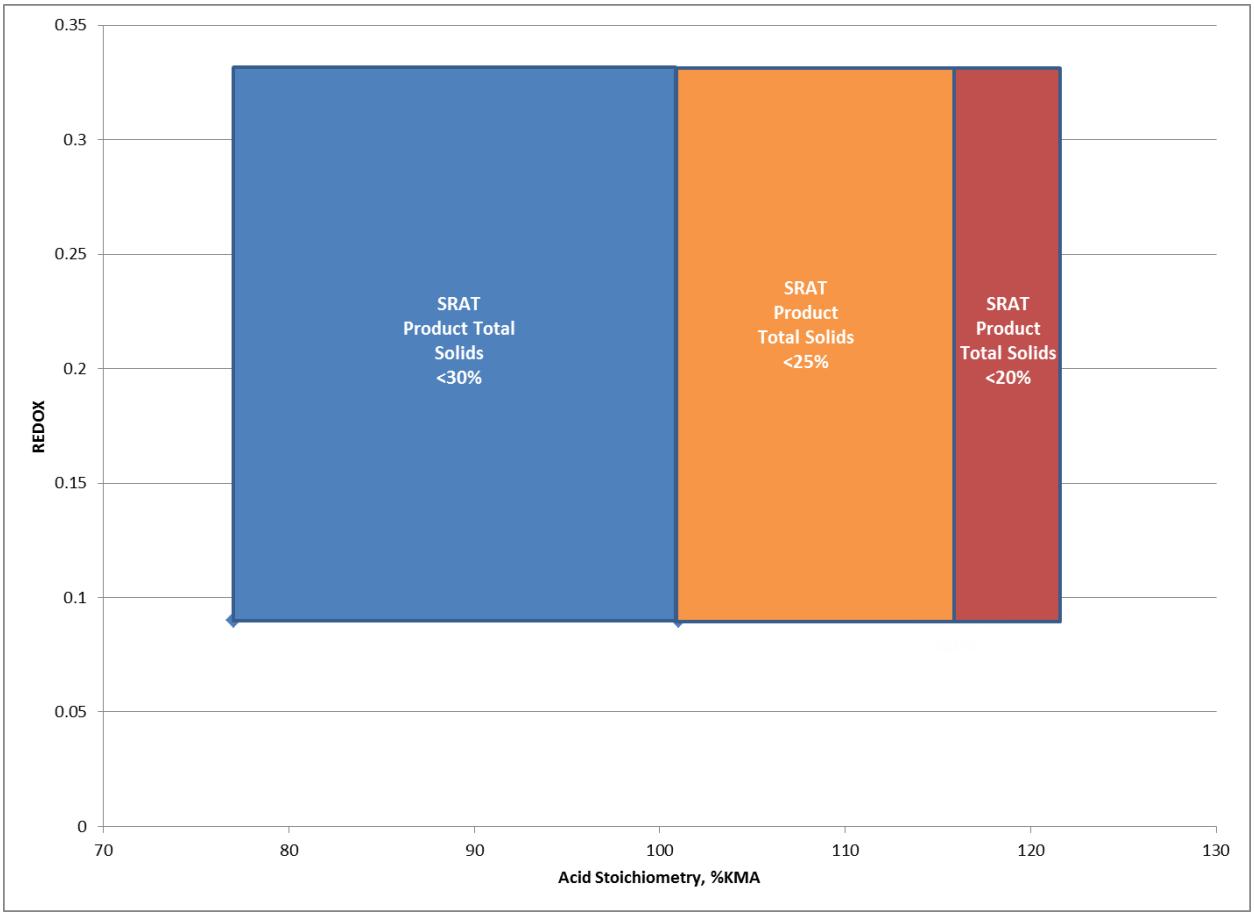

Figure 3-42. SB9 Processing Window

3.5.3 Transition from Nitric-Formic Acid Flowsheet to Nitric-Glycolic Acid Flowsheet

Because of the heels present in DWPF processing vessels, the transition from the nitric-formic acid flowsheet to the nitric-glycolic acid flowsheet will create some unique batches that can be challenging to determine the best processing conditions. Testing was not performed with SB9 simulant that specifically included nitric-formic flowsheet SRAT and SME heels with nitric-glycolic tests. However, past testing completed with varying mixtures of glycolic and formic acid provide analogous information that can be helpful during the transition, especially the runs that used an 80:20 molar blend of glycolic and formic acid.[24-27]

One key insight from this previous work is that little formic acid was left in the SRAT product even though 20% of the added organic acid was formic acid. This is because the formic acid is so much more reactive than glycolic acid in CPC processing. In addition, the hydrogen generation was much lower in runs with the 80:20 blend than for the nitric-formic flowsheet.

The result is that the transition from the nitric-formic to the nitric-glycolic acid flowsheet in the SRAT should be essentially complete after the first SRAT batch. During the first batch, hydrogen generation is expected, however it will be significantly lower than for a similar batch produced using the nitric-formic acid flowsheet. In subsequent SRAT cycles, the hydrogen generation is expected to be very low and may be below the GC's detection limit.

The transition in the SME cycle is expected to be slower, as less chemistry occurs in SME processing. The transition will be similar to a transition from one sludge batch to another. To ensure the hydrogen generation is less than the limit in the SME, the KMA acid stoichiometry should be targeted at 100% KMA to ensure the destruction of nitrite, which may lead to activation of the rhodium and higher hydrogen generation.

Due to the tank heels and the chemistry that occurs during each process step, the vessel contents at the end of each process step during transition can be approximated by a mixture of nitric-formic and nitric-glycolic flowsheet material. A projection was completed to determine the percent of nitric-formic flowsheet material that would be present in the SRAT, SME and MFT during the flowsheet transition. The assumption for the SRAT is that the first batch will result in a totally nitric-glycolic flowsheet SRAT product because formic acid is preferentially reduced and destroyed by active noble metal catalysts. The assumption was made that there is "no chemistry" in the SME so the percent of formic acid material was calculated by serial dilution of the heel knowing the heel and transfer volumes. In both the SRAT and SME, the heel was assumed to be 1,500 gallons and a 4,500 gallon transfer was made to the next tank. For the MFT, the assumption was the heel volume was 4,000 gallons. For the melter, the assumption was a 733 gallon continuously stirred tank reactor, fed by 1,100 gallons of new glass per batch based on the SC-18 SME product composition

Based on this analysis, the SME contains 6.25% nitric-formic flowsheet material by the completion of the SME batch NG2 and less than 0.39% by the completion of SME batch NG4. Because of the large heel in the MFT, the MFT contains 32% nitric-formic flowsheet material by the completion of the MFT batch NG2 and 7.6% by the completion of MFT batch NG4 (assuming no dilution by pump priming). To shorten the duration of transition, it is recommended that the heel volume in the MFT be reduced. If the MFT heel is decreased to 1,500 gallons the MFT contains 16% formic acid by the completion of the MFT batch NG2 and 1.6% by the completion of MFT batch NG4. The melter, assuming the large heel in the MFT, contains 40% nitric-formic flowsheet material by the completion of the melter batch NG2 and 10.9% by the completion of melter batch NG4 (assuming no dilution by pump priming). Note that these estimates for turnover times are calculated values based on optimal processing conditions. DWPF might experience longer turnover times than are predicted and plant data should be used to determine the extent of turnover. A graph summarizing this projection is summarized in Figure 3-43.

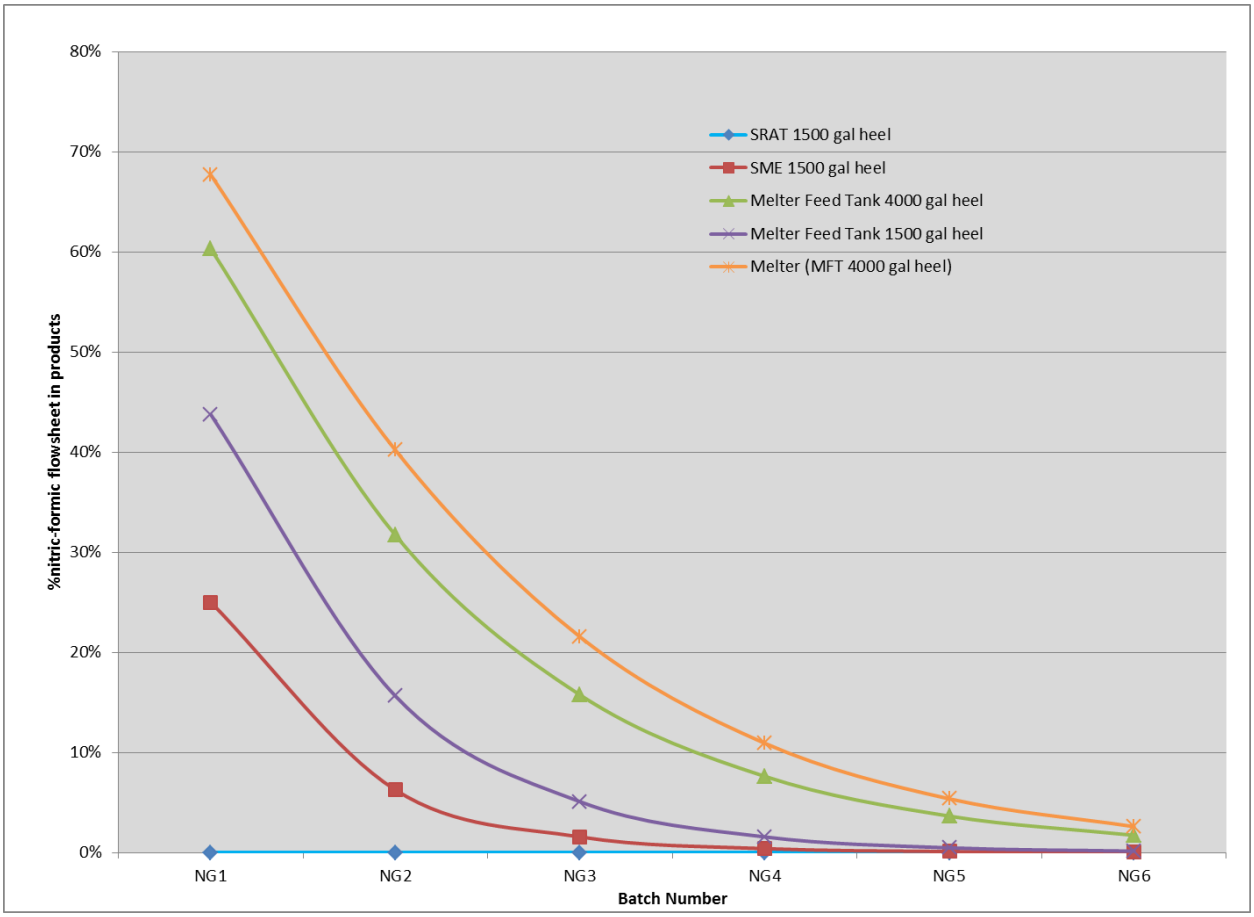

Figure 3-43. Percent Nitric-Formic Acid Flowsheet Present in SRAT, SME, MFT and melter during Transition

The recommended processing parameters during transition are the same as were recommended for flowsheet processing, as described in Table 3-44.

Table 3-44: Recommended CPC Processing Targets during Transition

Processing parameter	Recommended Value	Rationale
KMA Acid Stoichiometry	100%	Destroy nitrite in SRAT, ensure peak H_2 is in SRAT
Hsu Acid Stoichiometry	104.5%	
REDOX target	0.1 bubbled/0.2 unbubbled	Same target as formic acid processing
Antifoam Strategy	Nitric-glycolic acid	Needed to limit HMDSO peak within SB9 CPC flammability limits. Add antifoam more frequently if needed.
SRAT Total Solids Target, wt%	1% higher than nitric-formic processing each batch until 25% is reached	Nitric-glycolic flowsheet is thinner rheologically and can be concentrated further
SME Total Solids Target, wt%	1% higher than nitric-formic processing each batch until 42% is reached	Nitric-glycolic flowsheet is thinner rheologically and can be concentrated further
SRAT Acid Mix	Use final nitric-glycolic flowsheet REDOX and acid calculation equations to calculate	Acid mix is calculated to achieve REDOX target
Caustic boiling	Use same strategy as PRFT. More frequent additions may be needed. Not recommended during transition	Antifoam strategy was not demonstrated in testing with caustic boiling
Boilup Rate	Use current scheme	Eventually the boilup rates should be increased to minimize boiling time but not during the transition
Nitric Acid Addition rate, gpm	4.5 gpm of 50 wt%	179 mol/min addition rate
Glycolic Acid Addition rate, gpm	4 gpm of 70 wt%	179 mol/min addition rate

The following precautions are recommended during initial processing of SB9:

- The recommended antifoam strategy was not demonstrated at DWPF flux and was not demonstrated during caustic boiling. Extra attention should be paid to offgas measurements (CO_2, N_2, and O2), pressure, SRAT density, SMECT level and other indicators of foaming. If a camera is available in the SRAT it should be monitored during key processing evolutions such as carbonate destruction and initiation of boiling in the SRAT. The antifoam strategy was successful in simulant and actual waste testing, however the boiling flux is approximately 8 times higher during typical SRAT boiling.
- The SRAT and SME product analytical results should be carefully evaluated during transition in case the anion destruction or the slurry composition is different than projected. A projection of the SRAT and SME product is recommended and this should be compared to the measured results to ensure the REDOX target is met. Glycolic acid is a good complexing agent and may bring vessel or coil deposits into solution so the slurry composition might be different than projected. Remediation of the SME product with nitric or glycolic acid may be needed to achieve the REDOX target. Even the processing of samples might be slower in the laboratory as several of the methods have changed to support this flowsheet.
- The slurry rheology during SRAT and SME processing is important for adequate mixing and effective pumping to the next processing vessel. If the composition of the slurry changes due to recovered solids from the walls and coils, the slurry might be thicker than projected. If the slurry

is too thick rheologically, it can be diluted with water. The slurry thickens on cooling so it might process well but be too thick to transfer without dilution or heating

- Analysis of glass samples from the DWPF melter for REDOX is recommended to ensure the REDOX target is met. The correlations to predict REDOX were developed using simulated waste in crucibles and small melters, which may be more oxidizing than the DWPF melter
- On shift technical support from nitric-glycolic acid flowsheet experts might ease the anxiety of the operating staff as this is a more significant operational change than switching to a new sludge batch.

3.6 Qualification of Future Sludge Batches

The qualification of CPC processing can be radically changed due to elimination of catalytically generated hydrogen. The other key to qualifying the sludge batch is the fact that little chemistry is happening in the SME cycle; so much more can be learned by SRAT cycle testing. The SRAT products can be used to produce SME products by blending with frit combined with evaporation or dilution. This would save time and effort in qualifying a sludge batch.

The following is recommended as a minimum test matrix for use with simulated sludge (Figure 3-44). Assuming a REDOX target of 0.15 $Fe^{2+}/\Sigma Fe$, the acid stoichiometry range likely extends from about 80% to 110% KMA. Complete four runs at the extremes of this region, all SRAT cycles with PRFT and SEFT (typical DWPF processing). These runs are designed to develop the processing window. If any of these runs are unsuccessful due to rheology, additional runs, likely with a lower total solids target, will be needed to define the window.

Once the window has been defined, several SRAT/SME runs should be completed with sludge only and with varying PRFT and SEFT volumes to bound expected processing. In addition, further testing at various steam flow rates may be needed to understand the impact of the longer processing times (likely at 100% KMA or 104.5% Hsu acid stoichiometry). The shielded cells run should be completed with the same processing target as one of the simulant runs (actual sludge, actual PRFT, and simulated SEFT volumes, KMA, REDOX target).

The focus of the runs is demonstrating processability and verifying process chemistry. The data from the testing should be used to validate the Aspen Plus CPC model and demonstrate that it is capable of predicting the process chemistry. This can then be used as a process tool by SRNL or DWPF engineering to help optimize processing and troubleshoot upset conditions.

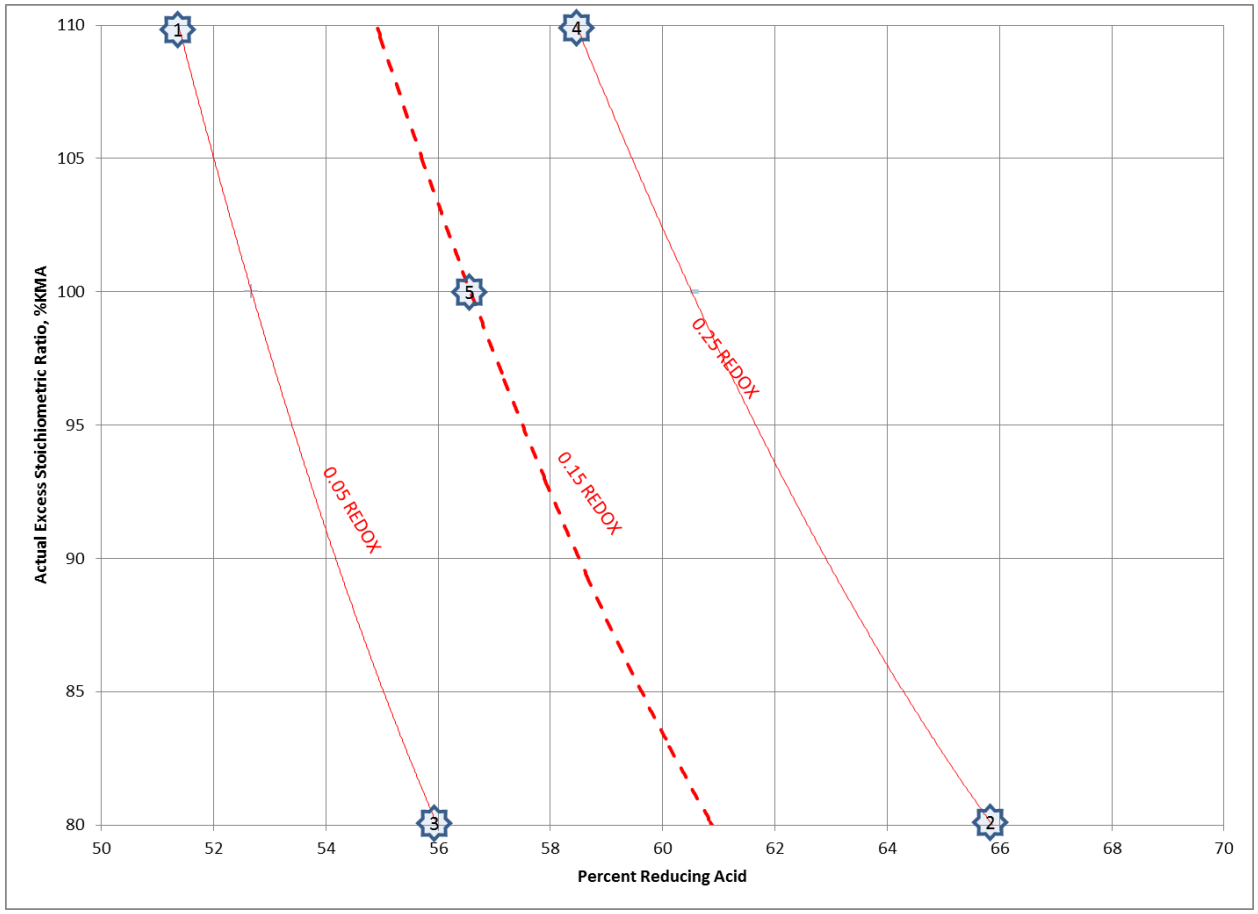

Figure 3-44. SRAT-only Matrix Showing Acid Stoichiometry and Percent Reducing Acid

3.7 Improvements in R&D Testing

The elimination of hydrogen and ammonia generation allows a different focus for future nitric-glycolic flowsheet testing. A number of suggested improvements are summarized below in an attempt to increase the magnitude and quality of the data collected during testing. It is also expected that few runs can be completed in developing future sludge batches due to the flowsheet changes and improvements in testing quality.

1. Add in situ slurry analysis using IR or Raman analyzers to track the anion concentration and metal oxidation state throughout processing, especially during acid addition and dewater, where most of the chemistry occurs. Mettler-Toledo sells an IR, Raman, and particle size instrument that can be easily used with their RC1 reactor calorimeter.
2. Add process tomography, which would allow determination of mixing homogeneity and foam height. ITS has instrumentation for measuring foam level (Froth-itometer) and mixing (Mix—itometer), both applications of tomography-based analytical process instrumentation; to allow seeing inside the process vessels. ITS is also developing an in situ rheometer, which would allow the measurement of rheology at process temperatures and throughout processing to better understand the rheology changes during semibatch processing.
3. Improve mixing of simulants and aliquots pulled for testing. Resodyn has mixers that use resonant frequencies to maximize mixing. They have developed larger mixers that are capable of mixing

drums and carboys and could be used to ensure the homogeneity of the slurries that are used throughout testing.

4. Measure the mercury mass, mercury form, and monitor the mercury stripping during SRAT/SME testing. Optimizing the mercury stripping and coalescence in the MWWT and SMECT will require equipment that can detect the mercury that condenses and then drops into the MWWT and SMECT. Localization of mercury across the length of the vessel can be detected via a linear probe using Electrical Resistance Tomography.

4.0 Conclusions

Testing was completed to develop an SB9 nitric-glycolic acid chemical process flowsheet for DWPF's CPC. CPC simulations were completed using sludge, ARP and PRFT simulants (10 SRAT cycles and 4 SRAT/SME cycles) and actual SB9 sludge (SRAT/SME cycle). As has been demonstrated in over 100 simulations, the replacement of formic acid with glycolic acid virtually eliminates the CPC's largest flammability hazards, hydrogen and ammonia. Recommended processing conditions are summarized in section 3.5.1.

Testing demonstrated that the interim chemistry and REDOX equations are sufficient to predict the composition of DWPF SRAT product and SME product. Additional reports will finalize the chemistry and REDOX equations. Additional testing developed an antifoam strategy to minimize the HMDSO peak at boiling, while controlling foam based on testing with simulant and actual waste.

Implementation of the nitric-glycolic acid flowsheet in DWPF is recommended. This flowsheet not only eliminates the hydrogen and ammonia hazards but will lead to shorter processing times, higher elemental mercury recovery, and more concentrated SRAT and SME products. The steady pH profile is expected to provide flexibility in processing the high volume of strip effluent expected once the Salt Waste Processing Facility starts up.

Important conclusions from the testing are summarized below:

- Successfully validated interim chemistry equations
    - Interim REDOX model predicts resulting REDOX trends.
- Demonstrated very low generation of two of DWPF's potential flammable gases, hydrogen and ammonia.
- Except for the first tests where the antifoam strategy was being developed, significant foaming was observed only during boiling, prior to completion of dewater, for the coupled run (NG62).
- The antifoam strategy developed during additional SB9 flowsheet testing, similar to the reduced antifoam addition strategy used during SC-18 qualification, should be implemented by DWPF for SB9 nitric-glycolic flowsheet processing. The peak HMDSO SRAT generation at boiling was 0.0041±0.0004 mmol/min at the experiment scale.
- The KMA operating window for SB9 processing is 77% to 100% for SRAT product total solid concentration of <30 wt % and can be extended to 123% for SRAT product total solid concentration of <20 wt %. Note the SB9 antifoam strategy was only tested up to 110% KMA.
- During sludge-only testing, mercury stripping and collection in the MWWT, averaging 71% mercury recovery in the MWWT during 100% KMA runs at design basis boilup, was much better than has been achieved in previous testing.
- In all experiments, nitrite was destroyed to <500 mg/kg. This is similar to the SC-18 actual-waste demonstration (at a relatively low 78% KMA) where the nitrite concentration was 304 mg/kg in the SRAT product slurry and 380 mg/kg in the SME product slurry.

- The peak carbon dioxide in the SRAT varied from 640 to 730 lb/hr at DWPF scale, significantly higher than the 342 lb/hr measured in the SC-18 actual-waste demonstration. The peak carbon dioxide in the SME varied from 4.9 to 6.1 lb/hr, significantly lower than the 19 lb/hr measured in the SC-18 shielded cells run.
- The peak nitrous oxide ranged from 0.23-1.0 vol% in the SRAT and <0.069 vol% in the SME. The peak nitrous oxide in the SC-18 actual-waste demonstration was 0.57 vol% in the SRAT and 0.08 vol% in the SME.
- Rheology is the most important parameter in defining the CPC operating window. The rheology was a strong function of acid stoichiometry. The highest acid stoichiometry runs (NG52, 54 and 59) had yield stress and consistency results that were higher than the DWPF SRAT product design basis. The rest of the runs had low yield stress and consistency values, often below the SRAT product design basis.
- NG58 was the closest simulant run for comparison to the SC-18 actual-waste demonstration. The NG58 SRAT product had a yield stress of 0.6 Pa and a consistency of 5.6 cP. The SC-18 shielded cells run had a SRAT product yield stress of 0 Pa and a consistency of 2.8 cP. Both SRAT products were rheologically thin. Since the NG58 SRAT product was higher in total solids (30% versus 25% for SC-18) it would be expected to have a higher yield stress and consistency.
- The final concentration of mercury in the SRAT product ranged from 0.02-0.61 wt% of the total solids, which was below the 0.45 wt% target in all runs except NG52.

5.0 Recommendations

Based on the results of this simulant study, SRNL recommends implementation of the nitric-glycolic acid flowsheet in DWPF.

- Except for runs NG52 and NG54, which both had thick rheology and high rod temperatures, Hydrogen generation was near or below the GC detection limit of <0.006 volume % or <0.0037 lb/hr DWPF scale.
- Throughout the SB9 qualification testing, no significant foaming was observed. DWPF should consider implementing a reduced antifoam addition strategy developed for SB9 in testing with simulants and actual waste
- Testing with simulants and actual waste confirmed that the Caustic Quench method previously developed should be used for anion measurement by IC for SRAT and SME product slurries and SRAT receipt slurry.

The following are recommendations for follow-on work utilizing the data from this study:

- Use SRAT and SME product data from these tests in regressions to refine the nitric-glycolic flowsheet CPC chemistry equations.
- Use SRAT and SME product from these tests and additional REDOX measurements to finalize the nitric-glycolic flowsheet REDOX model.
- Based on findings from additional study of mercury within the liquid waste flowsheet, it is recommended that future simulant work include CVAA for mercury analysis to compare method sensitivities during simulant tests.

Based on testing results and observations, SRNL recommends the following future testing to better align simulant studies with the facility in an effort to maximize mercury recovery. These recommendations are not tied to the implementation of the flowsheet for SB9.

- Complete back to back DWPF prototypic SRAT testing that includes a heel of mercury in the MWWT and SMECT, hot SRAT condenser outlet temperature, to better simulate prototypic DWPF processing.
- Determine if mercury collection is increased by refluxing the SRAT condensate (not dewatering) for the first 3 hours of SRAT boiling. This would return any dissolved mercury back to the SRAT allowing collection in the MWWT at a time when the condensate is less acidic.
- Determine whether pH control of the MWWT and/or SMECT can increase mercury recovery
- Determine whether a coalescer will improve the recovery of mercury in the MWWT

In future sludge batches, testing for CPC processing qualification can be radically changed due to elimination of catalytically generated hydrogen. Little chemistry is happening in the SME cycle; so much more can be learned by focusing on SRAT cycle testing. The following testing at prototypic processing conditions is recommended:

- Complete SRAT cycle testing at the extremes of the expected processing (in other words 80% to 110% KMA)
- Define rheological window
- Complete one sludge-only SRAT/SME cycle and several coupled SRAT/SME cycles with varying PRFT and SEFT volumes to bound expected processing
- Complete one shielded cells SRAT/SME cycle with actual sludge, actual PRFT, and SEFT simulant. , Use recommended acid stoichiometry and REDOX target from simulant testing.
- Validate the Aspen Plus CPC model using data generated in CPC testing.

6.0 References

1. T. Fellinger, "Sludge Batch 9 Simulant Runs Using the Nitric-Glycolic Flowsheet," Savannah River Remediation, Aiken, SC, X-TTR-S-00037, 2015.

2. D.P. Lambert, "Task Technical and Quality Assurance Plan for Sludge Batch 9 Simulant Runs Using the Nitric-Glycolic Flowsheet," Savannah River National Laborator, Aiken, SC, SRNL-RP-2015-00931, Revision 0, 2016.

3. F.C. Johnson and T.B. Edwards, "Reconfirmation of Frit 803 Based on the January 2016 Sludge Batch 9 Reprojection," Savannah River National Laboratory, Aiken, SC, SRNL-L3100-2016-00010, 2016.

4. F.C. Johnson, T.B. Edwards, and D.K. Peeler, "Confirmation of Frit 803 for Sludge Batch 9," Savannah River National Laboratory, Aiken, SC, SRNL-L3100-2015-00155, 2015.

5. F.C. Johnson, T.B. Edwards, and D.K. Peeler, "SB9 Frit Development: Mar Results Based on the August 26-27, 2015 Projections," Savannah River National Laboratory, Aiken, SC, SRNL-MS-2015-00175, Revision 0. , 2015.

6. D.P. Lambert, "Recommendations for Sludge Batch 9 Qualification Processing under the Nitric-Glycolic Acid Flowsheet in the Shielded Cells," Savannah River National Laboratory, Aiken, SC, SRNL-L3100-2016-00077, Rev. 1, 2016.

7. J.D. Newell, J. Pareizs, C.J. Martino, S.H. Reboul, C.J. Coleman, T.B. Edwards, and F.C. Johnson, "Actual Waste Demonstration of the Nitric-Glycolic Flowsheet for Sludge Batch 9 Qualification," Savannah River National Laboratory, Aiken, SC, SRNL-STI-2016-00327, Revision 0, 2016.

8. C.J. Bannochie, "Tank 40 Final Sludge Batch 8 Chemical Characterization Results," Savannah River National Laboratory, Aiken, SC, SRNL-STI-2013-00504, Revision 0, 2013.

9. H.B. Shah and M.A. Rios-Armstrong, "Sludge Batch 9 Qualification Blend Recommendation," Savannah River National Laboratory, Aiken, SC, SRR-LWP-2015-00037, Revision 0, 2015.

10. D.C. Koopman and J.R. Zamecnik, "DWPF Simulant CPC Studies for SB8," Savannah River National Laboratory, Aiken, SC, SRNL-STI-2013-00106, Rev. 0, 2013.

11. T.E. Smith, J.D. Newell, and W.H. Woodham, "Defense Waste Processing Facility Simulant Chemical Processing Cell Studies for Sludge Batch 9," Savannah River National Laboratory, Aiken, SC, SRNL-STI-2016-00281, Rev 0, 2016.

12. D.C. Koopman, D.R. Best, and B.R. Pickenheim, "SRAT Chemistry and Acid Consumption During Simulated DWPF Melter Feed Preparation," Savannah River National Laboratory, Aiken, SC, WSRC-STI-2008-00131, 2008.

13. J.R. Zamecnik, "DWPF Nitric-Glycolic Flowsheet Chemical Process Cell Chemistry: Part 1," Savannah River National Laboratory, Aiken, SC, SRNL-STI-2015-00681, Revision 0, 2016.

14. J.C. Marek and R.E. Eibling, "Calculational Algorithms for Nitric Acid Sludge Adjustment," Savannah River Technology Center, Aiken, SC, SRTC-PTD-92-0050, 1992.

15. J.W. Ray, "Waste Acceptance Criteria for Sludge, ARP, and MCU Process Transfers to 512-S and DWPF," Savannah River Remediation, LLC, Aiken, SC, X-SD-G-00008, Rev. 23, 2016. *Draft*

16. "Laboratory Scale Chemical Process Cell Simulations," Savannah River National Laboratory, Aiken, SC, 2016.

17. D.P. Lambert, "Task Technical and Quality Assurance Plan for Sludge Batch 9 Simulant Runs Using the Nitric-Glycolic Flowsheet," Savannah River National Laborator, Aiken, SC, SRNL-RP-2015-00931, Revision 1, 2016.

18. D.P. Lambert, "Run Plan for Sludge Batch 9 Nitric-Glycolic Acid " Savannah River National Laboratory, Aiken, SC, SRNL-L3100-2016-00121, 2016.

19. D.P. Lambert, "SB9 Nitric-Glycolic Acid Flowsheet Development," Savannah River National Laboratory, Aiken, SC, o7787-00055-19, 2016.

20. C. Jantzen, M. Williams, J.R. Zamecnik, and D. Missimer, "Interim Glycol Flowsheet Reduction/Oxidation (REDOX) Model for the Defense Waste Processing Facility (DWPF)," Savannah River National Laboratory, Aiken, SC, 2016.

21. D.P. Lambert, M. Williams, and C.H. Brandenburg, "Antifoam Degradation Testing to Support Development of Sludge Batch 9 Flammability Strategy," Savannah River National Laboratory, Aiken, SC, SRNL-L3100-2016-00146 Revision 2, 2016.

22. "Gum Workbench: User Manual for Version 1.2, 2.3, and 2.4,"

23. M.C. Clark, "DWPF Chemical Control Program: Antifoam Addition Attributes Description," Savannah River Remediation, LLC, Aiken, SC, X-ESR-S-00285, 2016.

24. B.R. Pickenheim, M.E. Stone, and J.D. Newell, "Glycolic - Formic Acid Flowsheet Development," Savannah River National Laboratory, Aiken, SC, SRNL-STI-2010-00523, Revision 0, 2010.

25. D.P. Lambert, B.R. Pickenheim, M.E. Stone, J.D. Newell, and D.R. Best, "Glycolic - Formic Acid Flowsheet Final Report for Downselection Decision," Savannah River National Laboratory, Aiken, SC, SRNL-STI-2010-00523, Revision 1, 2011.

26. D.P. Lambert, J. Pareizs, and D.R. Click, "Demonstration of the Glycolic-Formic Flowsheet in the SRNL Shielded Cells Using Actual Waste," Savannah River National Laboratory, Aiken, SC, SRNL-STI-2011-00622, Revision 0, 2011.

27. D.P. Lambert and D.C. Koopman, "Glycolic-Formic Acid Flowsheet Sludge Matrix Study," Savannah River National Laboratory, Aiken, SC, SRNL-STI-2011-00275, Revision 0, 2011.